Forschungszentrum Jülich

Institut für Festkörperforschung

# The Motion of the Solidification Front of a Binary Alloy with Quenched Disorder

Xia Feng

Jül-3613

# *The Motion of the Solidification Front of a Binary Alloy with Quenched Disorder*

*Xia Feng*

Berichte des Forschungszentrums Jülich ; 3613
ISSN 0944-2952
Institut für Festkörperforschung Jül-3613
D82 (Diss. RWTH Aachen)

Zu beziehen durch: Forschungszentrum Jülich GmbH · Zentralbibliothek
D-52425 Jülich · Bundesrepublik Deutschland
☎ 02461/61-6102 · Telefax: 02461/61-6103 · e-mail: zb-publikation@fz-juelich.de

# Abstract

In this work, we studied the motion of the solidification front of a disordered binary alloy. Here we assume that the atoms are frozen not only in the solid state but also in the liquid state. This assumption is justified if the system is quenched from its melt so fast that the atoms in both phases do not have time to jump as the solidification front passes. Both analytical results and results obtained from MC-simulations are presented. The quenched disorder in the system, which is caused by concentration fluctuations, leads to spatial and temporal correlations through the propagation of the solidification front. By investigating a two-dimensional lattice model, we found the non-trivial effects of the quenched disorder on the behavior of the solidification front.

In the one-phase region of an equilibrium phase diagram, the interface moves with a constant velocity. However, in the two-phase region it demonstrates a complicated behavior, which strongly depends on the system parameters. The average displacement $h$ of the interface as a function of time $t$ obeys a power law, $h(t) \sim t^{\nu}$, with the exponent $\nu < 1$. For very large bond energy, the exponent $\nu$ decreases to the value of a one-dimensional system; for moderate bond energy, the exponent increases to about $1$, and for small bond energy, it reverts to the value of a one-dimensional system. Therefore, the propagation of the solidification front is blocked by the quenched disorder at very small as well as very large bond energies.

The energy range where $\nu = 1$ increases with increasing system size. For a very large system with finite bond energy the interface moves with a constant velocity. This movement corresponds to the thermal creep motion of the front. A finite temperature smears out the sharp pinning-depinning transition at zero temperature. The dynamic behavior of the front has been studied by means of a scaling theory. It has been found that under small driving force, at low temperature or relatively high bond energy, the velocity $v$ of the front as a function of bond energy $\varepsilon$ and concentration $c$ can be factorized: $v(\varepsilon, c) \sim e^{-\varepsilon/T} e^{\Delta/T(Co-c)}$. Here $\Delta$ characterizes the relative strength of the disorder in the system and $Co$ represents the concentration that separates the solid from liquid state in the equilibrium phase diagram.

In addition to the diffusionless solidification we also studied the effects of the material diffusion on the motion of the front through MC-simulation of a one-dimensional system. Without diffusion the exponent $\nu$ has a value between $0$ and $1$. Typically, the exponent of a diffusion process is $0.5$. The MC-simulation shows that the exponent $\nu$ increases to $0.5$ for the concentration range where without diffusion $\nu$ would be smaller than $0.5$. Here the diffusion process dominates. For other concentrations the exponent remains unchanged and the interface dynamics dominates.

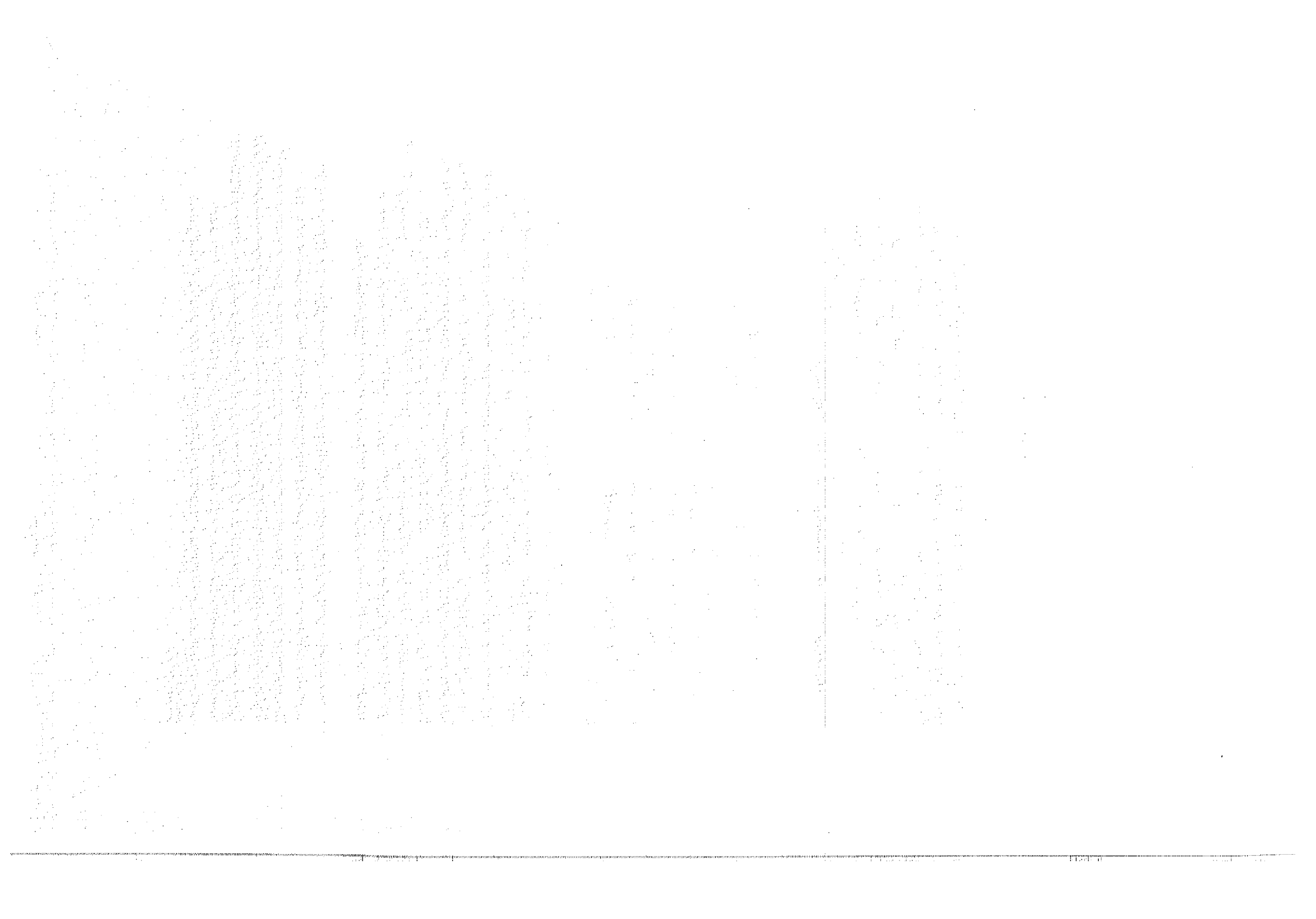

# Contents

# Chapter 1

# Introduction

## 1.1 General Introduction of the Thesis

An ideal crystal, ie., a crystal with perfect lattice and periodic boundary conditions, does not exist in nature. Indeed, most properties of real materials depend crucially on the presence of imperfections - bulk vacancies, dislocations, surface roughness and local variations in density and compositions - which are remnants of the nonequilibrium conditions under which the material has formed. Over the centuries, the art and science of crystal growth has progressed to ever more closely approximate the ideal of a perfect, crystalline solid, as evidenced impressively by modern techniques such as molecular beam epitaxy (MBE), which allows for the engineering of solid state devices at the level of individual atomic planes. Nevertheless, the success of this and other techniques depends crucially on the ability to control the disordering effects of the nonequilibrium growth conditions, and to assess, at least empirically, the relationship between the growth conditions and the resulting structures.

In a more general sense one may consider crystal growth also as a moving interface in a random media. The quenched noise, which does not change with time, generated by the randomness of the medium, has a nontrivial effect on the motion and morphology of an interface. In general, it is agreed that quenched noise produces anomalous roughening of the advancing interface [1]-[17]. The understanding of roughening dominated by quenched noise is

especially important for interpreting the results of various experiments, for which it is generally believed that the disorder of the substrate determines the morphology of the interface. There are many examples in various disciplines of physics: the interface[18, 19] between two phases in random media, such as between two fluids in a porous medium [20], or domain walls in a random ferromagnetic alloy; lattices of vortices in dirty type II superconductors[21, 22, 23]; Charge Density Waves(CDWs)[23]-[28], which are spatially periodic modulations of the electron density that occur in certain solids; the contact line of fluid drop [29, 31]; the motion of geological faults[23]; and ultimately even dry friction between two solids.

In all of these systems, a driving force, call it F, can be applied which acts to try to make the object move, but this will be resisted by the random pinning forces exerted by the medium or substrate. The primary questions of interest will involve the response of the system to such an applied driving force. If F is small, then one might guess that it will not be sufficient to overcome the resistance of the pinning forces; sections of the object would just move a bit and it would deform in response to F, but would afterwards be at rest. If the force is increased, some segment might go unstable and move only to be stopped by the remaining parts. But for large enough $F$, it should be possible to overcome the pinning forces, unless they are so strong that the object is broken up, and then object will move, perhaps attaining some steady-state velocity $v$.

Some basic questions one might ask are: is there a unique $F_c$ separating the static from the moving regime? How does $v$ depend on $F$? Are there some kinds of non-equilibrium critical phenomena when $v$ is small? In CDWs, the role of $F$ is played by the external electric field; a finite CDW current appears only beyond a threshold applied electric field. Interfaces in porous media, domain walls in random magnets, are stationary unless the applied magnetic field is sufficiently strong. A key feature of these examples is that they involve the collective depinning of many degrees of freedom that are "elastically" coupled. The elastic manyfold is pinned by disorder if the driving force is small, but for forces just above the critical threshold $F_c$, the interface

advances by jumping from one pinning path to another. At the absolute zero temperature a sharp pinning-depinning transition takes place at a finite strength of an external driving force, but at a finite temperature, the pinning transition is smeared out by the creep motion of the interface.

In this thesis we shall study the motion of the solidification front or the interface between the liquid and solid part of a binary alloy system with quenched disorder. We consider a disordered two-component alloy system which consists of A and B atoms. Each species of atoms can change its state from liquid to solid during the solidification as the interface between the two phases is advancing towards the liquid. Without allowing for diffusion, the positions of the atoms are assumed to be fixed, so that no rearrangement can occur. This corresponds to a very rapid solidification, as, for example, achievable during the formation of metallic glasses. The growth of such a binary alloy is controlled not only by the temperature but also the relative concentration of the alloy in the mother phase. In Fig.1.1, the two-component equilibrium phase diagram with three regions : the solid (S), the liquid (L) and the two-phase coexistence in between, is shown. If an initially liquid melt is suddenly cooled down to a temperature corresponding to the solid one-phase region for the corresponding relative AB-concentration, the stable solid grows steadily with a constant speed. The situation changes if the melt is cooled down into the two-phase coexistence region of the corresponding equilibrium phase diagram. The process then becomes unstable with time-dependent growth rate, since there will now be spatial regions with local alloy concentrations, which want to solidify, and other regions which preferably remain liquid. The spatial regions of the alloy with concentration close to the solidus line can solidify, but the other parts with concentrations close to the liquidus line act as an obstacle to the solidification front and stop the solidification front to advance. Thus the propagation of the solidification front becomes pinned by the fluctuations in the concentrations. In consequence, whether the solidification front advances with a constant speed or is pinned by quenched disorders and eventually stops to move depends on the relative AB-concentration or the driving force. There exists a critical concentration

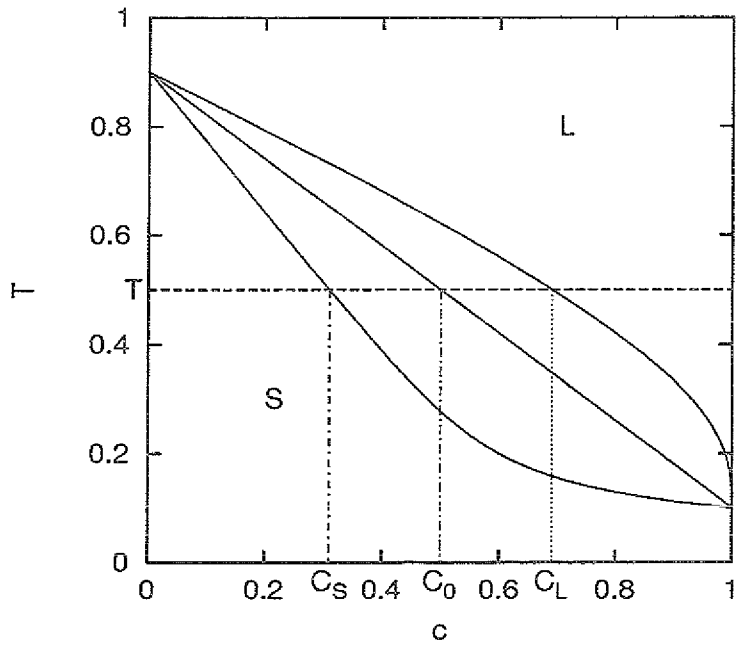


Figure 1.1: The equilibrium phase diagram for an ideal AB solution with temperature T versus concentration c of the B-atom species. S and L denote the solid and liquid phase, respectively. The area between the lower solidus line $C_S(T)$ and upper liquidus line $C_L(T)$ is the two-phase coexistence region. $C_0(T)$ is the concentration at which the thermodynamic potential per atom in the liquid and solid phase are equal.

which separates a static and a moving interface, but the transition between them is smeared out by the creep motion.

The problem in a one-dimensional (1D) system with a zero-dimensional interface has been studied extensively[32]-[54]. The equilibrium phase diagram in the concentration and temperature phase space is found to determine regions, where depinning-pinning transitions of the interface occur. In a one-phase region, the interface moves steadily, and in the two-phase region the steady velocity vanishes. The atomic species which prefers to remain in the liquid state acts as a quenched obstacle to hinder the propagation of the solidification front. The system is found to be equivalent to the random hopping model with a power-law distribution of jump waiting time[40]-[48]. In the

two-phase region the interface position $h(t)$ shows an anomalous time dependence as a power law behavior $h(t) \sim t^{\nu_1}$ with an exponent $\nu_1 < 1$, which is not a universal number but depends on both concentration of the alloy and the temperature.

For a two-dimensional(2D) system with a 1D interface extending in the direction normal to its propagating direction, a new degree of freedom comes into play: the interface tension tries to keep the interface straight, and counteracts the roughening effect by the quenched randomness. The elastic restoring effect caused by the interface tension leads to correlations along the interface, and the correlation length increases slowly with time. Therefore one can expect a finite size effect. All these make a 2D system much more complicated than a 1D one. One can ask the same questions here as those for a 1D system. For example, under which condition can the interface realize a steady-state velocity $v$? Is it possible only in the one-phase region of the equilibrium phase diagram like in the 1D system; or it is also possible in the two-phase region? How does $v$ depend on the driving force and the bond energy? There are many interesting but difficult questions about a 2D system. The behavior of the interface depends on many parameters: concentration c, bond energy $\epsilon$, system size N and the temperature T. It is almost impossible to have a theory taking the effects of all these parameters into account. Fortunately, things sometimes become a little bit simper when one handles the problem in the limit of some parameters and the corresponding asymptotics usually act as a very useful guide to investigate the behavior of the system. For a finite size system with large restoring force, we develop a theory which shows the same asymptotic dynamics in many respects as the 1D system.

It means that the interface achieves a steady-state velocity in the one-phase region of the equilibrium phase diagram, but it vanishes in the two-phase region. However, for a large system with a moderate restoring force, the interface propagates steadily even in the two-phase region. This is quite a surprise because it is totally impossible in a 1D system. Absence of a critical pinning force in a large 2D system was already shown by the Monte Carlo study by Jackson et al.[59]. It has been found that for low temperatures and

driving forces well below the $T = 0$ depinning threshold, $F_c$, the dynamics of the driven manyfold is controlled by thermally activated jumps of correlated regions over the pinning energy barriers separating different metastable states. In this region the mean velocity of the driving manyfold is highly nonlinear and has been evaluated via a scaling approach [62, 63] with the result, $v \simeq exp[-U(F)/T]$, where $U(F)$ is the optimal energy barrier for creep between favorable metastable states. Under the action of the external driving force, sections of the manyfold that are initially pinned move to a more favorable metastable state, determined by the condition that the energy gain due to the driving force equals the "elastic" deformation and the pinning energy of the medium. For $F \ll F_c$, large sections of the manyfold hop long distances to find the next optimal-energy state. This yields a large energy barrier that diverges algebraically with vanishing force, $U(F) \sim (F_c/F)^{\mu}$, where $\mu$ is a characteristic exponent. This problem was attacked in numerous works[64]-[80]. We shall study the front propagation in the two-phase region systematically and find that the steady-state velocity $v$ depends on the driving force $F$ as $v \propto \exp(-F^{-1})$. The results can be also analyzed in terms of random field Ising (RFI) model [81].

In reality, atoms are not completely quenched as we assumed but are moving, and concentrations follow the diffusion law. The natural question one may ask is then how the diffusion affects the motion of the interface. We address the question by the Monte Carlo simulation of the one-dimensional system and compare the results with an approximate analysis which neglects the correlations in the concentration distribution. We found that there exists competition between the kinetics and diffusion mechanics. If the growth is controlled by the diffusion of the alloy atoms, the anomalous propagation of the interface, the variance $\sigma(t) \sim t^{\nu_2}$, cross over to the $t^{1/2}$ law in the two-phase region, at least for the situation, where the quenched system would grow with a small exponent than the diffusion exponent $1\nu_2 < 1/2$. In the one phase region on the other hand steady-growth is obtained and controlled always by the kinetics of the advancing interface.

## 1.2 Outline

The structure of the thesis is as follows. The basic concepts about pinning-depinning transition are introduced in **Chapter 2** through a simple example. **Chapter 3** is devoted to diffusionless solidification of a 1D alloy system. Special attention will be paid to the interface behavior in the two-phase region. The problem will be modeled by a random walk in a 1D disordered lattice in Section 3.1. The results we get in this section become the theoretical basis for the work in the following chapters. Section 3.2 introduce the 1D lattice model and section 3.3 mainly summarize simulation results.

In chapter 4 - 7 the model is extended into two dimensions where the energy cost for the interface deformation is taken into account. Practically we restrict our investigations to models of solid-on-solid (SOS) type, where overhangs on the interface are not allowed. The 2D lattice model is introduced in **Chapter 4**. In particular, we also show that the model can be mapped to a random-field Ising (RFI) model with temperature-dependent random fields. Emphasis will be put on the different system behavior both inside and outside the two-phase coexistence region.

Since there are so many factors interplaying in a 2D system, the problem becomes extremely complicated. We start with a relatively simple system: a finite size system with very large bond energy, in **Chapter 5**. In this limit it is found theoretically that a 2D system has the same asymptotics in many respects as that for a 1D system. However, we can not analytically handle the problem for arbitrary value of the bond energy since mathematically too demanding. The alternative is the Monte Carlo Simulation. **Chapter 6** deals with the Algorithm and tests of the program for a 2D system.

**Chapter 7** is one of the main parts of the thesis where numerical results of a 2D system obtained from computer simulations are summarized. The behavior of the interface is found to depend on bond energy, concentration of alloy, temperature, the system size and the simulation time in a complicated manner. The correlation along the interface plays an important role. In section 7.1 the theoretical expectations for a 2D system with large bond energy

studied in chapter 5 is verified by compute simulations. Section 7.2 and 7.3 show that the 2D system has a finite size effect and the interface motion varies with the bond energy in a complicated way. For a large system the simulations in section 7.4 show that the interface always settles to a motion with a constant velocity. Even inside the two-phase region such a large system is not pinned but moves at a slow creeping velocity. This creep motion is analyzed in terms of RFI model, and our numerical results confirm quantitatively the analytical estimates of the dependence of the creep velocity upon the driving force and the bond energy. The development of the correlation along the interface in section 7.6 explains the finite size and the finite time effects observed in the asymptotic behavior of small systems.

Before chapter 8 we deal with a quenched system where atoms are frozen. In other words, there is no diffusion of particles in the system. In **Chapter 8** we will treat a more realistic system by taking the diffusion into account. In section 8.1 and 8.2 we introduce the diffusion into the diffusionless 1D model and write a corresponding Algorithm. Section 8.3 attempts to provide an approximate analysis of transient random fluctuations of the interface which neglects the correlations in the concentration distribution. A set of diffusion equations is obtained, and therefore we can numerically integrate them to obtain the motion of the interface. The comparison between Monte Carlo simulation and numerical integration of the diffusion equations is presented in section 8.4.

Finally, a conclusion about the whole work is given in **Chapter 9.**

# Chapter 2

# Pinning-Depinning Transition

For a class of interface phenomena we have an interface that moves in a disordered medium. The fluid flow in porous media, propagation of flam fronts, flux lines in a superconductor and the solidification front in a disordered alloy lattice are some examples. This apparently different phenomena actually can be discussed using a common framework. It is coming to be appreciated that all the systems display essentially the same physics: an elastic interface ('elastic' in the sense that it does not break, but tries to remain smooth) propagates in a disordered material. The randomness of the substrate acts to pin the interface, thereby making the interface rough. In the fluid case, local inhomogeneities may block the fluid flow. Some parts of the paper do not burn as rapidly as others, so the flam is halted. Impurities attract the flux line and pin it down in random positions. The atoms in favor of being in the liquid state pin some sections of the solidification front. Thus the velocity of the interface is affected by the inhomogeneities of the medium: the resistance of the medium against the motion of the interface is different from point to point ; we call this quenched noise, because it does not change with time. In the case of fluid flow, fluid pressure and capillary force drive the fluid and disorder in the medium slows its propagation. If the disorder wins the competition, the interface becomes pinned. Conversely, if the driving force wins, the interface stays depinned. This transition from a pinned to a moving interface - obtained by changing the driving force - is called the depinning transition.

In this chapter, we discuss how quenched disorder leads to interface pinning and depinning. The problem of a moving interface in the presence of quenched noise is a new type of critical phenomena, arising from "quenched randomness". Although the investigation of this problem by numerical simulation and renormalization group approach results in many important results, the diversity and richness of the underlying phenomena continue to present us with a large number of unanswered questions.

## 2.1 One Particle

Depinning is a non-equilibrium critical phenomenon involving an external force and a pinning force. A simple example is provided by a point mass on a plane. In Fig.2.1(a), a particle of mass m on a plane, driven by an external force F is shown. There are two friction forces acting: static friction, $F_R$, and dynamic friction $\rho dr/dt$, proportional to the velocity. There exists a critical force $F_c$. For $F < F_c$, $v = 0$. For $F > F_c$, the equation of motion is

$$m\frac{d^2r}{dt^2} = F - F_c - \rho\frac{dr}{dt}, \tag{2.1}$$

here $\rho$ is a dissipative coefficient. Solving Eq.(2.1), one can easily find the velocity of the particle

$$v = \frac{1}{\rho}(F - F_c - e^{-\frac{\rho}{m}t}). \tag{2.2}$$

So after a transit period, the particle will reach a constant velocity $v$. There are two regimes as a function of the external force $F$, as shown in Fig.2.1(b).
*Pinned phase* - If $F < F_c$, the driving force can not overcome the static friction, thus the velocity of the particle is zero.
*Moving phase* - If $F > F_c$, the velocity is $v = \frac{F-F_c}{\rho}$, a linear function of $F$.
The transition from a pinned to a moving phase is called a depinning transition, and takes place at a critical threshold $F_c$. In the vicinity of the depinning

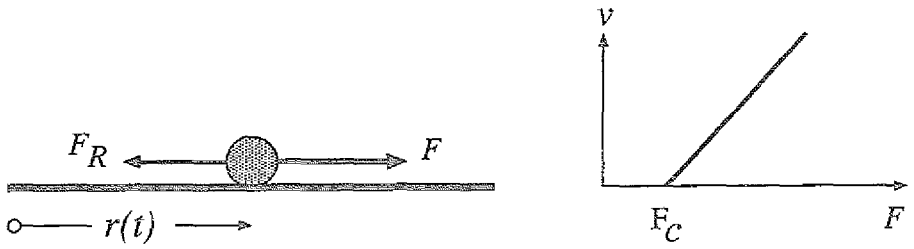


Figure 2.1: Depinning transition of a single particle on a plane. (a) The particle of mass $m$ is driven by the external force, $F$, to the right, and the friction force,$F_R$, acts against its motion. (b) The velocity of the particle as a function of the external driving force. $F_c$ is the critical driving force.

transition, the average velocity has the form

$$v \sim (F - F_c)^\theta, \tag{2.3}$$

where $\theta$ is the velocity exponent. In the example, $v \propto (F - F_c)$, so $\theta = 1$.

## 2.2 Random Force

In Fig.2.2(a), a particle of mass m on a rough plane is driven by the force $F$. The plane is randomly distributed some obstacles and the average distance between two obstacles is $a$. Then the velocity of the particle is given by[31]

$$\rho\frac{dr}{dt} = F + f(r(t)), \tag{2.4}$$

with $f(r(t))$ representing the random pinning forces of the static heterogeneous medium on the place. The resistance of the medium against the motion is different from point to point and does not change with time. Three regimes are predicted by the motion equation (2.4) as shown in Fig.2.2(b). *(a) Pinned phase* - If we add a small driving force, the particle tends to move in the direction of $F$, but will eventually become pinned by obstacles.
*(b) Critical moving phase* - If we increase the driving force, the particle overcome the pinning force of impurities at a criticle force $F_c$, and begins to move

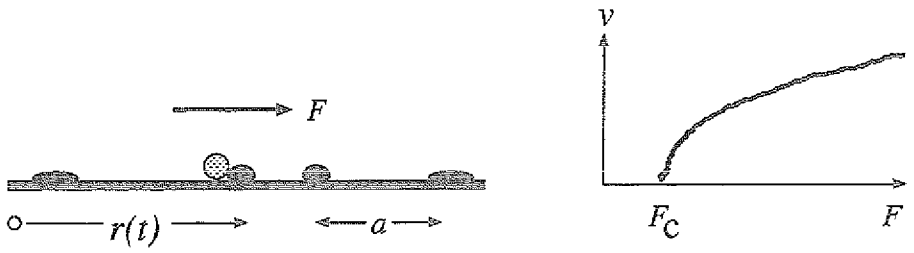


Figure 2.2: Depinning transition of a single particle on a rough plane. (a) The particle of mass $m$ is driven by the external force, $F$, to the right, and the randomly distributed obstacles act against its motion. $a$ is the average spacing between two obstacles. (b) The velocity of the particle as a function of the external driving force. $F_c$ is the critical driving force.

with a finite velocity. In the immediate vicinity of $F_c$, the velocity follows (2.3). The motion of the particle just above the threshold is not uniform and sometime slow and sometime fast.

*(c) Large velocity regime* - If $F \gg F_c$, the particle feels a rapidly fluctuating noise, so the velocity increase linearly with $F$.

## 2.3 Interface in a Disordered Medium

Consider the general situation of an interface in a porous medium, as shown in Fig.2.3(a) with a driving force $F$ acting on the interface in a vertical direction. This is in fact a generalization of a single particle motion shown in Fig.2.2. Instead of a single particle, we have a spatially extended string that has a surface tension and so tries to remain straight. The disorder acts as an inhomogeneous friction force, pinning parts of the interface. However, other parts are free to advance, and they try to drive the neighboring parts of the interface as well. The configuration of the interface at time t is described by the function $h(x,t)$. The function h is assumed to be single valued, thus excluding configurations with overhangs. In many cases[18, 19], where viscous forces dominate over inertia, the local velocity of a point on the interface is

given by

$$\frac{dh(x,t)}{dt} = F + f(x,h(x,t)) + \kappa_x[h(x',t)]. \tag{2.5}$$

The first term on the right hand side is the driving force on the interface which is also the external control parameter. Fluctuations in the force due to randomness and impurities are represented by the second term. With the assumption that the medium is on average translationally invariant, the average of $f(x,h)$ can be set to zero. The final term in eq.(2.5) describes the "elastic" forces between different parts of the interface. Short range interactions can be described by a gradient expansion; for example, a line tension leads to $\kappa[h(x)] = \Delta^2 h(x)$ or $\kappa[h(q)] = -q^2 h(q)$ for the Fourier modes. The surface of a drop of non-wetting liquid terminates at a contact line on a solid substrate[29]. Deformations of the contact line are accompanied by distortions of the liquid/gas surface. As shown by Joanny and de Gennes[30], the resulting energy and forces are non-local, described by $\kappa[h(q)] = -|q|^\alpha h(q)$.

When $F$ is small, the interface is trapped in one of many metastable states in which $\partial h/\partial t = 0$ at all points. The interface is therefore in pinned phase. For $F$ larger than a threshold $F_c$, the interface is depinned from the last metastable state, and moves with an average velocity $v$. On approaching the threshold from above, the velocity vanishes as $v \sim (F - F_c)^\theta$. A mean-field estimate for $\theta$ was obtained by Fisher in the context of CDWs[27]. It corresponds to the limit $\alpha = 0$, where every point is coupled to all others, and hence experiences a restoring force proportional to $< h(x) > - h(x)$. The resulting equation of motion,

$$\frac{dh(x,t)}{dt} =< h(x) > - h(x) + F + f(x,h(x,t)), \tag{2.6}$$

has to be supplemented with the condition $< h(x) >= vt$. The self-consistent solution for the velocity indeed vanishes as $(F - F_c)^\theta$, with an exponent that dependents on the details of the random force.

The motion just above the threshold is not uniform, composed of rapid jumps as large segments of the interface depin from strong pinning centers, superposed on the slower steady advance. Theses jumps have a power law distribution in size, cutoff at a correlation length $\xi$ which diverges at the

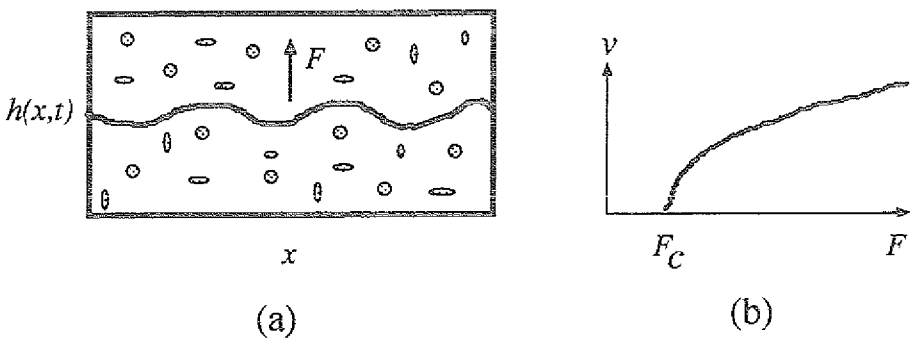


Figure 2.3: (a) Schematic representation of an interface h(x,t) in a random environment. The shaded circles represent randomly distributed pinning centers, whose position and pinning strength is independent of time (quenched). $F$ is the external driving force. (b) The velocity of the interface as a function of the external driving force. $F_c$ is the critical driving force.

transition as

$$\xi \sim (F - F_c)^{-\lambda}. \tag{2.7}$$

This phase we call critical moving phase. If $F$ is much larger than $F_c$, the interface attains some steady-state velocity $v$ which increases linearly with $F$. Then the interface is in the large velocity regime. The above three regimes are shown in Fig.2.3(b).

Although, the underlying issues of collective depinning for CDWs have been around for some time, only recently a systematic perturbative approach to the problem was developed. This functional renormalization group approach to the dynamic equations of motion was originally developed in the context CDWs by Narayan and Fisher[27, 28], and extended to interfaces by Nattermann et al[66].

## 2.4 Thermal Noise

The results discussed in the previous sections were obtained in the zero-temperature limit, where the thermal noise is negligible. However, thermal noise is always present in experiments, so its effect on the motion of interfaces

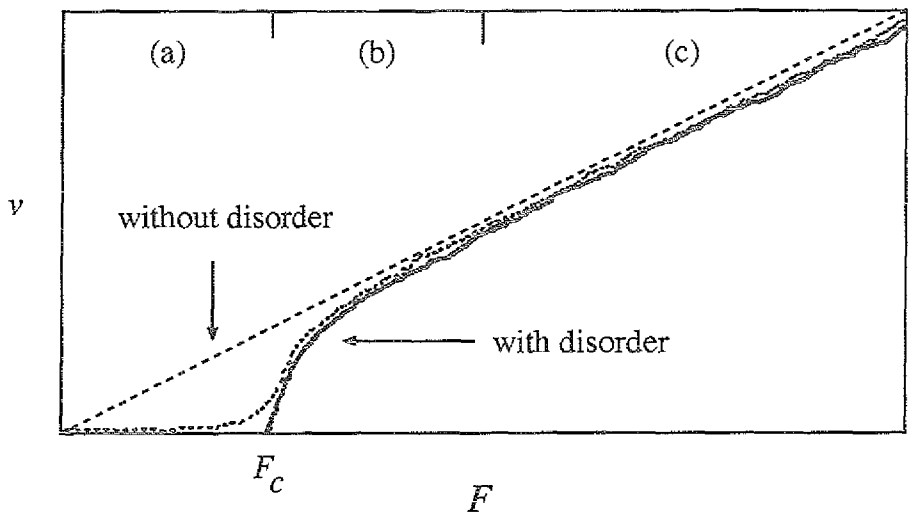


Figure 2.4: Dependence of the velocity on the driving force at nonzero temperature (middle curve), compared with idealized behavior at $T = 0$ (bottom curve). Thermal fluctuations help the interface advance even at forces smaller than $F_c$.

in a medium with quenched randomness must be discussed. The thermal noise affects the motion of the interface close to and below the depinning transition. At finite temperature the transition from an unpinned to a pinned interface is somewhat rounded; the interface moves with a nonzero average velocity even for $F < F_c$, which can be understood by looking more closely at the nature of the thermal fluctuations. Let us consider that the interface is trapped in a local potential minimum, generated by the quenched disorder. In order to advance further, it must pass a potential barrier $\Delta V$. At zero temperature the interface remains in the local minimum forever, its velocity being zero. However, at finite temperature, the interface can pass the barrier with a probability $P \sim \int_{\Delta V}^{\infty} dE exp(-E/k_B T)$. A schematic illustration of the resulting velocity-driving force diagram at finite temperature is shown in Fig.2.4.

# Chapter 3

# Diffusionless Solidification of a One-Dimensional System

In this chapter we shall study the propagation of the solidification front of a 1D binary system. This problem can be modeled by a random walk in a 1D disordered lattice. From a theoretical point of view, it seems to be one of the simplest models of disordered system. However, it gives a satisfactory understanding of conductivity experiments on some anisotropic organic conductors [85] and serves as the theoretical basis of the following work. In a discrete-time version, one can formulate the problem as follows. Consider a particle on a one-dimensional lattice. If the particle is on site n at time t, it will be at time $t+1$ either on site $n+1$ with probability $p_n$ or on site $n-1$ with probability $q_n = 1 - p_n$. The problem is obvious if all the $p_n$ are equal. However, if the $p_n$ are randomly chosen with some probability distribution $\rho(p_n)$, one can observe very unexpected behaviors. One of the most striking results was obtained by Sinai [48] who has shown that, for random hopping rates $p_n$ and the distribution $\rho(p_n)$ which satisfy

$$\left\langle ln\frac{p_n}{1-p_n} \right\rangle = \int \rho(p_n)\, dp_n\, ln\frac{p_n}{1-p_n} = 0, \tag{3.1}$$

the particle is at a distance of order $log^2 t$ from its starting point after time t. When the hopping rates do not satisfy the condition (3.1), one finds [45, 49,

42, 40] that the mean position $< h(t) >$ of the particle increases linearly with time, i.e., with a finite velocity only if

$$\left\langle \frac{q_n}{p_n} \right\rangle < 1 \qquad or \qquad \left\langle \frac{p_n}{q_n} \right\rangle < 1. \tag{3.2}$$

It was found that

$$< h(t) > \simeq \left\langle \frac{1}{p_n} \right\rangle^{-1} \left( 1 - \left\langle \frac{q_n}{p_n} \right\rangle \right) t \qquad \text{if} \qquad \left\langle \frac{q_n}{p_n} \right\rangle < 1, \tag{3.3}$$

whereas

$$< h(t) > \simeq \left\langle \frac{1}{q_n} \right\rangle^{-1} \left( 1 - \left\langle \frac{p_n}{q_n} \right\rangle \right) t \qquad \text{if} \qquad \left\langle \frac{q_n}{p_n} \right\rangle < 1. \tag{3.4}$$

On the contrary, if the conditions (3.2) is not satisfied, the mean position $\overline{h(t)}$ increases like a power law $t^{\nu_1}$ with $\nu_1 < 1$. Then, if $\nu_1$ is the nonzero solution of

$$\left\langle \left( \frac{1 - p_n}{p_n} \right)^{\nu_1} \right\rangle = 1, \tag{3.5}$$

one finds

$$< h(t) > \sim t^{\nu_1} \qquad if \quad \nu_1 > 0,$$

$$< h(t) > \sim -t^{-\nu_1} \qquad if \quad \nu_1 < 0. \tag{3.6}$$

Bernasconi and Schneider[40] found that these power laws (3.6) are modulated by a periodic function of $\log t$ for some particular distributions of $p_n$.

## 3.1 One-Dimensional Hopping Model

In the following, we shall give the explicit derivation of the dependence of the exponent $\nu_1$ on the system parameters. The basic results are identical to the ones given in [41]. For this problem, the first equation that one can write is the Master equation

$$P_n(t+1) = q_{n+1} P_{n+1}(t) + p_{n-1} P_{n-1}(t). \tag{3.7}$$

Here $P_n(t)$ is the probability of finding the particle on site n at time t, and we use the periodic boundary conditions for a lattice with N sites, which means the site $N+n$ is identified with the site n.

After a very long time, the probability $P_n(t)$ converges to an equilibrium probability distribution $Q_n$ which satisfies

$$Q_n = q_{n+1}Q_{n+1} + p_{n-1}Q_{n-1}. \tag{3.8}$$

Our aim is to determine the long-time asymptotic behavior of the particle's velocity which is given by

$$v = [\sum_{n=1}^{N}(p_n - q_n)Q_n]/[\sum_{n=1}^{N} Q_n]. \tag{3.9}$$

If the transition rates have fixed values p, independent of n, one immediately derives the result: $v = p - q$. This is the case of pure atoms. In the case of random transition rates, $Q_n$ can be solved by using the recurrence (3.8). Taking equation (3.8) into account, subtracting a term $p_nQ_n$ in both sides and reordering terms, we obtain

$$q_{n+1}Q_{n+1} - p_nQ_n = q_nQ_n - p_{n-1}Q_{n-1}. \tag{3.10}$$

The above equation has the same structure on two sides, therefore each of them can be nothing but a constant $C_1$

$$q_{n+1}Q_{n+1} - p_nQ_n = C_1 \tag{3.11}$$

We define three new functions $f_n$, $g_n$ and $s_n$ which satisfy

$$Q_n = f_n/p_n, \qquad g_n \equiv \frac{1}{s_{n+1}} \equiv \frac{p_{n+1}}{q_{n+1}} \tag{3.12}$$

Inserting $f_n$ and $g_n$ in equation (3.11), we get the following recursion relation

$$f_{n+1} = g_n(f_n + C_1). \tag{3.13}$$

Using the recurrence (3.13), $f_{N+1}$ can be derived as following

$$f_2 = g_1f_1 + g_1C_1$$

$$
\begin{aligned}
f_3 &= g_2 g_1 f_1 + (g_2 g_1 + g_2) C_1 \\
f_4 &= g_3 g_2 g_1 f_1 + (g_3 g_2 g_1 + g_3 g_2 + g_3) C_1 \\
&\cdots \\
f_{n+1} &= g_n g_{n-1} \cdots g_1 f_1 + (g_n g_{n-1} \cdots g_1 + g_n g_{n-1} \cdots g_2 + \ldots + g_n g_{n-1} + g_n) C_1 \\
&= f_1 \left( \prod_{i=1}^{n} g_i \right) + \left( \prod_{i=1}^{n} g_i + \prod_{i=2}^{n} g_i + \prod_{i=3}^{n} g_i + + \prod_{i=n-1}^{n} g_i + g_n \right) C_1 \\
&\cdots \\
f_{N+1} &= f_1 \left( \prod_{i=1}^{N} g_i \right) + \left( \prod_{i=1}^{N} g_i + \prod_{i=2}^{N} g_i + \prod_{i=3}^{N} g_i + + \prod_{i=N-1}^{N} g_i + g_N \right) C_1 \\
&= f_1 \left( \prod_{i=1}^{N} g_i \right) + C_1 \left( \prod_{i=1}^{N} g_i \right) \left( 1 + \sum_{i=1}^{N-1} \prod_{j=1}^{i} \frac{1}{g_j} \right) \qquad (3.14)
\end{aligned}
$$

Here $\prod_{i=1}^{N} g_i$ is a constant for given lattice, replacing it by a constant $C_2$ and using the periodic boundary condition $f_1 = f_{N+1}$ and (3.12) for $s_n$, we obtain

$$f_1 = f_1 C_2 + C_1 C_2 \left( 1 + \sum_{i=1}^{N-1} \prod_{j=1}^{i} s_{j+1} \right), \qquad (3.15)$$

then

$$f_1 = C \left( 1 + \sum_{i=1}^{N-1} \prod_{j=1}^{i} s_{j+1} \right). \qquad (3.16)$$

Generally,

$$f_n = C \left( 1 + \sum_{i=1}^{N-1} \prod_{j=1}^{i} s_{j+n} \right) \qquad (3.17)$$

here $C = C_1 C_2/(1 - C_2)$ is a constant. It turns out that $Q_n$ can be determined explicitly as a function of all the $p_i$ from equation (3.12) and (3.17)

$$Q_n = \frac{C}{p_n} \left[ 1 + \sum_{i=1}^{N-1} \left( \prod_{j=1}^{i} s_{j+n} \right) \right]. \qquad (3.18)$$

From expressions (3.9) and (3.18), we can now calculate the velocity $v$ for any choice of the $p_n$. In order to have a quantity which is simple to average

and to study, we give the expression of the inverse velocity:

$$v^{-1} = \frac{\sum_{i=1}^{N} \frac{1}{p_n} \left(1 + \sum_{i=1}^{N-1} \left(\prod_{j=1}^{i} s_{j+n}\right)\right)}{N\left(1 - \prod_{i=1}^{N} s_i\right)}. \tag{3.19}$$

Now let us try to average $v^{-1}$ over the possible choice of $p_n$. Consider first the case where $< lns > < 0$ [*i.e.*, $< lnp > >< ln(1-p) >$]. Then the product in the denominator of (3.19) can be neglected with probability 1 in the limit $N \to \infty$ and it becomes easy to average the right side of equation (3.19):

$$\begin{aligned}
< v^{-1} > &= \frac{1}{N}\left\langle \sum_{i=1}^{N} \frac{1}{p_n} + \sum_{i=1}^{N} \frac{1}{p_n} \left[\sum_{i=1}^{N-1} \left(\prod_{j=1}^{i} s_{j+n}\right)\right]\right\rangle \\
&= \frac{1}{N}\left\langle \sum_{i=1}^{N} (1+s_n)\right\rangle + \left\langle \sum_{i=1}^{N} (1+s_n) \left[\sum_{i=1}^{N-1} \left(\prod_{j=1}^{i} s_{j+n}\right)\right]\right\rangle \\
&= (1+< s >) + (1+< s >) \sum_{i=1}^{N-1} < s >^i \\
&= (1+< s >)\left(1 + \sum_{i=1}^{N-1} < s >^i\right)
\end{aligned} \tag{3.20}$$

The series is convergent in the limit $N \to \infty$ only if $< s > \ < 1$. We conclude that there is a finite velocity for this problem only if $< s > \ < 1$ and in this case, the velocity is given by

$$< v^{-1} >= \frac{1+< s >}{1-< s >} \tag{3.21}$$

If the distribution $\rho$ was chosen such that $< lns > < 0$ but $< s > > 1$, the inverse velocity would be infinite. We shall see later that in this case, the distance h covered by the particle during the time t is no longer promotional to t but to $t_1^{\nu}$ with $0 < \nu_1 < 1$.

The calculation of $< v^{-1} >$ can be done in the case $< lns > > 0$ in the same way as for $< lns > < 0$. One starts by neglecting 1 in the denominator of Equation (3.19) and then one finds that $< v^{-1} >$ is finite only if $< s^{-1} > < 1$. The result for $< v^{-1} >$ is, in this case,

$$< v^{-1} >= -\frac{1+< s^{-1} >}{1-< s^{-1} >} \tag{3.22}$$

It may look arbitrary to average the inverse velocity $v^{-1}$. However , if $< s > < 1$ or $< s^{-1} > < 1$, one can show that the fluctuations of $v^{-1}$ are small in the large-N limit. This indicates that the velocity has small fluctuations, and therefore $\left\langle \frac{1}{v} \right\rangle \simeq \frac{1}{<v>}$.

At this stage, the main question is what happens if $< s > > 1$ or $< s^{-1} > > 1$. In order to simplify the calculations, we shall restrict ourself to a simple distribution $\rho$ which depends on two parameters $\alpha$ and p (for convenience we choose $p > \frac{1}{2}$):

$$\rho(p_n) = \alpha\,\delta(p_n - p) + (1-\alpha)\,\delta(p_n - (1-p)) \tag{3.23}$$

For the distribution (3.23),

$$< s >= \alpha \frac{1-p}{p} + (1-\alpha)\frac{p}{1-p} \tag{3.24}$$

and

$$< s^{-1} >= \alpha \frac{p}{1-p} + (1-\alpha)\frac{1-p}{p} \tag{3.25}$$

$$< lns >= \alpha\, ln\left(\frac{1-p}{p}\right) + (1-\alpha)\, ln\left(\frac{p}{1-p}\right) \tag{3.26}$$

From equation (3.24) and (3.25) we can see that a finite velocity exists if $< s > < 1$, i.e., $\alpha > p$ or $< s^{-1} > < 1$, i.e., $\alpha < 1-p$. So the region we want to study is $1-p < \alpha < p$. Let us come back to formula (3.19). If $< lns > < 0$ (here it means that $\alpha > \frac{1}{2}$ from formula (3.26)), we can neglect the product in the denominator. Then by regrouping terms in (3.19), one can write $< v^{-1} >$ as

$$v^{-1} = 1 + 2\sum_{n=1}^{N-1} S_n + S_N \tag{3.27}$$

where $S_n$ (capital S,not $s_n$) is defined by

$$S_n = \frac{1}{N}\sum_{i=1}^{N}\prod_{j=1}^{n} s_{i+j} \tag{3.28}$$

In the limit $N \to \infty$, if n remains finite, $S_n \to < s >^n$ and so $S_n$ increases with n. On the other hand, $S_N = \prod_{j=1}^{N} s_j$ vanishes with probability

1. Therefore, there are certainly in the sum (3.27) terms between $n = 1$ and $n = N$ which are maximum and give the dominant contribution to $v^{-1}$ in the limit $N \to \infty$. $S_n$ is a sum of N terms and one could be tempted to use the central-limit theorem. This would be wrong because for most values of n, the number of terms in the sum (3.28) is too small to give the average $< s >^n$. Therefore, with probability 1, $S_n$ is not equal to $< S_n >$. The main idea used in the following is that the most probable value of the quantity $S_n$ can be very different from its average $< S_n >$. We denote the term in the summation in (3.28) as $I_{nm} = \frac{1}{N} \prod_{j=1}^{n} S_{i+j}$. Among the n terms in $I_{nm}$, there are m times $s = \frac{p}{1-p}$ with probability $\alpha$ and $(n-m)$ times $s = \frac{1-p}{p}$ with probability $(1-\alpha)$. Therefore we have

$$I_{nm} = \frac{1}{N}(\frac{1-p}{p})^{n-m}(\frac{p}{1-p})^{n} = \frac{1}{N}(\frac{1-p}{p})^{n-2m} \tag{3.29}$$

We define $\Omega(m)$ as the number of terms in the sum $S_n$ which are equal to $I_{nm}$ . The average $\Omega(m)$ is

$$< \Omega(m) >= NC_n^m \alpha^{(n-m)}(1-\alpha)^m. \tag{3.30}$$

For large n, we see that, depending on m, $\Omega(m)$ can be either much bigger than 1 or much smaller than 1. The critical values $m_{min}$ and $m_{max}$ can be estimated by requiring that $\Omega(m) \approx 1$. If $m_{min} < m < m_{max}$, then $\Omega(m) \gg 1$; therefore with probability 1, $\Omega(m) =< \Omega(m) >$. This is due to the fact that the fluctuations of $\Omega(m)$ are of order $< \Omega(m) >^{\frac{1}{2}}$ only. On the other hand, if $m < m_{min}$ or $m > m_{max}$, $< \Omega(m)$ is small ($\ll 1$) and then $\Omega(m) = 0$ with probability 1. For large n, the values $m_{min}$ and $m_{max}$ are the two solutions of

$$lnN + mln(\frac{n(1-\alpha)}{m}) + (n-m)ln(\frac{n\alpha}{n-m}) \tag{3.31}$$

Since $p > \frac{1}{2}$, $\frac{1-p}{p}$ must be less than 1. Therefore $(\frac{1-p}{p})^{n-2m}$ increases with increasing m and give the dominant contribution when $m \approx m_{max}$. It follows that $S_n$ is given with probability 1 by

$$S_n = \sum_{m=m_{min}}^{m=m_{max}} C_n^m \alpha^{n-m}(1-\alpha)^m(\frac{1-p}{p})^{n-2m} \tag{3.32}$$

$$\tag{3.33}$$

$$\approx C_n^{m_{max}} \alpha^{n-m_{max}} (1-\alpha)^{m_{max}} (\frac{1-p}{p})^{n-2m_{max}} \tag{3.34}$$

$$\tag{3.35}$$

$$= \frac{1}{N} (\frac{p}{1-p})^{2m_{max}-n} \tag{3.36}$$

Now we try to solve $m_{max}$. Let

$$u(n) = 2m_{max} - n \tag{3.37}$$

then

$$m_{max} = (u+n)/2 \tag{3.38}$$

The maximum of $u(n)$ gives the dominant $S_n$. Replacing m in (3.31) by $(u+n)/2$, performing derivative with regard to n and letting $\partial u/\partial n = 0$, we have found $u = n(2\alpha - 1)$, and therefore $m_{max} = n\alpha$. With this evaluation of $S_n$, we can come back to the calculation of $v^{-1}$ by looking for the value $\overline{n}$ which is dominant in sum (3.27). One finds by replacing m by $m_{max} = n\alpha$ in equation (3.31)

$$\overline{n} = \frac{lnN}{(2\alpha-1) ln(\frac{\alpha}{1-\alpha})} \tag{3.39}$$

and

$$v^{-1} \sim S_{\overline{n}} \sim N^{z-1} \tag{3.40}$$

with

$$z = \frac{ln\frac{p}{1-p}}{ln\frac{\alpha}{1-\alpha}}. \tag{3.41}$$

To obtain the most probable value of $S_n$, we have completely ignored the correlations between the terms in the sums (3.27) and (3.28). A calculation taking these correlations into account would be more complicated, but the result would be the same apart from some factors $lnN$ in equation (3.40). We have chosen $< \Omega(m) > \sim 1$ to determine $m_{min}$ and $m_{max}$. If we had replaced 1 by any other finite constant, the result would have been the same. The fact

that sum (3.27) was replaced by $S_{\overline{n}}$ can be justified by looking at the behavior of $S_n$ around $\overline{n}$. One can estimate that there are $\sim lnN$ terms in (3.27) which are comparable to $S_n$ around $\overline{n}$. Therefore (3.40) is again valid apart from factors of order $lnN$

We have shown that the inverse velocity $v^{-1} \sim N^{z-1}$ for a chain of N sites with periodic boundary conditions when $\frac{1}{2} < \alpha < p$. This means that to cover a distance $h \sim N$ the particle needs a time $t = v^{-1}N \sim N^z$. It is equivalent to say that the distance h covered by the particle during the time t behaves like $h \sim t^{\nu_1}$ with $\nu_1 = 1/z$. It is interesting to notice that in (3.27), all the terms are positive and therefore the sign of $v^{-1}$ is positive. This means that when $\alpha > \frac{1}{2}$, there is a systematic displacement to the right. If $\alpha < \frac{1}{2}$, $v^{-1}$ becomes negative because the dominant term in the denominator of (3.19) is the product(see Fig.3.1).

In the limit $\alpha \to \frac{1}{2}$, $\nu_1$ vanishes and we find that h increases less rapidly than any power law. This is in good agreement with $h \sim ln^2 t$ found by Sinai. In the limit where $< s > \to 1$ (here $\alpha \sim p$) $\nu_1$ tends to 1. We recover that in this limit, the distance starts to be promotional to the time.

In conclusion, it is found that a 1D lattice with random hopping rates behaves differently from the one with regular hopping rates. The particle of the former system does not always have a steady-state velocity. When the hopping rates satisfy the condition $\left\langle \frac{q_n}{p_n} \right\rangle < 1$ or $\left\langle \frac{p_n}{q_n} \right\rangle < 1$, one finds the velocity

$$v \simeq \left\langle \frac{1}{p_n} \right\rangle^{-1} \left(1 - \left\langle \frac{q_n}{p_n} \right\rangle\right) \quad \text{if} \quad \left\langle \frac{q_n}{p_n} \right\rangle < 1$$

$$v \simeq \left\langle \frac{1}{q_n} \right\rangle^{-1} \left(1 - \left\langle \frac{p_n}{q_n} \right\rangle\right) \quad \text{if} \quad \left\langle \frac{q_n}{p_n} \right\rangle < 1 \tag{3.42}$$

from equations (3.12), (3.21) and (3.22). However when $\left\langle \frac{q_n}{p_n} \right\rangle > 1$ and $\left\langle \frac{p_n}{q_n} \right\rangle > 1$, the displacement of the particle follows a power law of time as: $< h(t) > \simeq t^{\nu_1}$. Then[40, 42, 45, 49] the exponent $\nu_1$ is the nonezero solution of

$$\left\langle \left( \frac{1 - p_n}{p_n} \right)^{\nu_1} \right\rangle = 1. \tag{3.43}$$

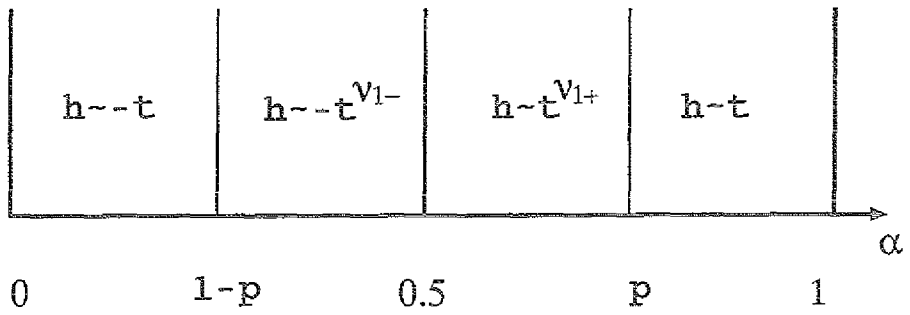


Figure 3.1: Phase diagram for the distribution $\rho(p_n) = \alpha\,\delta(p_n - p) + (1-\alpha)\delta(p_n - (1-p))$. If $\alpha > \frac{1}{2}$, there is a systematic displacement to the right. The velocity is finite only if $\alpha > p$. For $\frac{1}{2} < \alpha < p$, the displacement h covered during the time t is given by $h \sim t^{\nu_{1+}}$ with $\nu_{1+} = ln\frac{\alpha}{1-\alpha}/ln\frac{p}{1-p}$, The situation for $\alpha < \frac{1}{2}$ is symmetric.

## 3.2 One-Dimensional Lattice Model

The formation of interfaces and surfaces is influenced by a large number of factors, and it is almost impossible to distinguish all of them. Nevertheless, a scientist always hopes that there is a small number of basic laws determining the morphology and the dynamics of growth. The action of these basic laws can be described in microscopic detail through discrete growth model which mimics the essential physics but bypass some of the less essential details. The following one-dimensional model of a binary alloy generates a nonequilibrium interface that exemplifies many of the essential properties of a growth process.

The microscopic model was originally proposed by Temkin [32, 33, 35] as follows: On a one-dimensional lattice chain two species of atoms, A and B, are distributed uniformly with the concentration $c$ of B species. This atomic chain is separated by a solid-liquid interface into two parts: the liquid in the right and the solid in the left, for example. The atomic configuration is frozen and atoms cannot move, but can only change their state between the solid and the liquid. The solidification and melting frequency for an A atom (or probability of phase-change per time-unit) are denoted by $\omega_{+A}$ and $\omega_{-A}$, respectively. $\omega_{+B}$ and $\omega_{-B}$ denote the corresponding frequencies for a B atom. The interface position $h$ is defined then as the lattice site of the rightmost solid

atom which can be either a species of A or B. Here we assume that only the two atoms adjoining the interface are allowed to chang their states. If the solid atom on the left side of the interface melts the interface-height decreases by one: $h \to h-1$. If the liquid atom solidifies, the interface advances by one: $h \to h+1$. The interface motion is assumed to take place stochastically following the master equation

$$\begin{aligned}\frac{\partial P(h,t)}{\partial t} = \quad & W(h+1 \to h)P(h+1,t) \\ & -[W(h \to h+1)+W(h \to h-1)]P(h,t) \\ & +W(h-1 \to h)P(h-1,t),\end{aligned} \tag{3.44}$$

where $P(h,t)$ is the probability that the interface is at a site $h$ at time $t$. The transition probabilities $W$ depend on the atomic configurations around the interface. We consider a model where the transition probability $W$ depends only locally on the type of particle which changes its state during melting or solidification. If the solid site $h$ is occupied by an X (= A or B) atom and the liquid site $h+1$ by a Y (= A or B) atom, the transition probability of the interface advancement is given as

$$W(h \to h+1) = \omega_{+Y}, \tag{3.45}$$

and that of the interface retardation as

$$W(h \to h-1) = \omega_{-X}. \tag{3.46}$$

The detailed balance condition requires that the kinetic ratio $\omega_{-X}/\omega_{+X}$ should be equal to $\exp(-\Delta\mu_X/T)$ determined by the thermodynamics:

$$\frac{\omega_{-X}}{\omega_{+X}} = e^{-\Delta\mu_X/T} \tag{3.47}$$

where $\Delta\mu_X$ is the chemical potential difference of atom X(=A or B) between liquid and solid state. At a temperature T near the equilibrium melting temperature $T_X$ of a X atom the chemical potential difference is approximately written as

$$\Delta\mu_X = \frac{L_X}{T_X}(T_X - T) \tag{3.48}$$

with the specific latent heat $L_X$. For the mixture of A and B atoms an ideal solution without mixing energy but with a mixing entropy is assumed. Then the equilibrium phase diagram is obtained with the solidus line $C_s(T)$, the liquidus line $C_l(T)$ and the concentration $C_0(T)$ at which the free energy per liquid atom is equal to the free energy per solid atom as

$$\begin{aligned} C_s(T) &= \frac{1-e^{-\Delta\mu_A/T}}{e^{-\Delta\mu_B/T}-e^{-\Delta\mu_A/T}}, \\ C_l(T) &= \frac{(1-e^{-\Delta\mu_A/T})e^{-\Delta\mu_B/T}}{e^{-\Delta\mu_B/T}-e^{-\Delta\mu_A/T}}, \\ C_0(T) &= \frac{\Delta\mu_A}{\Delta\mu_A-\Delta\mu_B}. \end{aligned} \tag{3.49}$$

The phase diagram with solidus line $C_s(T)$ and the liquidus line $C_l(T)$ as well as the concentration $C_0(T)$ is depicted in Fig.1.1 with the following set of parameters: $T_A = 0.9$, $T_B = 0.1$, $L_A/T_A = L_B/T_B = 1$.

In the diffusionless crystal growth considered here, the solidification proceeds via the propagation of a single solid-liquid interface over a frozen configuration of A and B atoms. Although each atom has fixed probability to solidify or melt, the solidification and melting take place only at the interface position. In other words, we exclude the possibility of nucleation of the energetically favorable phase in positions away from the solid-liquid-interface.

The above 1D growth model can be mapped onto the 1D hopping model. The interface located between the solid atom $X_h$ (=A or B) and the liquid atom $Y_{h+1}$ (=A or B) in the growth model can be considered as a "particle" in the hopping model which sits at the site h at a time $t$ (see Fig. 3.2). At the time $t+1$, the interface jumps either one lattice unit forward to the site $h+1$ by solidifying the liquid atom $Y_{h+1}$ with a probability

$$p_h = \frac{\omega_{+Y_{h+1}}}{\omega_{+Y_{h+1}} + \omega_{-X_h}} \tag{3.50}$$

or one lattice unit backward to the site $h-1$ by melting the solid atom $X_h$ with a probability

$$q_h = \frac{\omega_{-X_h}}{\omega_{+Y_{h+1}} + \omega_{-X_h}}. \tag{3.51}$$

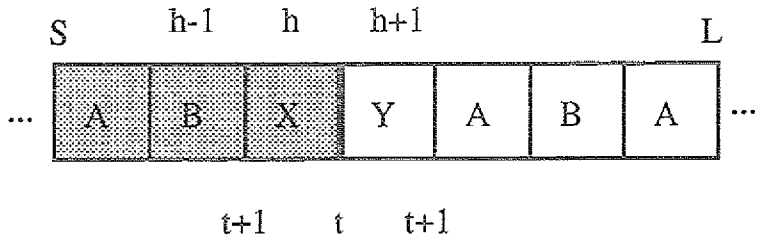


Figure 3.2: Mapping of the 1D model of a binary alloy onto the 1D hopping model. The hopping probabilities of a particle, $p_n$ and $q_n$, are related to the transition frequencies, $\omega_{+Y_{h+1}}$ and $\omega_{-X_h}$, of the liquid atom Y and the solid atom X at the interface by (3.50) and (3.51).

From the results of the previous section, it is possible that the interface has a steady-state velocity for some distribution of A and B atoms, but it vanishes for other distributions.

The theoretical analysis by Temkin[32, 33, 35] has revealed that for our lattice model the interface has a steady-state motion in one-phase regions, but in the two-phase region the average velocity of the interface advancement vanishes with time. In a one phase region the mean displacement $\langle h(t)\rangle$ of the interface is linear in time $t$ as

$$\begin{aligned} \langle h(t)\rangle &= v_+ t \qquad (c < Cs), \\ \langle h(t)\rangle &= -v_- t \qquad (c > C_l), \end{aligned} \tag{3.52}$$

with the velocities

$$\begin{aligned} v_+ &= (1 - \langle\frac{\omega_-}{\omega_+}\rangle)\Big/\langle\frac{1}{\omega_+}\rangle \\ &= \left\{1 - \left[(1-c)\frac{\omega_{-A}}{\omega_{+A}} + c\frac{\omega_{-B}}{\omega_{+B}}\right]\right\}\left[\frac{1-c}{\omega_{+A}} + \frac{c}{\omega_{+B}}\right]^{-1}, \\ v_- &= (1 - \langle\frac{\omega_+}{\omega_-}\rangle)\Big/\langle\frac{1}{\omega_-}\rangle \\ &= \left\{1 - \left[(1-c)\frac{\omega_{+A}}{\omega_{-A}} + c\frac{\omega_{+B}}{\omega_{-B}}\right]\right\}\left[\frac{1-c}{\omega_{+A}} + \frac{c}{\omega_{+B}}\right]^{-1}. \end{aligned} \tag{3.53}$$

Here $\omega_+(=\omega_{+A}$ or $\omega_{+B})$ refers to the solidification frequency and $\omega_-(=\omega_{-A}$ or $\omega_{-B})$ to the melting frequency. The angular bracket means the ensemble average of the quantity within the brackets.

The fact that at $C_s$ and $C_l$ the average $\langle\omega_-/\omega_+\rangle$ and $\langle\omega_+/\omega_-\rangle$ are equal to unity and therefore the velocities $v_+$ and $v_-$ vanish, respectively reveals that the phase boundaries $C_s$ and $C_l$ serve as the critical concentrations where the system undergoes a phase transition between the pinning and depinning states. In the two phase coexistence region $C_s < c < C_l$, the mean displacement is no longer linear in time. For example, the position $\langle h(t)\rangle$ of the solidification front instead advances as a power law $\langle h(t)\rangle \sim t^{\nu_{1+}}$ in the concentration range $C_s < c < C_0$ and $\langle h(t)\rangle \sim -t^{\nu_{1-}}$ in the concentration range $C_0 < c < C_l$ with the exponent $\nu_{1+}$ ($\nu_{1-}$) being less than unity and decreasing on leaving the phase boundary $C_s$ ($C_l$). So the steady-state velocity vanishes in the two-phase region. According to Derrida's general treatment of the 1D hopping model, the exponent are determined from the relation

$$\langle(\frac{\omega_-}{\omega_+})^{\nu_{1+}}\rangle = 1, \quad \langle(\frac{\omega_+}{\omega_-})^{\nu_{1-}}\rangle = 1. \tag{3.54}$$

In the present case, this equation can be written explicitly as

$$(1-c)(\frac{\omega_{-A}}{\omega_{+A}})^{\nu_{1+}} + c(\frac{\omega_{-B}}{\omega_{+B}})^{\nu_{1+}} = 1,$$

$$(1-c)(\frac{\omega_{+A}}{\omega_{-A}})^{\nu_{1-}} + c(\frac{\omega_{+B}}{\omega_{-B}})^{\nu_{1-}} = 1. \tag{3.55}$$

At $c = C_0$,

$$\langle ln(\frac{\omega_-}{\omega_+})\rangle = \langle ln(\frac{\omega_+}{\omega_-})\rangle = 0. \tag{3.56}$$

and $\nu_{1+} = \nu_{1-} = 0$.

In addition, Derrida[42] also obtained the expression of the diffusion constant

$$\begin{aligned} D &= \frac{1}{2}\lim_{t\to\infty}\frac{d}{dt}\{< [h(t) - < h(t) >]^2 >\} \\ &= \frac{1}{2}\lim_{t\to\infty}\frac{d}{dt}\sigma^2(t) \end{aligned}$$

$$= \frac{1-\left\langle\frac{\omega_-}{\omega_+}\right\rangle^2}{1-\left\langle\left(\frac{\omega_-}{\omega_+}\right)^2\right\rangle}\left\langle\frac{1}{\omega_+}\right\rangle^{-3}\left[\left\langle\frac{1}{\omega_+}\right\rangle\left\langle\frac{\omega_-}{\omega_+^2}\right\rangle+\frac{1}{2}\left\langle\frac{1}{\omega_+^2}\right\rangle\left(1-\left\langle\frac{\omega_-}{\omega_+}\right\rangle\right)\right], \tag{3.57}$$

for the region $<(\omega_-/\omega_+)^2>\!<1$. When c is larger than

$$c_2 = \frac{1-(\frac{\omega_{-A}}{\omega_{+A}})^2}{(\frac{\omega_{-B}}{\omega_{+B}})^2-(\frac{\omega_{-A}}{\omega_{+A}})^2}, \tag{3.58}$$

D is expected to diverge even in the one-phase region.

## 3.3 Simulation Results

In order to understand the fact that the mean displacement and the variance becomes anomalous at different concentrations, Monte Carlo simulations have been performed. The parameters are chosen as : $T_A = 0.9$, $T_B = 0.1$, $T = 0.5$, $L_A/T_A = L_B/T_B = 1$ From the phase diagram we can see that the equilibrium concentrations are $C_s = 0.310$ and $C_l = 0.690$. Parameters for the interface dynamics are set as $\omega_{+A} = \omega_{+B} = 1$, $\omega_{-A} = 1/\omega_{-B} = 0.4493$. The results presented here was obtained by Saito[34] and we repeated all of them. The random walk of the interface position has been simulated up to the time $10^5$. Physical quantities have been averaged over $10^5$ chains. The mean displacement of the interface $\langle h(t)\rangle$ at various concentrations of B atoms are plotted in Fig.3.3(a). The time dependence is fitted to a single power law of the time as $\langle h(t)\rangle = a_1 t^{\nu_1} + b_1$, and the obtained dynamic exponent $\nu_1$ is plotted in Fig.3.5. Up to the equilibrium concentration $C_s = 0.31$, the exponent remains about unity, and afterwards it starts to decrease on increasing c to the point $C_0 = 0.5$. By forcing a linear fit of $\langle h(t)\rangle$ to the time t, the velocity $v$ of the interface is obtained. It varies as is shown in Fig.3.4, and agrees quite

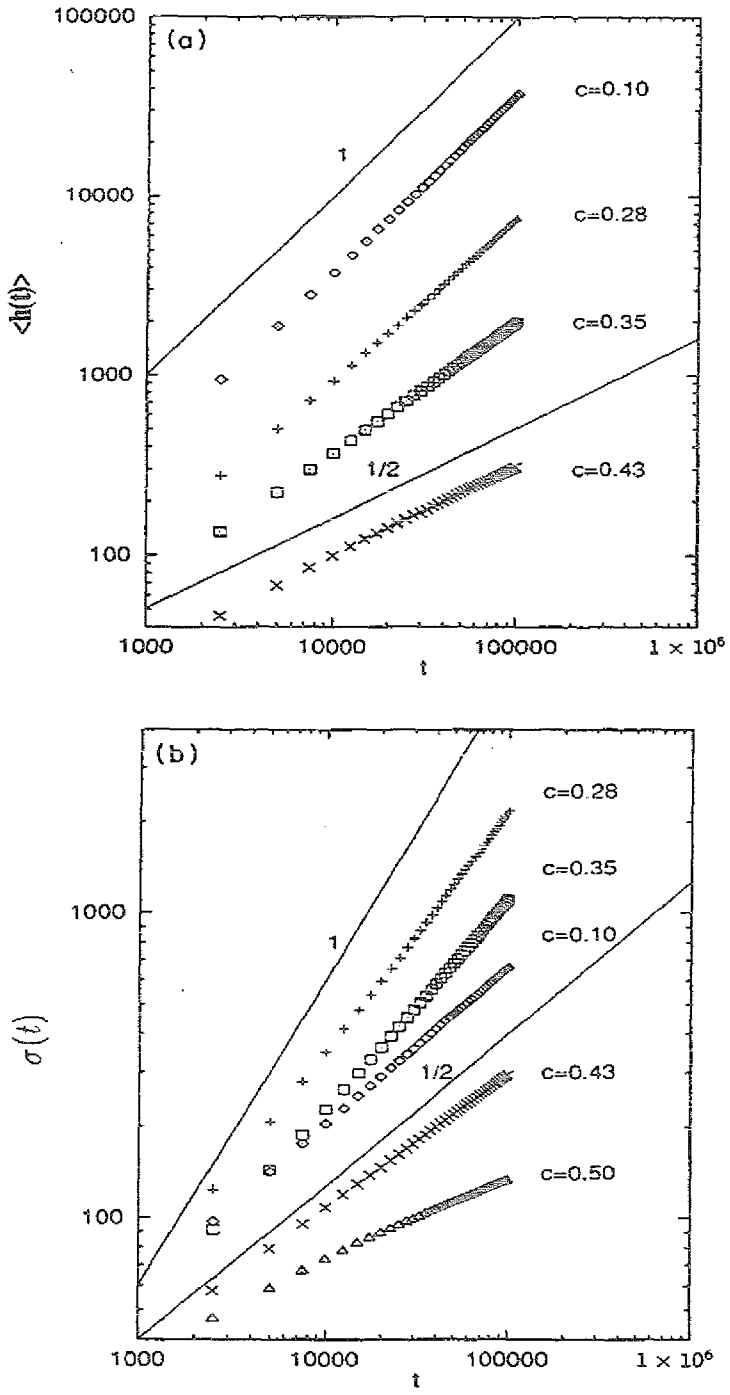


Figure 3.3: Time variation of (a) the mean displacement $\langle h(t) \rangle$ and (b) the variance $\sigma(t)$ for various concentrations c of B atoms in the double logarithmic way at $T = 0.5$. Two straight lines represent the asymptotic behavior with exponent 1 and 1/2.

well with the theoretical expectation Eq.(3.53) in the one phase region, which is shown by a solid line. In the two-phase region, $C_s < c < C_l$, $\nu_1$ depends on the concentration and varies between unity and zero. The variation of $\nu_1$ agrees well with the theoretical expectation (3.55), which can be simplified in the present case as

$$\nu_1 = 1.25\, ln\left(\frac{1-c}{c}\right), \tag{3.59}$$

and is shown by a solid line in Fig.3.5.

The time evolution of the variance $\sigma(t) = \sqrt{< [h(t) - < h(t) >]^2 >}$ is plotted in Fig.3.3(b). It is also fitted to a single power law, $\sigma(t) = a_2 t^{\nu_2} + b_2$, and the exponent $\nu_2$ is shown in Fig.3.5. $\nu_2$ starts from 1/2 of the normal Brownian motion for a pure system, $c = 0$, up to about $c_2 = 0.168$ given by Eq.(3.58), and increases to 1 near $C_s$. From $C_s$ on, $\nu_2$ decreases similarly with the velocity exponent $\nu_1$.

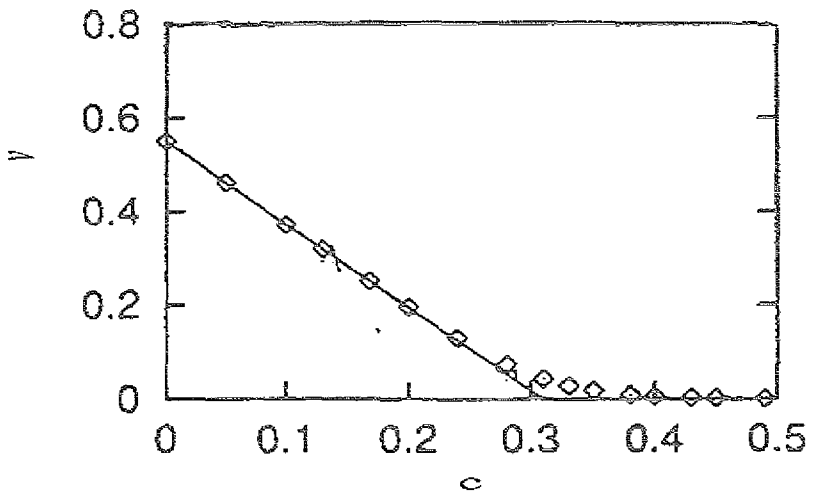


Figure 3.4: The stead-state velocity $v$ versus concentration c. The solid line represents the theoretical expectations from Eq.(3.53) and dots represent the MC results.

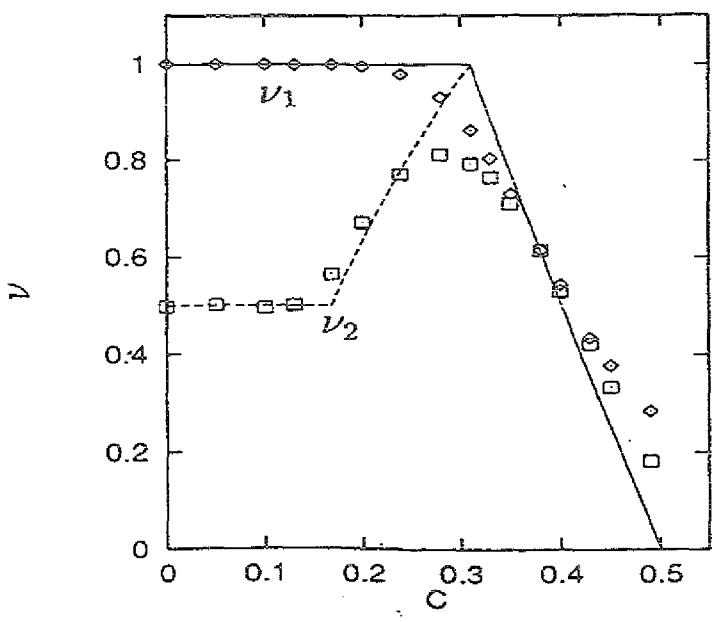


Figure 3.5: Exponent $\nu_1$ of the mean displacement, $< h(t) > \sim t^{\nu_1}$, and exponent $\nu_2$ of the variance, $\sigma(t) \sim t^{\nu_2}$, at various concentrations of B atoms. The solid-liquid phase boundary is at $C_s = 0.31$, and the anomaly in $\sigma$ is at $c_2 = 0.168$. The solid line represents the theoretical expectations from Eq.(3.55) and dots represent MC simulation results.

# Chapter 4

# Two-Dimensional Model of Binary Alloy

In this chapter the 1D diffusionless binary alloy model will be extended into 2D system and the model will be also mapped onto the Random Field Ising model.

## 4.1 Thermodynamics and Kinetics of the Alloy Model

We consider a simple square lattice which is randomly occupied by A and B atoms and decomposed into two parts by a 1D solid-liquid interface, liquid above solid, for example. The solidification or melting takes place only at the interface: Only those atoms which have both solid and liquid nearest neighbors have the possibility to transform to the other phase. Atoms are not allowed to change their positions, and therefore the atomic configuration is quenched. For simplicity we assume that the cohesive forces act only between nearest neighboring atoms of the same phase but they do not depend on the type of atoms:

$$\epsilon^{\beta}_{AA} = \epsilon^{\beta}_{AB} = \epsilon^{\beta}_{BB} = \epsilon_{\beta} \qquad (\beta = s, l). \tag{4.1}$$

Here the superscripts $s$ and $l$ refer to solid and liquid state, respectively. Since the mixing energy

$$\epsilon^{\beta}_{AB} - \frac{\epsilon^{\beta}_{AA} + \epsilon^{\beta}_{BB}}{2} \tag{4.2}$$

is zero both phases are ideal solutions. The interface thus corresponds to the place where the atomic cohesion is broken and each broken bond costs interface energy. We study the effect of the interface energy on the dynamics of the alloy solidification.

The phase transformation is assumed to take place stochastically at the interface. The phase change of an atom is associated with the breaking of cohesion of nearest neighboring atoms in the same phase which costs energy. Fig.4.1 highlights the possible configures of the interface and transitions of atoms at successive time intervals, so that the growth process can be followed qualitatively. Depending on the process (freezing or melting) and the number $j(= 1 \sim 3)$ of nearest neighboring atoms in the same phase, there are 12 transition frequencies: six solidification frequencies denoted as $\omega_{+X}(j)$ and six melting frequencies denoted by $\omega_{-X}(j)$ with X referring to A or B atom. In Fig.4.1(a), the liquid atom X has one nearest liquid neighbor, so it transforms into solid state with the frequency $\omega_{+X}(1)$. In Fig.4.1(c), the liquid atom X has two nearest liquid neighbors, one is above and the other is at the right, so it transforms into solid state with the frequency $\omega_{+X}(2)$ (or $\omega_{+X}$). Fig.4.1(e) shows a liquid atom surrounded by three nearest liquid neighbors which can transform into solid state with the frequency $\omega_{+X}(3)$. Fig.4.1(b),(d) and (f) represent the cases where a solid atom surrounded by one, two and three solid neighbors transforms into liquid state with the frequencies $\omega_{-X}(1)$, $\omega_{-X}(2)$ (or $\omega_{-X}$) and $\omega_{-X}(3)$, respectively. All these frequencies should satisfy the detailed balance condition to ensure the equilibrium phase diagram as

$$\begin{aligned} \omega_{+X}(j) &= \omega_{+X} \exp[-(j-2)\epsilon_l/T], \\ \omega_{-X}(j) &= \omega_{-X} \exp[-(j-2)\epsilon_s/T]. \end{aligned} \tag{4.3}$$

The transition frequencies $\omega_{\pm X}$ of component X at the kink position $(j = 2)$ are related to the chemical potential difference $\Delta\mu_X$ between liquid and solid phases as

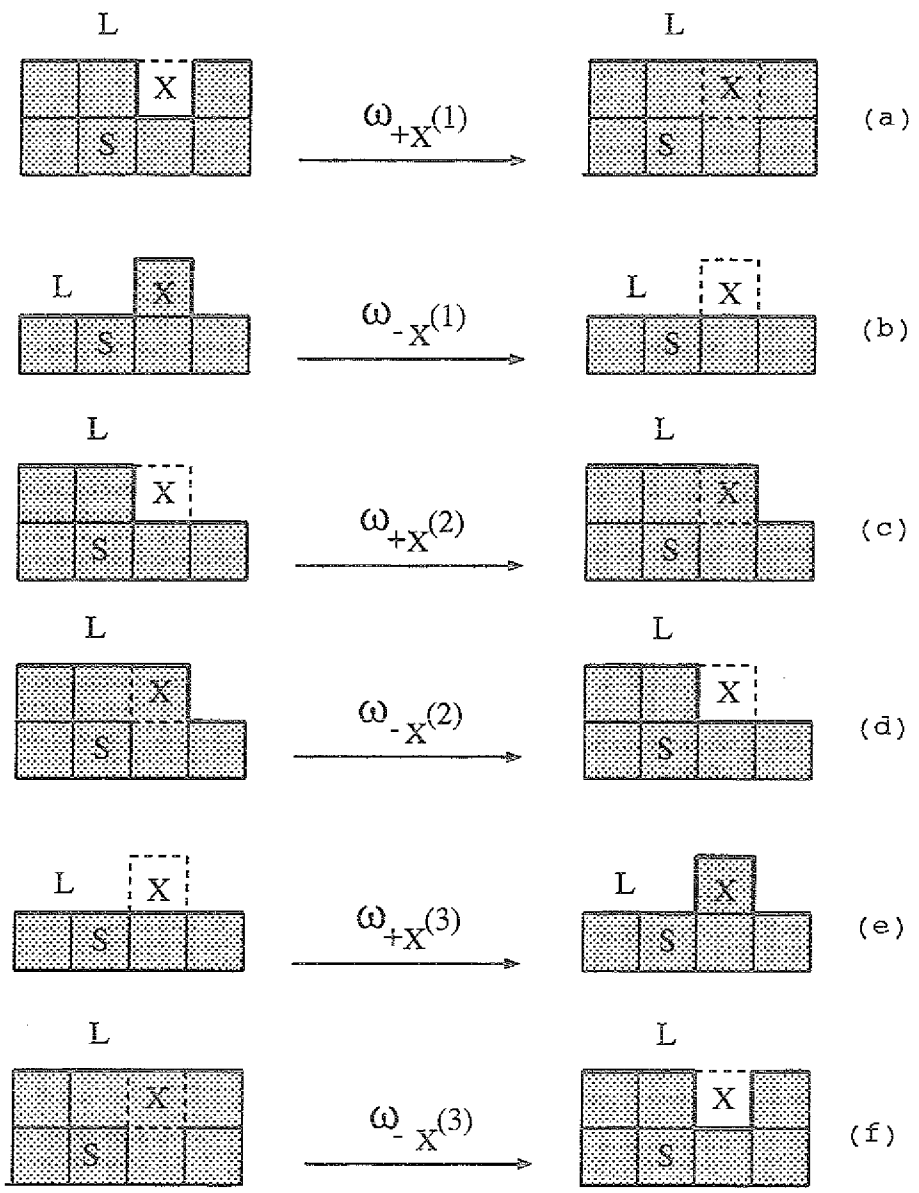


Figure 4.1: The two-dimensional solidification model illustrates three solidification and melting possibilities. The letter X represents A or B atoms. Doted sites are the solid phase denoted by S and empty is the liquid phase denoted by S. The interface is represented by the bold solid lines. Shown is the case N=4, where N is the number of columns or the system size.

$$\frac{\omega_{+X}}{\omega_{-X}} = \exp(\frac{\Delta\mu_X}{T}) \tag{4.4}$$

with

$$\Delta\mu_X = \mu_X^l - \mu_X^s \cong L_X \frac{T_X - T}{T_X}. \tag{4.5}$$

Here $T_X$ and $L_X$ are the melting temperature and the latent heat for pure $X(= A, B)$ atoms. The solidus $C_s(T)$ and the liquidus lines $C_l(T)$ obey the detailed balance principle in the form

$$\begin{aligned} (1 - C_s)\omega_{-A} &= (1 - C_l)\omega_{+A}, \\ C_s\omega_{-B} &= C_l\omega_{+B}, \end{aligned} \tag{4.6}$$

and they are obtained as

$$\begin{aligned} C_s(T) &= \frac{1 - e^{-\Delta\mu_A/T}}{e^{-\Delta\mu_B/T} - e^{-\Delta\mu_A/T}}, \\ C_l(T) &= \frac{(1 - e^{-\Delta\mu_A/T})e^{-\Delta\mu_B/T}}{e^{-\Delta\mu_B/T} - e^{-\Delta\mu_A/T}}. \end{aligned} \tag{4.7}$$

At the equal-free energy line $C_0$, the free energy $\phi_s$ per solid atom is equal to the free energy $\phi_l$ per liquid atom;

$$\begin{aligned} &\phi_s \equiv (1 - C_0)\mu_A^s(T) + C_0\mu_B^s(T) \\ = \ &\phi_l \equiv (1 - C_0)\mu_A^l(T) + C_0\mu_B^l(T), \end{aligned} \tag{4.8}$$

or

$$(1 - C_0)\Delta\mu_A + C_0\Delta\mu_B = 0. \tag{4.9}$$

From equations (4.4) and (4.9), we obtain $C_0$ as

$$C_0(T) = \frac{\Delta\mu_A}{\Delta\mu_A - \Delta\mu_B}. \tag{4.10}$$

Equation (4.9) is equivalent to Eq.(3.56) and we shall see later that the interface velocity of a large 2D system vanishes at this concentration $C_0$.

The phase diagram with coexistence lines $C_s(T)$ and $C_l(T)$ as well as $C_0(T)$ is depicted in Fig.1.1 with the following set of parameters: $T_A = 0.9$,

$T_B = 0.1$, $L_A/T_A = L_B/T_B = 1$. It is seen that the solidification or melting of the system depends not only upon the cooling condition but also on the alloy composition. At a fixed temperature $T$ between $T_A$ and $T_B$, the system remains in the solid state as long as the concentration $c$ is smaller than $C_s(T)$. When c comes to lie between $C_s(T)$ and $C_l(T)$, the solid and liquid phase coexist, but when c becomes larger than $C_l(T)$ the system melts completely.

## 4.2 Random Field Ising Model

The above 2D growth model can be mapped onto the random field Ising (RFI) model with external field which depends explicitly on the temperature. The RFI model is defined by spins with two possible values $s_i = \pm 1$ that are placed on site i of a lattice. Its Hamiltonian is given by,

$$\mathcal{H} \equiv -J \sum_{<i,j>} s_i s_j - \sum_i (f_i + F)\, s_i. \tag{4.11}$$

Here $s_i = +1$ represents the solid state, $s_i = -1$ represents the liquid state, $\sum_{<i,j>}$ denotes the summation over all nearest-neighbor pairs $< i, j >$, $\sum_i$ is the sum over all spins in the system. J is the exchange energy between the ferromagnetically-coupled nearest-neighbor spins and determined by the bond energies as

$$J = \frac{1}{4}(\epsilon_s + \epsilon_l). \tag{4.12}$$

F is the external uniform driving force which is proportional to the concentration difference $(C_0 - c)$. $f_i$ is the quenched local field caused by the concentration fluctuation from the average concentration $c$ of the B-atoms. Since each lattice site $i$ is occupied by either A atom with the probability $(1 - c)$ (the average concentration of A atoms) or B atom with the probability $c$ (the average concentration of B atoms), the probability distribution of the quantity $(f_i + F)$ is

$$\rho(f_i + F) = (1 - c)\delta(f_i + F - f_A) + c\,\delta(f_i + F - f_B). \tag{4.13}$$

Here $f_A$ and $f_B$ depend on the temperature and the latent heat and are defined as,

$$\begin{aligned} f_A(T) &= -\frac{1}{2}\Delta\mu_A = -\frac{1}{2}L_A(1-\frac{T}{T_A}), \\ f_B(T) &= -\frac{1}{2}\Delta\mu_B = -\frac{1}{2}L_B(1-\frac{T}{T_B}). \end{aligned} \tag{4.14}$$

In addition, the driving force $F(T)$, or the average free energy gain by solidifying one atom is

$$F(T) = (1-c)\, f_A(T) + c\, f_B(T), \tag{4.15}$$

here c is the average concentration of B atoms. Accordingly, the randomly quenched field $f_i$ has a zero average value

$$< f_i >= 0. \tag{4.16}$$

Here the angular bracket represents the average over the different realization of randomness. $f_i$ then is assumed uncorrelated for different sites.

# Chapter 5

# Diffusionless Solidification at Large Bond Energy

In the previous chapter, we have introduced a 2D model for difussionless solidification of a disordered binary alloy. Comparing to the 1D model, two more parameters are introduced, the system size and the bond energy. This makes the system extremely complicated: effects of all parameters (concentration, bond energy and system size) on the motion of the interface interplay. Due to the mathematical difficulty, we were not able to solve the model exactly for arbitrary parameters. However, in this chapter, we will present the exact solution of the diffusionless solidification at large bond energy limit where the interface is found to have the same asymptotics as its 1D counterpart in many respects. It means that the interface moves steadily in the one-phase region but the velocity vanishes in the two-phase region.

We consider the alloy solidification starting from a flat interface configuration. The solidification is initiated by the formation of a single nucleus or an island with two kinks on a flat one-dimensional interface. For infinitely large bonding energies, $\epsilon_s$ and $\epsilon_l$, transition frequencies of atoms differ orders as

$$\omega_{\pm X}(1) = \omega_{\pm X} e^{\epsilon_{l(s)}/T} \gg \omega_{\pm X} \gg \omega_{\pm X}(3) = \omega_{\pm X} e^{-\epsilon_{l(s)}/T}. \qquad (5.1)$$

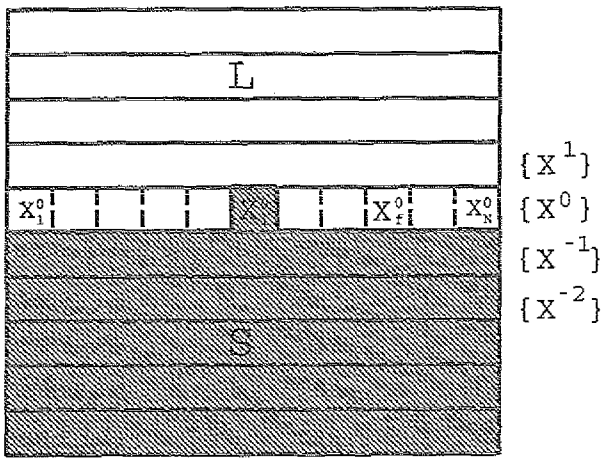


Figure 5.1: The layer-by-layer growth mechanism for large bond energy limit. $\{X^n\} = \{X_1^n, X_2^n \ldots X_N^n\}$ is the atom arrangement in the n-th layer respective to the interface with $n \geq 0$ in the liquid phase and $n < 0$ in the solid phase, respectively. $X_i^n$ can be either A or B atom.

So the comparatively small $\omega_{\pm X}(3)$ makes this nucleation process very slow compared to the lateral growth of the island with $\omega_{\pm X}(2)(= \omega_{\pm X})$ afterwards. The solidification proceeds layer-by-layer by the single-nucleation and growth mechanism and the probability of multi-layers and multi-nuclei processes is negligible small: Once a cluster appears, it soon spreads laterally until the whole layer is filled. If the bond energy $\epsilon_s$ is large the melting also proceeds by a layer-by-layer mechanism. In these cases the jump of a flat interface to the neighboring layer positions may be considered as a single "elementary" action. Then one may construct an effective 1D model where the "elementary" transition frequencies $\Omega_\pm$ of a "layer" jumping forward $(+)$ and backward $(-)$ play the same role as $\omega_\pm$ play in a real 1D system. In reality these "elementary" jumps consist of many atomic solidification-melting subprocesses. We can calculate the elementary frequencies $\Omega_\pm$ in terms of atomic frequencies $\omega_\pm$. From the analysis, we shall find the remarkable result that the exponent $\nu_1$ obeys the same equation (3.54) as in the 1D system. This result will be tested by the Monte Carlo simulation in the section 7.1.

First consider the situation when the layer has just been completed and the

flat interface is located between the solid layer with an atomic arrangement $\{X^{-1}\} = \{X_1^{-1}, X_2^{-1} \ldots X_N^{-1}\}$ and the liquid layer above with an arrangement $\{X^0\} = \{X_1^0, X_2^0 \ldots X_N^0\}$ as shown in Fig.5.1. Here $X_i^n$ denotes A or B atom with $n \geq 0$ in the liquid phase and $n < 0$ in the solid phase, respectively. The index $i$ $(= 1, 2...N)$ denotes the column-number in the square lattice. The solidification, for instance, starts from the nucleation at a site $i$ in the liquid layer. The solid nucleus grows to the right or to the left, but can also melt back. Finally the layer is completed by the solidification at the last site $f$. We call here the sequence of events starting from the site $i$ and ending at the site $f$ as a "trajectory" . After an average waiting time $\Upsilon$, the interface has moved one layer forward with a probability $P$ or one layer backward with a probability $Q$ where $P + Q = 1$ obviously. Then the transition frequencies of layer-jump are given by

$$\Omega_+ = P/\Upsilon \qquad \text{and} \qquad \Omega_- = Q/\Upsilon. \tag{5.2}$$

The forward transition probability $P$ obeys the following iterative equation

$$P = \sum_{i=1}^{N} p_i P_i + P \sum_{i=1}^{N} \left[ p_i(1 - P_i) + q_i(1 - Q_i) \right]. \tag{5.3}$$

Here

$$p_i = \frac{\omega_{+i}(3)}{\sum_{i=1}^{N} \omega_{+i}(3) + \sum_{j=1}^{N} \omega_{-j}(3)} \equiv \omega_{+i}(3)\tau \tag{5.4}$$

is the probability that a solid island first nucleates at the site $i$ on the initial flat interface $\{X^0\}$. Similarly

$$q_i = \omega_{-i}(3)\tau \tag{5.5}$$

gives the probability of the first melting event at the $i$th site in the solid layer $\{X^{-1}\}$. We introduced the abbreviated notation $\omega_{\pm i}$ for $\omega_{\pm X_i^{l(s)}}$. $\tau$ represents the mean waiting time before the first solid or liquid nucleus is created on the flat interface. In Eq.(5.3) $P_i$ represents the probability that the solid cluster which started from the site $i$ completely covers the interface without being molten back before finishing the coverage, so that the interface never comes

back to the initial flat configuration during the solidification process. Similarly $Q_i$ defines the probability that the liquid cluster started from the site $i$ completely melts the interface layer without being completely resolidified to the original interface configuration. Therefore the first term on the RHS of Eq.(5.3) represents the contribution from all the possible trajectories which never come back to the initial flat interface during solidification process. The second term gives the contribution from those trajectories which lead to the initial interface configuration during solidification. Those started by solidification but remelted have a probability $p_i(1-P_i)$ to return to the original interface configuration, and those started by melting and resolidified has a probability $q_i(1-Q_i)$. Afterwards the interface has the same probability $P$ to be solidified. Eq.(5.3) has a solution

$$P = \frac{\sum_{i=1}^{N} p_i P_i}{\sum_{i=1}^{N} [p_i P_i + q_i Q_i]}. \tag{5.6}$$

Obviously $Q = 1 - P$. In the same spirit we can derive the equation for the average waiting time $\Upsilon$:

$$\begin{aligned} \Upsilon &= \tau \sum_{i=1}^{N} [p_i P_i + q_i Q_i] + \\ &\quad (\tau + \Upsilon) \sum_{i=1}^{N} [p_i(1-P_i) + q_i(1-Q_i)]. \end{aligned} \tag{5.7}$$

Equation (5.7) is approximate because we take into account only a single nucleation and growth during the interface evolution. It has the solution

$$\Upsilon = \frac{\tau}{\sum_{i=1}^{N} [p_i P_i + q_i Q_i]}. \tag{5.8}$$

Now we obtain the transition frequencies:

$$\begin{aligned} \Omega_+ &= \frac{1}{\tau} \sum_{i=1}^{N} p_i P_i = \sum_{i=1}^{N} \omega_{+i}(3) P_i, \\ \Omega_- &= \sum_{i=1}^{N} \omega_{-i}(3) Q_i. \end{aligned} \tag{5.9}$$

The important feature of the obtained result, Eq.(5.9), is that in the used approximation the frequency of solidification, $\Omega_+$, depends only on the atomic configuration of the solidifying liquid-layer above the interface. Similarly the melting frequency $\Omega_-$ depends only on the atomic configuration of the melting solid-layer at the interface.

In terms of the introduced frequencies $\Omega_\pm$ we can write down some important characteristics using the known 1D results. The solidification velocity $v_+$ and the melting velocity $v_-$ are given as

$$\begin{aligned} v_+ &= +\left[1- < \frac{\Omega_-}{\Omega_+} >\right] / < \frac{1}{\Omega_+} >, \\ v_- &= -\left[1- < \frac{\Omega_+}{\Omega_-} >\right] / < \frac{1}{\Omega_-} > . \end{aligned} \tag{5.10}$$

The frequencies $\Omega_+$ and $\Omega_-$ depend on the sequence $\{X_1 X_2 \ldots X_N\}(X_i$ =A or B) of A and B atoms in the solidification or melting layer and $< \ldots >$ means the average over all possible configurations in the layer, for example,

$$\langle \frac{\Omega_-}{\Omega_+} \rangle = \sum_{X_1=A,B} \cdots \sum_{X_N=A,B} \frac{\Omega_-(X_1 \ldots X_N)}{\Omega_+(X_1 \ldots X_N)} \prod_{i=1}^{N} c_i, \tag{5.11}$$

where $\prod_{i=1}^{N} c_i$ (with $c_i = c$ for $X_i = B$ and $c_i = 1 - c$ for $X_i = A$) is the probability of finding the configuration $\{X_i X_2 \ldots X_N\}$. These steady-state velocities, $v_+$ and $v_-$, vanish under the following conditions

$$\begin{aligned} < \Omega_-/\Omega_+ > &= 1, \\ < \Omega_+/\Omega_- > &= 1. \end{aligned} \tag{5.12}$$

In the region where steady-state motion of the interface is impossible, the mean displacement $< h(t) >$ shows a power law behavior $< h_+(t) > \sim t^{\nu_{1+}}$ and $< h_-(t) > \sim -t^{\nu_{1-}}$ with the exponents $\nu_{1+}$ and $\nu_{1-}$ determined from the relations

$$\begin{aligned} < (\Omega_-/\Omega_+)^{\nu_{1+}} > &= 1, \\ < (\Omega_+/\Omega_-)^{\nu_{1-}} > &= 1. \end{aligned} \tag{5.13}$$

At the point where

$$< \ln(\Omega_-/\Omega_+) > = 0, \tag{5.14}$$

the mean displacement vanishes, $< h_+(t) >=< h_-(t) >= 0$ and $\nu_{1+} = \nu_{1-} = 0$. Note that in accord with the 1D-results[32, 33, 35] the frequencies $\Omega_-$ and $\Omega_+$ in equations (5.10) to (5.14) should be taken for the same layer.

In order to proceed further we need to calculate the probabilities $P_i$ and $Q_i$ in Eq.(5.9). For $P_i$ with $i = 1, 2, \cdots, N$, one can write the following set of equations:

$$P_i = \frac{1}{W_{i,i}} \left\{ \omega_{+(i-1)} P_{i-1,i} + \omega_{+(i+1)} P_{i,i+1} \right\},$$

$$P_{i,\ldots,i+n} = \frac{1}{W_{i,i+n}} \left\{ \omega_{-i} P_{i+1,\ldots,i+n} + \omega_{-(i+n)} P_{i,\ldots,i+n-1} + \omega_{+(i-1)} P_{i-1,\ldots,i+n} + \omega_{+(i+n+1)} P_{i,\ldots,i+n+1} \right\},$$
$$\text{for} \quad n = 1, \ldots, N-3$$

$$P_{i,\ldots,i+N-2} = \frac{1}{W_{i,i+N-2}} \{ \omega_{-i} P_{i+1,\ldots,i+N-2} + \omega_{-(i+N-2)} P_{i,\ldots,i+N-3} + \omega_{+(i+N-1)}(1) \}. \tag{5.15}$$

Here $P_{i,\ldots,i+n}$ is the probability that the solid cluster with $(n+1)$ particles which occupies the sites from $i$ to $(i+n)$ finally fills the layer of $N$ atoms without being completely remelted. The denominators are the total rate of possible events for the nucleus occupying the sites $i$ to $i+n$;

$$\begin{aligned} W_{i,i} &= \omega_{-i}(1) + \omega_{+(i-1)} + \omega_{+(i+1)}, \\ W_{i,i+n} &= \omega_{-i} + \omega_{-(i+n)} + \omega_{+(i-1)} + \omega_{+(i+n+1)}, \\ W_{i,i+N-2} &= \omega_{-i} + \omega_{-(i+N-2)} + \omega_{+(i+N-1)}(1). \end{aligned} \tag{5.16}$$

We consider Eqs. (5.15) and (5.16) with periodic boundary conditions. Namely, $\omega_{\pm(k+N)} = \omega_{\pm k}$, and a cluster which reaches a boundary of the layer can continue to grow from the other side of the layer.

For a given configuration of the layer one can solve linear equations (5.15) numerically. The closed analytical form of the solution is obtained only for $N = 2, 3, 4$ and $\Omega_+$ is given by:

For $N = 2$,

$$\Omega_+ = \omega_{+1}\omega_{+2}\left\{\frac{1}{\omega_{+2}(1)+\omega_{-1}(1)}+\frac{1}{\omega_{+1}(1)+\omega_{-2}(1)}\right\}. \tag{5.17}$$

For $N = 3$,

$$\Omega_+ = \frac{\exp[-(\epsilon_s+\epsilon_l)/T]}{\omega_{-1}\omega_{-2}\omega_{-3}} \times [\omega_{+1}\omega_{-1}(\omega_{+2}\omega_{-3}+\omega_{-2}\omega_{+3})$$

$$+\omega_{+2}\omega_{-2}(\omega_{+1}\omega_{-3}+\omega_{-1}\omega_{+3})+\omega_{+3}\omega_{-3}(\omega_{+1}\omega_{-2}+\omega_{-1}\omega_{+2})] \tag{5.18}$$

For $N = 4$,

$$\Omega_+ = \frac{\exp[-(\epsilon_s+\epsilon_l)/T]}{\prod_{i=1}^{4}\omega_{-i}}\sum_{i=1}^{4}\omega_{+i}\omega_{+(i+1)}\omega_{-(i+2)}\omega_{-(i+3)}$$

$$\times\frac{(\omega_{+(i+2)}+\omega_{+(i+3)})(\omega_{-i}+\omega_{-(i+1)})}{\omega_{+(i+2)}+\omega_{+(i+3)}+\omega_{-i}+\omega_{-(i+1)}}. \tag{5.19}$$

Equations (5.17)-(5.19) are obtained by using the fact that

$$\omega_{\pm i}(1) = \omega_{\pm i}\exp(\epsilon_{l(s)}/T) \gg \omega_{\pm i} \gg \omega_{\pm i}(3) = \omega_{\pm i}\exp(-\epsilon_{l(s)}/T). \tag{5.20}$$

The expressions for $\Omega_-$ can be obtained from the corresponding expressions for $\Omega_+$ by replacing $\omega_{+i}$ with $\omega_{-i}$ and vice versa. The solidification velocity $v_+$ can also be calculated explicitly as follows:
For $N = 1$,

$$v_+ = e^{-\epsilon_l/T}(1-S_+e^{(\epsilon_l-\epsilon_s)/T})/\left(\frac{1-c}{\omega_{+A}}+\frac{c}{\omega_{+B}}\right). \tag{5.21}$$

For $N = 2$,

$$v_+ = (1-S_+^2)\Big/\left\{\frac{(1-c)^2}{2\omega_{+A}^2}\left(\omega_{+A}e^{\epsilon_l/T}+\omega_{-A}e^{\epsilon_s/T}\right)\right.$$

$$+ \quad \frac{2c(1-c)}{\omega_{+A}\omega_{+B}} \times \frac{\left(\omega_{+A}e^{\epsilon_l/T} + \omega_{-B}e^{\epsilon_s/T}\right)\left(\omega_{+B}e^{\epsilon_l/T} + \omega_{-A}e^{\epsilon_s/T}\right)}{(\omega_{+A}+\omega_{+B})e^{\epsilon_l/T} + (\omega_{-A}+\omega_{-B})e^{\epsilon_s/T}}$$

$$+ \quad \frac{c^2}{2\omega_{+B}^2}\left(\omega_{+B}e^{\epsilon_l/T} + \omega_{-B}e^{\epsilon_s/T}\right)\Bigg\}. \tag{5.22}$$

For $N = 3$,

$$v_+ = e^{-(\epsilon_s+\epsilon_l)/T}(1-S_+^3)\Big/$$

$$\left\{\frac{(1-c)^3\omega_{-A}}{6\omega_{+A}^2} + \frac{3(1-c)^2c\omega_{-A}\omega_{-B}}{2\omega_{+A}(\omega_{+A}\omega_{-B}+\omega_{+B}\omega_{-A}+\omega_{+B}\omega_{-B})}\right.$$

$$\left. + \frac{3(1-c)c^2\omega_{-A}\omega_{-B}}{2\omega_{+B}(\omega_{+A}\omega_{-B}+\omega_{+B}\omega_{-A}+\omega_{+A}\omega_{-A})} + \frac{c^3\omega_{-B}}{6\omega_{+B}^2}\right\}. \tag{5.23}$$

For $N = 4$,

$$v_+ = e^{-(\epsilon_s+\epsilon_l)/T}(1-S_+^4)\Big/$$

$$\{\,(1-c)^4\frac{\omega_{-A}(\omega_{+A}+\omega_{-A})}{8\omega_{+A}^3} + (1-c)^3c\frac{\omega_{-A}\omega_{-B}}{\omega_{+A}^2}$$

$$\times\left(\frac{(\omega_{+A}+\omega_{+B})\omega_{-B}}{2\omega_{-A}+\omega_{+A}+\omega_{+B}} + \frac{(\omega_{-A}+\omega_{-B})\omega_{+B}}{2\omega_{+A}+\omega_{-A}+\omega_{-B}}\right)^{-1}$$

$$+2c^2(1-c)^2\frac{\omega_{-A}\omega_{-B}}{\omega_{+A}\omega_{+B}}\left(\frac{\omega_{+A}\omega_{-B}}{\omega_{-A}+\omega_{+B}}\right.$$

$$\left.+\frac{(\omega_{+A}+\omega_{+B})(\omega_{-A}+\omega_{-B})}{\omega_{+A}+\omega_{-A}+\omega_{+B}+\omega_{-B}} + \frac{\omega_{-A}\omega_{+B}}{\omega_{+A}+\omega_{-B}}\right)^{-1}$$

$$+\frac{c^2(1-c)^2}{2}\frac{\omega_{-A}\omega_{-B}(\omega_{+A}+\omega_{-A}+\omega_{+B}+\omega_{-B})}{\omega_{+A}\omega_{+B}(\omega_{+A}+\omega_{+B})(\omega_{-A}+\omega_{-B})}$$

$$+(1-c)c^3\frac{\omega_{-A}\omega_{-B}}{\omega_{+B}^2} \times \left(\frac{(\omega_{+A}+\omega_{+B})\omega_{-A}}{\omega_{+A}+\omega_{+B}+2\omega_{-B}} + \frac{(\omega_{-A}+\omega_{-B})\omega_{+A}}{\omega_{-A}+2\omega_{+B}+\omega_{-B}}\right)^{-1}$$

$$\left.+c^4\frac{\omega_{-B}(\omega_{+B}+\omega_{-B})}{8\omega_{+B}^3}\right\}. \tag{5.24}$$

Here $S_+$ is defined as

$$S_+ = < \frac{\omega_{-i}}{\omega_{+i}} > = (1-c)\frac{\omega_{-A}}{\omega_{+A}} + c\frac{\omega_{-B}}{\omega_{+B}}. \tag{5.25}$$

We should note that result for $N = 1$ in Eq.(5.21) differs from the usual result, Eq.(3.53), for the pure one-dimensional-system by the presence of the exponential factors. This difference is due to the periodic boundary condition.

The analytical result of the velocity $v_+$ is compared with numerical simulation results explicitly for the case with system size $N = 4$ in section 7.1. We have also checked the results for smaller systems and found good agreements, within 2 %.

The remarkable result found in the analysis is the relation

$$\frac{\Omega_-}{\Omega_+} = \prod_{i=1}^{N} \left( \frac{\omega_{-i}}{\omega_{+i}} \right), \tag{5.26}$$

for $N = 2, 3, 4$. So far this result has been explicitly shown only for systems with finite sizes $N = 2, 3, 4$, but it can be extended to an arbitrary large $N$ by a plausible argument. It is clear that each trajectory which gives contribution to $\Omega_+$ has the common factor $\prod_{i=1}^{N} \omega_{+i}$, because all atoms in the liquid layer have to be solidified at least once. An exponential factor contained at the initiation of a solid nucleus, $\omega_{+i}(3) = \omega_{+i} \exp(-\epsilon_l/T)$, is compensated by the factor at the end: $\omega_{+N}(1) = \omega_{+N} \exp(\epsilon_l/T)$. Index "1" here simply is the place from where the nucleation of the new layer has started. Additional melting and resolidification at the site $j$ in the intermediate stage introduces a factor $\omega_{-j}\omega_{+j}$. Thus we can formally write $\Omega_+$ as a sum over all possible trajectories

$$\Omega_+ = (\prod_{i=1}^{N} \omega_{+i}) \sum_k f_{+k}(\{\omega_{-j}\omega_{+j}\}, W_{n,m}), \tag{5.27}$$

where function $f_{+k}$ describes the contribution from the $+k$th trajectory. $W_{n,m}$ is given in Eq.(5.16). The similar formal expression can be written for $\Omega_-$ for the same layer:

$$\Omega_- = (\prod_{i=1}^{N} \omega_{-i}) \sum_k f_{-k}(\{\omega_{+j}\omega_{-j}\}, W_{n,m}). \tag{5.28}$$

We cannot calculate the trajectory sum in the general case, but we can show that $\sum_k f_{+k} = \sum_k f_{-k}$. For each $+k$th trajectory there exists a $-k$th trajectory with precisely the opposite sequence of elementary events, like a movie film forward for the $+k$th trajectory and backward for the $-k$th one. Through this one-to-one correspondence between trajectories, one gets $f_{+k} = f_{-k}$ and the relation (5.26).

From the property, Eq. (5.26), that the ratio $\Omega_-/\Omega_+$ is just the product of the ratios of the frequencies $\omega_{-i}/\omega_{+i}$, We can derive that the 2D system with large $\epsilon_s$ in many respects behaves similarly as the pure 1D system. The average of the ratio reduces to

$$< \frac{\Omega_-}{\Omega_+} > = S_+^N. \tag{5.29}$$

From Eq.(5.10) the growth rate $v_+$ then vanishes at $S_+ = 1$. This is precisely the same condition for the absence of steady growth in the 1D system Eq.(3.53), and it corresponds to the solidus line on the phase diagram. Moreover, Eq.(5.13) for the exponent $\nu_{1+}$ has the form

$$[(1-c)\left(\frac{\omega_{-A}}{\omega_{+A}}\right)^{\nu_{1+}} + c\left(\frac{\omega_{-B}}{\omega_{+B}}\right)^{\nu_{1+}}]^N = 1, \tag{5.30}$$

and gives the same exponent $\nu_{1+}$ as for the 1D system (see Eq.(3.55)). All these results obtained for the solidification front can be easily converted into the melting front just by exchanging the indices $+$ and $-$. For example the melting velocity $v_-$ vanishes at the concentration which satisfies

$$S_- \equiv (1-c)\frac{\omega_{+A}}{\omega_{-A}} + c\frac{\omega_{+B}}{\omega_{-B}} = 1. \tag{5.31}$$

In above, we have verified that the 2D system with a large bond energy is effectively one-dimensional with the transition rates $\Omega_+$ and $\Omega_-$. Then we can use some additional results for a real one-dimensional system. For example, following the procedure of Ref.[33] we can derive the expression $W(\{X^n\})$ for the probability of finding a configuration $\{X^n\} \equiv \{X_1^n \ldots X_N^n\}$ in the $n$th

layer from the steadily growing interface:

$$W(\{X^n\}) = \begin{cases} \prod_{i=1}^{N} c_{X_i^n} & \text{for } n \leq -1, \text{ in the solid,} \\ \prod_{i=1}^{N} c_{X_i^n} \left\{ 1 + S_+^{Nn} [\frac{\Omega_-(\{X^n\})}{\Omega_+(\{X^n\})} - 1 + \frac{1 - S_+^N}{\Omega_+(\{X^n\}) < 1/\Omega_+ >}] \right\} & \\ \text{for } n \geq 0, \text{ in the liquid.} & \end{cases}$$

Here $\prod_{i=1}^{N} c_{X_i^n}$ is the probability of finding the configuration $\{X^n\} = \{X_1^n, X_2^n \ldots X_N^n\}$ in the n-th layer respective to the interface. From Eq.(5.32) one can calculate the average concentration of $B$-atoms, $c(n)$, in the $n$-th layer from the interface, by fixing the configuration of one lattice site, say $i = 1$, to a B atom ($X_1^n = B$ ), and summing $W(\{X^n\})$ over all possible configurations $\{X^n\} = \{B, X_2^n \ldots X_N^n\}$. For example, when the initial concentration is $c = C_S$ where $S_+ = 1$ and the steady-state velocity $v_+ = 0$, $c(n)$ is obtained as

$$c(n) = \begin{cases} C_S & \text{for} \quad n \leq -1, \\ C_L & \text{for} \quad n \geq 0. \end{cases}$$

Both phases have the equilibrium compositions, as one finds in the case of the real one-dimensional system[33].

# Chapter 6

# Monte Carlo Simulation

Due to intractable mathematical difficulties, numerical methods are used to investigate the problem of interface motion from this chapter on. This chapter deals with the algorithm and tests of the program. Meanwhile we obtain a closed solution for a two-column ordered system.

## 6.1 Implementation of the Algorithm

For the analysis of a 2D alloy solidification with general values of bond energies we perform Monte Carlo (MC) simulations of the lattice model introduced before. On a square lattice with $N$ columns and $M$ rows, A and B atoms are distributed randomly with a mean concentration $c$ of the B component. We introduce the state variable $m_{ij}$ which takes the value 0 or 1 according to whether the lattice site (i,j) is occupied by an A or B atom,

$$m_{ij} = \begin{cases} 0 & \text{for A atom} \\ 1 & \text{for B atom} \end{cases} \tag{6.1}$$

The average of $m_{ij}$ over the whole lattice sites $N \times M$ should be the given concentration c:

$$c = \frac{1}{NM} \sum_{i=1}^{N} \sum_{j=1}^{M} m_{ij}. \tag{6.2}$$

Each atom can be in either solid or liquid state. We use the solid-on-solid (SOS) model, and therefore overhangs are forbidden and the interface is single-

valued. We put the lattice sample in such a way that the liquid phase stays above the solid phase. Then, the interface is defined to be the set of column heights $\{h_i\}$ for columns $i = 1$ to $N$ in the solid phase. The growth starts from a horizontal line at a height $h_i(t = 0) = h(0)$ for all the columns. Each row is assumed periodic and both ends of each column are assumed free.

For the motion of the interface, only 2N atoms adjacent to the interface are involved. Let us denote the interface configuration as $\{h_i\}$, the solid-atom arrangement below the interface as $\{X^s(h_i)\}$ and the liquid-atom arrangement above the interface as $\{X^l(h_i + 1)\}$. The melting rate of a solid atom on the $i$th column depends on the number $j_i$ of neighboring solid atoms as $\omega_{-i} \equiv \omega_{-X^s(h_i)}(j_i)$ and the solidification rate of a liquid atom above the interface depends on the number $j_i'$ of neighboring liquid atoms as $\omega_{+i} \equiv \omega_{+X^l(h_i+1)}(j_i')$. Then, during the time interval

$$\Delta t = 1/(\sum_{i=1}^{N} \omega_{+i} + \sum_{i=1}^{N} \omega_{-i}), \tag{6.3}$$

an atom in the $i$th column in the liquid or solid layer changes its state with the transition probability

$$P_{\pm}(i) = \omega_{\pm i}\Delta t, \tag{6.4}$$

where $i = 1, \cdots, N$. Here +(-) refers to the solidification (melting) of the atom at the height $h_i + 1$ ($h_i$). Since the probability (6.4) is normalized, some event must take place within the time interval $\Delta t$. Therefore, our simulation algorithm runs as follows; Pick up a random number between 0 and 1. If it falls in the interval between $\sum_{n=1}^{i-1} P_+(n)$ and $\sum_{n=1}^{i} P_+(n)$ then the liquid atom at the site $(i, h_i + 1)$ solidifies and the interface height at column i increases by one unit: $h_i \to h_i + 1$. If the random number falls in the interval between $\sum_{n=1}^{N} P_+(n) + \sum_{n=1}^{i-1} P_-(n)$ and $\sum_{n=1}^{N} P_+(n) + \sum_{n=1}^{i} P_-(n)$, then the solid atom at the site $(i, h_i)$ melts and the interface height at column i decreases by one unit: $h_i \to h_i - 1$. After each attempt the configuration of the interface changes and the time increases by $\Delta t$: $t = t + \Delta t$. To describe the growth quantitatively, we introduce two functions.

(i) The displacement of the interface ,h, is defined by

$$h(t) \equiv \frac{1}{N}\sum_{i=1}^{N} h_i(t) - h(0), \tag{6.5}$$

where $h_i(t)$ is the height of column i at time t and $h(0)$ is the initial position of the interface.

(ii) The interface width, which characterizes the roughness of the interface, is defined by the root-mean-square fluctuation in the height,

$$\begin{aligned} \sigma(t) &\equiv \sqrt{\frac{1}{N}\sum_{i=1}^{N}\left[h_i(t) - \frac{1}{N}\sum_{i=1}^{N} h_i(t)\right]^2} \\ &= \sqrt{\frac{1}{N}\sum_{i=1}^{N} h_i^2(t) - \left[\frac{1}{N}\sum_{i=1}^{N} h_i(t)\right]^2}. \end{aligned} \tag{6.6}$$

## 6.2 Tests of the Program

Several tests of the program are performed in this chapter. First of all, using this 2D growth program with zero bond energy ($\epsilon_s = \epsilon_l = 0$), we have repeated all main results in the section 3.3 for a 1D chain. Secondly, we have tried to find out some analytic results for simple 2D systems, for example, a two-column system consisting of one column A atoms and one column B atoms and a 2D pure system at equilibrium state. The simulation results agree very well with the theoretical expectations. In order to make a further checking of the program, we have used our program to perform Voronkov's model which has the analytic expression of the interface velocity. Again, the simulation results and the analytic expectation are in good agreement!

### 6.2.1 Two-column system

We consider a two-column lattice system which consists of one column A atoms and one column B atoms. The structure of the interface can be classified into

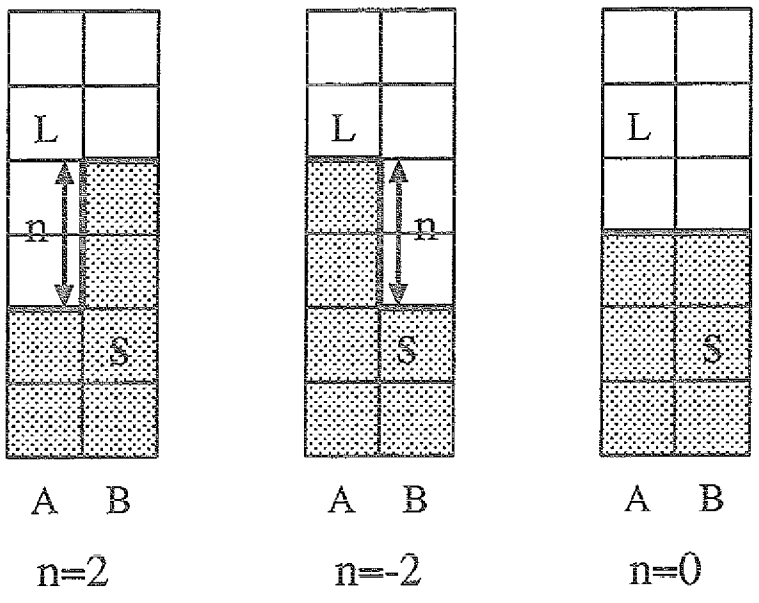


Figure 6.1: The interface configuration of two-column system. n is the height difference between the interface positions of the two columns. $n > 0$ refers to a plus interface; $n < 0$ refers to a minus interface; and $n = 0$ refers to a flat interface.

three types: plus, minus and flat interfaces as shown in Fig.6.1 from left to right. Plus interface refers to the interface configuration in which the interface position in the right column is higher than that in the left; The minus interface is just opposite of the plus; And the flat one has equal interface height. At a given time, the interface can have one of these three structures. We introduce the probability $\rho(n)(n = 0, \pm 1, \pm 2, \cdots)$ of finding an interface configuration with a height difference n between left and right column. So $\rho(0)$ denotes the probability of finding a flat interface. Each row is assumed periodic and both ends of each column are assumed free. Since the interface position in each column can hop at one elementary act only one unit, the process must be controlled by the following set of Master equations. For $n > 0$

$$\begin{aligned}\frac{d\rho(n)}{dt} &= -\rho(n)[\omega_{+A}(1) + \omega_{-A}(3) + \omega_{+B}(3) + \omega_{-B}(1)] \\ &\quad +\rho(n-1)[\omega_{-A}(3) + \omega_{+B}(3)] + \rho(n+1)[\omega_{+A}(1) + \omega_{-B}(1)].\end{aligned} \tag{6.7}$$

For $n < 0$

$$\begin{aligned}\frac{d\rho(n)}{dt} &= -\rho(n)[\omega_{+A}(3) + \omega_{-A}(1) + \omega_{+B}(1) + \omega_{-B}(3)] \\ &\quad +\rho(n+1)[\omega_{-A}(1) + \omega_{+B}(1)] + \rho(n-1)[\omega_{+A}(3) + \omega_{-B}(3)].\end{aligned} \tag{6.8}$$

For $n = 0$

$$\begin{aligned}\frac{d\rho(0)}{dt} &= -\rho(0)[\omega_{+A}(3) + \omega_{-A}(3) + \omega_{+B}(3) + \omega_{-B}(3)] \\ &\quad +\rho(-1)[\omega_{-A}(1) + \omega_{+B}(1)] + \rho(+1)[\omega_{+A}(1) + \omega_{-B}(1)].\end{aligned} \tag{6.9}$$

In the long time limit, one expects that the interface reaches a steady-state and the probability $\rho(n)$ does not change with time. Set $\frac{d\rho(n)}{dt} = 0$ and rewrite the equation (6.7) as

$$\begin{aligned}&\rho(n)[\omega_{+A}(1) + \omega_{-B}(1)] - \rho(n-1)[\omega_{-A}(3) + \omega_{+B}(3)] \\ =\ &\rho(n+1)[\omega_{+A}(1) + \omega_{-B}(1)] - \rho(n)[\omega_{-A}(3) + \omega_{+B}(3)] \\ =\ &C(\text{constant}).\end{aligned} \tag{6.10}$$

Dividing the above equation from the two sides by $[\omega_{+A}(1) + \omega_{-B}(1)]$, we have got

$$\rho(n) = \rho(n-1)\eta_+ + C1, \tag{6.11}$$

$$\eta_+ = \frac{\omega_{-A}(3) + \omega_{+B}(3)}{\omega_{+A}(1) + \omega_{-B}(1)} < 1. \tag{6.12}$$

Due to $\rho(\infty)$ being zero the constant C1 must be zero too. Using the recursion relation (6.11), one can get a relation for the probability $\rho(n)$ of the plus interface

$$\rho(n) = \rho(0)\eta_+^n \qquad (n \geq 0). \tag{6.13}$$

Similarly, we can obtain the probability of the minus interface from equation (6.8)

$$\rho(n) = \rho(0)\eta_-^n \qquad (n \leq 0), \tag{6.14}$$

here

$$\eta_- = \frac{\omega_{-A}(1) + \omega_{+B}(1)}{\omega_{+A}(3) + \omega_{-B}(3)} > 1. \tag{6.15}$$

The probabilities must satisfy the normalization requirement

$$\sum_{n=-\infty}^{+\infty} \rho(n) = 1, \tag{6.16}$$

namely

$$\rho(0)(\eta_+ + \eta_+^2 + \cdots) + \rho(0) + \rho(0)(\frac{1}{\eta_-} + \frac{1}{\eta_-^2} + \cdots) = 1. \tag{6.17}$$

Solving the above equation, we get

$$\rho(0) = [\frac{\eta_-}{\eta_- - 1} + \frac{\eta_+}{1 - \eta_+}]^{-1}. \tag{6.18}$$

The velocity of the interface $v$ is the average velocity over three interface configurations

$$\begin{aligned} 2v &= \rho(0)v_{flat} + \sum_{n=1}^{+\infty} \rho(0)\eta_+^n v_{plus} + \sum_{n=-\infty}^{-1} \rho(0)\eta_-^n v_{minus} \\ &= \rho(0)\left(v_{flat} + v_{plus}\sum_{n=1}^{+\infty}\eta_+^n + v_{minus}\sum_{n=-\infty}^{-1}\eta_-^n\right) \\ &= \rho(0)\left(v_{flat} + v_{plus}\frac{\eta_+}{1-\eta_+} + v_{minus}\frac{1}{\eta_- - 1}\right). \end{aligned} \tag{6.19}$$

For pure atom at steady-state, the velocity of the interface is determined purely by the dynamics: $v = \omega_+ - \omega_-$, so we have

$$\begin{aligned} v = \quad & \frac{1}{2}\rho(0)\{[\omega_{+A}(3) - \omega_{-A}(3) + \omega_{+B}(3) - \omega_{-B}(3)] \\ + \quad & \frac{\eta_+}{1-\eta_+}[\omega_{+A}(1) - \omega_{-A}(3) + \omega_{+B}(3) - \omega_{-B}(1)] \\ + \quad & \frac{1}{\eta_- - 1}[\omega_{+A}(3) - \omega_{-A}(1) + \omega_{+B}(1) - \omega_{-B}(3)]\}. \end{aligned} \tag{6.20}$$

Because $\eta_+$ is smaller than 1 and $\eta_-$ is bigger than 1, we conclude that the interface of the AB structure has always a steady-state velocity. This is different from the system with quenched randomness where the interface does not always move with a steady-state velocity. For AA structure or pure A atoms, $\eta_+ = \frac{1}{\eta_-}$ from equation (6.12) and (6.15), so we have $\rho(0) = \frac{1-\eta_+}{1+\eta_+}$. In this case, the expression of the velocity can be simplified as

$$\begin{aligned} v &= \frac{1-\eta_+}{1+\eta_+}[\omega_{+A}(3) - \omega_{-A}(3)] + \frac{\eta_+}{1+\eta_+}[\omega_{+A}(1) + \omega_{+A}(3) - \omega_{-A}(1) - \omega_{-A}(3)] \\ &= 2\omega_{-A}(2) \times \frac{e^{\Delta\mu_A/T} - 1}{e^{\epsilon_l/T} + e^{-\epsilon_l/T}}. \end{aligned} \tag{6.21}$$

In the following table we have shown that the simulation results and the analytic predictions from equation (6.20) for AB structure and (6.21) for AA structure. The parameters are chosen as : $T_A = 0.9$, $T_B = 0.1$, $L_A/T_A = L_B/T_B = 1$, $\epsilon_s/T_A = \epsilon_l/T_A = 1$ and $\omega_{-A} = \omega_{-B} = 1$. From the table we can see that under various temperature for both pure and AB structure, the analytic and simulation results agree quite well.

| Temperature | analytic $v_a$ | numeric $v_n$ | time | structure |
|---|---|---|---|---|
| 0.2 | 0.1381 | 0.1381 | $2.3 \times 10^5$ | AB |
| 0.4 | 0.0609 | 0.0607 | $1.5 \times 10^5$ | AB |
| 0.5 | 0.0000 | 0.0004 | $1.5 \times 10^5$ | AB |
| 0.4 | 0.0609 | 0.0607 | $1.3 \times 10^5$ | AB |
| 0.7 | -0.1264 | -0.1268 | $7.5 \times 10^4$ | AB |
| 0.7 | 0.1698 | 0.1690 | $7.5 \times 10^4$ | AA |
| 0.9 | 0.0000 | -0.0006 | $7.4 \times 10^5$ | AA |
| 1.1 | 0.1228 | 0.1229 | $6.6 \times 10^4$ | AA |

### 6.2.2 Two-dimensional Pure System at Equilibrium State

For a two-dimensional pure system, the interface may contain many structures like those shown in Fig.6.1. Structures can distinguish from each other

by the interface height difference $n$ between the two neighboring columns. At nonequilibrium state, we do not know the probability $\rho'(n)$ of finding a structure with a given height $n$, but at equilibrium state it should obey Boltzman's distribution

$$\rho'(n) = e^{-\frac{|n|\epsilon}{T_A}} = \eta_0^{|n|}, \qquad n = 0, \pm 1, \pm 2 \cdots \tag{6.22}$$

and

$$\eta_0 \equiv e^{-\frac{\epsilon}{T_A}}. \tag{6.23}$$

The partition function is

$$z = \sum_{n=-\infty}^{+\infty} \rho'(n) = 1 + 2(\eta_0 + \eta_0^2 + \cdots) = \frac{1+\eta_0}{1-\eta_0}, \tag{6.24}$$

and then the normalized probability can be expressed as

$$\rho(n) = \frac{\rho'(n)}{z} = \eta_0^{|n|}\rho(0), \qquad \rho(0) = \frac{1-\eta_0}{1+\eta_0}. \tag{6.25}$$

If the bond energy is set to be $T_A$: $\epsilon = T_A$, then $\eta_0 = \frac{1}{e}$ and $\rho(0) = 0.462$. In the following table we have shown the analytic predictions (6.25) and the simulation results for the probabilities $\rho(n)$ and we can see that they are in a good agreement (within 0.2%). Other parameters are chosen as: $L_A/T_A = 1$ and the system size $N = 100$.

| height n | analytic $\rho(n)$ | numeric $\rho(n)$ |
|---|---|---|
| 0 | 0.462 | 0.461 |
| 1 | 0.170 | 0.172 |
| 2 | 0.063 | 0.063 |
| 3 | 0.023 | 0.023 |
| ⋮ | ⋮ | ⋮ |

### 6.2.3 Voronkov's Model

For a pure material, Voronkov introduced a special model which defines the transition frequencies $\omega_{\pm}(j)$ in such a way that no correlation along the interface exists. The transition frequencies are so defined

$$\begin{aligned}
\omega_+(2) &= (1+f)\omega_-(2), \\
\omega_+(3) &= \omega_+(2)\frac{2s^2}{1+s^2}, \\
\omega_+(1) &= \omega_+(2)\frac{2}{1+s^2}, \\
\omega_-(1) &= \omega_+(3)\frac{1}{(1+f)s^2}, \\
\omega_-(3) &= \omega_+(1)\frac{s^2}{1+f},
\end{aligned} \tag{6.26}$$

here

$$\begin{aligned}
f &= \exp(\frac{\mu_l - \mu_s}{T}) - 1, \\
s &= \exp(-\frac{\epsilon_l + \epsilon_s}{2T}).
\end{aligned} \tag{6.27}$$

So $\omega_-(2)$ is the only dynamic parameter. Under this model he found that the velocity of the interface can be expressed as

$$v = \frac{2sf\omega_-(2)}{1+s^2} \tag{6.28}$$

By replacing the transition frequencies (4.3) of our model by Voronkov's ones (6.26) in our program, we have simulated Voronkov's model using our program. The parameters are chosen as : $T_A = 0.9$, $T_B = 0.1$, $L_A/T_A = L_B/T_B = 1$, $\epsilon_s/T_A = \epsilon_l/T_A = 1$ and $\omega_{-A} = \omega_{-B} = 1$. We have performed simulations for pure A and pure B atoms and the simulation results as well as analytic

prediction are summarized in the following table. From the table we can see that the numeric and analytic velocities are in a good agreement!

| temperature | analytic velocity | numeric velocity | atom |
|---|---|---|---|
| 0.5 | 0.3944 | 0.3948 | A |
| 1.2 | -0.1709 | -0.1703 | A |
| 0.5 | -0.1772 | -0.1752 | B |

### 6.2.4 Two-Dimensional Periodic Structure

We consider a 2D periodic lattice consisting of alternate columns of either A or B atoms. This ordered lattice can be considered as repetitions of the two-column AB system studied in the section 6.2.1 to arbitrary size. Even for this ordered system we are not able to give an exact theory. However, for the specialization to Voronkov's model we do obtain an expression for the velocity of the interface.

First we introduce two distribution functions $\rho_A(n)$ and $\rho_B(n)$ of the height n of a break, the vertical part of the interface between two neighboring columns. $\rho_A(n)$ is defined as the probability of finding a break located between A-column on the left side of the break and B-column on the right side of the break and $\rho_B(n)$ is the probability of finding a break located between B-column on the left side of the break and A-column on the right side of the break. When the highest solid atom on the right side column of the break is higher than the one on the left column, n is positive : $n > 0$. Otherwise n is negative : $n < 0$. For breaks $\rho_A(n) = \rho_B(-n)$ and $\rho_B(n) = \rho_A(-n)$ should hold due to the symmetry. Then under the assumption of the absence of correlation among the breaks, one can write down the Master equations. For $\rho_B(n)$ when $n \geq 0$, the Master equation is

$$\frac{d\rho_B(n)}{dt} =$$
$$\rho_B(n+1)\left\{\left[\omega_{-A}(2)+\omega_{+B}(2)\right]\sum_{n=0}^{\infty}\rho_A(n)+\left[\omega_{-A}(1)+\omega_{+B}(1)\right]\sum_{n=-\infty}^{1}\rho_A(n)\right\}$$
$$+\rho_B(n-1)\left\{\left[\omega_{+A}(2)+\omega_{-B}(2)\right]\sum_{n=1}^{\infty}\rho_A(n)+\left[\omega_{+A}(3)+\omega_{-B}(3)\right]\sum_{n=-\infty}^{0}\rho_A(n)\right\}$$
$$-\rho_B(n)\left\{\left[\omega_{+A}(2)+\omega_{-B}(2)\right]\sum_{n=1}^{\infty}\rho_A(n)+\left[\omega_{+A}(3)+\omega_{-B}(3)\right]\sum_{n=-\infty}^{0}\rho_A(n)\right.$$
$$\left.+\left[\omega_{-A}(2)+\omega_{+B}(2)\right]\sum_{n=0}^{\infty}\rho_A(n)+\left[\omega_{-A}(1)+\omega_{+B}(1)\right]\sum_{n=-\infty}^{1}\rho_A(n)\right\}. \tag{6.29}$$

At the steady-state this equation can be simplified and hence the following relation is obtained

$$\rho_B(n) = \rho(0)\,S_B^n,$$
$$\rho_A(-n) = \rho_B(n), \qquad \text{when} \quad n \geq 1, \tag{6.30}$$

The similar equation for $\rho_A(n)$ when $n \geq 0$ as (6.29) can be written and the similar relation as (6.30) is obtained

$$\rho_A(n) = \rho(0)\,S_A^n,$$
$$\rho_B(-n) = \rho_A(n), \qquad \text{when} \quad n \geq 1. \tag{6.31}$$

Here

$$\rho(0) = \frac{(1-S_A)(1-S_B)}{1-S_A\,S_B}, \tag{6.32}$$

provided that $S_A < 1$ and $S_B < 1$. $\rho(0)$ is the probability of the absence of any break and $S_A$ and $S_B$ satisfy the conditions

$$(1-S_B)\left\{S_A[\omega_{+A}(2)+\omega_{-B}(2)] - S_B[\omega_{+B}(2)+\omega_{-A}(2)]\right\}$$
$$+(1-S_A)\left\{[\omega_{+A}(3)+\omega_{-B}(3)] - S_B^2[\omega_{+B}(1)+\omega_{-A}(1)]\right\} = 0,$$

$$(1-S_A)\left\{S_B[\omega_{+B}(2)+\omega_{-A}(2)] - S_A[\omega_{+A}(2)+\omega_{-B}(2)]\right\}$$
$$+(1-S_B)\left\{[\omega_{+B}(3)+\omega_{-A}(3)] - S_A^2[\omega_{+A}(1)+\omega_{-B}(1)]\right\} = 0. \tag{6.33}$$

These are highly nonlinear equations and generally we can not solve them. We guess that (6.33) has the following specific solution under Voronkov's model

$$\begin{aligned} S_A &= S\sqrt{\frac{\omega_{+B}(3)+\omega_{-A}(3)}{\omega_{+A}(1)+\omega_{-B}(1)}} = S\sqrt{\frac{\omega_{+B}(2)+\omega_{-A}(2)}{\omega_{+A}(2)+\omega_{-B}(2)}}, \\ S_B &= S\sqrt{\frac{\omega_{+A}(3)+\omega_{-B}(3)}{\omega_{+B}(1)+\omega_{-A}(1)}} = S\sqrt{\frac{\omega_{+A}(2)+\omega_{-B}(2)}{\omega_{+B}(2)+\omega_{-A}(2)}}, \end{aligned} \tag{6.34}$$

where S is defined as

$$S = \sqrt{\frac{\omega_{+A}(3)+\omega_{+B}(3)+\omega_{-A}(3)+\omega_{-B}(3)}{\omega_{+A}(1)+\omega_{+B}(1)+\omega_{-A}(1)+\omega_{-B}(1)}}. \tag{6.35}$$

Note for an alloy consisting of A and B atoms, the transition frequencies of A atoms defined in (6.26) differ from those of B atoms. It turns out that (6.34) is a solution of (6.33) since it satisfies the equations (6.33). The velocity is found to satisfy

$$\begin{aligned} \frac{2v}{\rho(0)^2} &= \frac{S_A^2}{(1-S_A)^2}[\omega_{+A}(1)-\omega_{-B}(1)] \\ &+ \frac{S_B^2}{(1-S_B)^2}[\omega_{+B}(1)-\omega_{-A}(1)] \\ &+ \frac{1}{(1-S_A)^2}[\omega_{+B}(3)-\omega_{-A}(3)] \\ &+ \frac{1}{(1-S_B)^2}[\omega_{+A}(3)-\omega_{-B}(3)] \\ &+ \frac{2S_A}{(1-S_A)(1-S_B)}[\omega_{+A}(2)-\omega_{-B}(2)] \\ &+ \frac{2S_B}{(1-S_A)(1-S_B)}[\omega_{+B}(2)-\omega_{-A}(2)], \qquad \text{when} \quad S_A, S_B \leq 1. \end{aligned} \tag{6.36}$$

This general expression of the velocity has a finite value when $S_A = 1$ or $S_B = 1$ and we found

$$\begin{aligned} v &= \frac{1}{2}[\omega_{+B}(3)-\omega_{-A}(3)+\omega_{+A}(1)-\omega_{-B}(1)] \qquad \text{when} \quad S_A \geq 1, \\ v &= \frac{1}{2}[\omega_{+B}(1)-\omega_{-A}(1)+\omega_{+A}(3)-\omega_{-B}(3)] \qquad \text{when} \quad S_B \geq 1. \end{aligned} \tag{6.37}$$

For pure material under Voronkov's model (6.26) we have

$$S_A = S_B = S = \sqrt{\frac{\omega_+(3) + \omega_-(3)}{\omega_+(1) + \omega_-(1)}} = s = \exp(-\frac{\epsilon_l + \epsilon_s}{2T}). \tag{6.38}$$

Using the relations among transition frequencies in (6.26) and (6.38) we can recover the velocity expression (6.28) for a pure material under Voronkov's model.

Diffusionless growth of a 2D periodic structure is simulated. In order to overcome the finite size effect, we keep $\epsilon_{s(l)}/T$ being 1, so that 100 columns always can be seen as "infinite" size no matter how low the temperature is. Parameters are chosen as: $L_A/T_A = L_B/T_B = 1$, $\epsilon_s/ = \epsilon_l = T$ and $\omega_{-A}(2) = \omega_{-B}(2) = 1$.. The width of the system is 100 and the numbers of sample is one. Under these parameters we found $S_B = 1$ at the temperature $T_c = 0.27$. Fig.6.2 shows the velocity of the interface as a function of temperature. The curve is drawn from (6.36) for $T \geq 0.27$ and from (6.37) for $T \leq 0.27$ and the empty diamond symbols represent the Monte Carlo simulation results. It is clear that the theoretical expectations are in a good agreement with Monte Carlo simulation results.

One remark worth mentioning is that a disordered 1D chain differs from an ordered chain [35]. The former does not always have a steady-state solidification front, but the latter does. For a 2D ordered system, for example AB structure, like the 1D ordered chain, the interface moves steadily when $\epsilon_{s(l)}$ not very large.

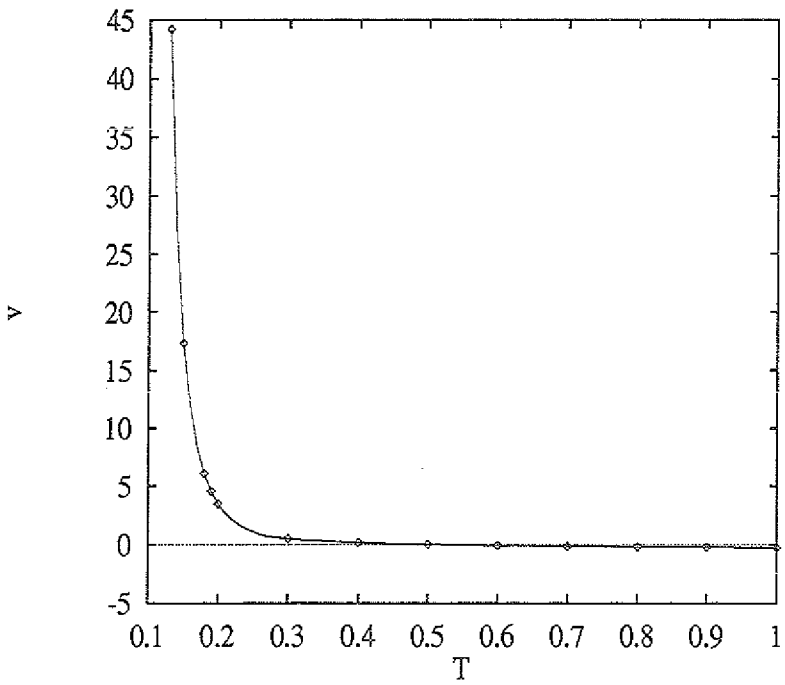


Figure 6.2: The stead-state velocity of the interface of a 2D periodic system versus temperature under Voronkov's model. $\epsilon_{s(l)}/T$ is kept 1.

# Chapter 7

# Numerical Results and Discussions

The goal of understanding the effect of quenched noise on interface motion and morphology has motivated a large number of numerical studies. In this chapter, we study the diffusionless solidification front more systematically. Special effort is put on the two-phase region.

In the two-phase region, bond energy effects are examined in the whole range. For both very small and very large value the solidification front is found to become pinned in the sense that the velocity of the interface decays due to the pinning force. For moderate energy, however, the interface of a finite size system obtains a steady-state velocity. A very large system is always in a depinning state, which is related to the creep motion. The height-height correlation on the interface is studied, by that the finite size effect found in the system can be well explained .

## 7.1 Large Bond Energy Limit

In the chapter 5, we proved that when the bond energies $\epsilon_s$ are infinitely large and the system width is finite the 2D system has asymptotics equivalent to the 1D system. In order to check this, we simulate the interface motion of a four-column lattice: $N = 4$, for which we have obtained a closed solution.

The parameters governing the phase diagram are : $T_A = 0.9$, $T_B = 0.1$ and $L_A/T_A = L_B/T_B = 1$. The correspondent phase diagram is shown in Fig.1.1. Other parameters are chosen as: $\epsilon_s/T_A = \epsilon_l/T_A = 3.0$, $\omega_{-A} = \omega_{-B} = 1$ and $T = 0.5$. The equilibrium concentrations at this temperature are $C_s = 0.310$ and $C_l = 0.690$. By solving equations (4.4), (4.5) and (3.55), the exponent for the displacement of the interface is obtained as

$$\nu_1 = 1.25 \ln(\frac{1-c}{c}) \qquad (0.31 < c < 0.50). \tag{7.1}$$

Since the bond energies $\epsilon_s/T = \epsilon_l/T = 5.4$ are so large that the thermally excited kink density is very small; Then the solid-liquid interface is expected to advance by the single nucleation and growth mechanism as is discussed in chapter 5. The exponent $\nu_1$ and the velocity $v$ obtained by the simulation are presented as functions of the concentration $c$ in Fig.7.1 and Fig.7.2, respectively. The exponents $\nu_1$ in Fig.7.1 are determined from the asymptotic slope of the logarithm of displacement versus time. The solid line in Fig.7.1 represents the theoretical expectations Eq.(7.1). In the one phase region far from the equilibrium concentration $C_s$, simulation results have a very good agreement with the theoretical expectations: $\nu_1 = 1$. However, there is a deviation of simulated $\nu_1$ from the theoretical value near the phase boundary $C_s$. The deviation is also observed in a 1D case [34] and is probably due to the finite simulation time effect. The velocity in Fig.7.2 is determined from the asymptotic slope of the displacement versus time and it has a non-zero value even in the two-phase region due to the creep motion. The solid line in Fig.7.2 is the velocity obtained theoretically from Eq.(5.24) for $N = 4$. Comparing the analytic prediction (solid line) with the simulation results (symbols), we can conclude that the 2D diffusionless crystal growth in the infinite bond energy limit obeys the same law as the 1D counterpart. It means that the interface advances steadily in the one phase region, but the steady-state velocity vanishes in the two phase region.

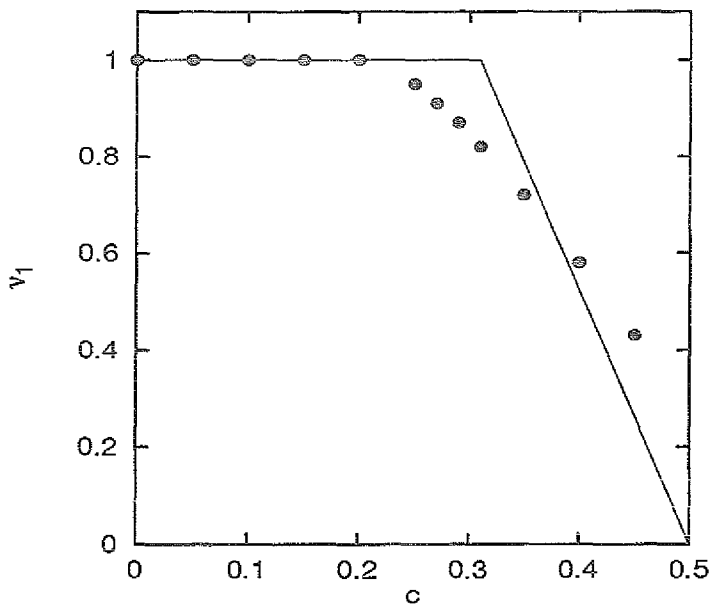


Figure 7.1: Exponent $\nu_1$ of the mean displacement at various concentrations of B atoms for four-column system: $N = 4$. The solid line represents the theoretical expectation Eq.(7.1) and dots represent MC results.

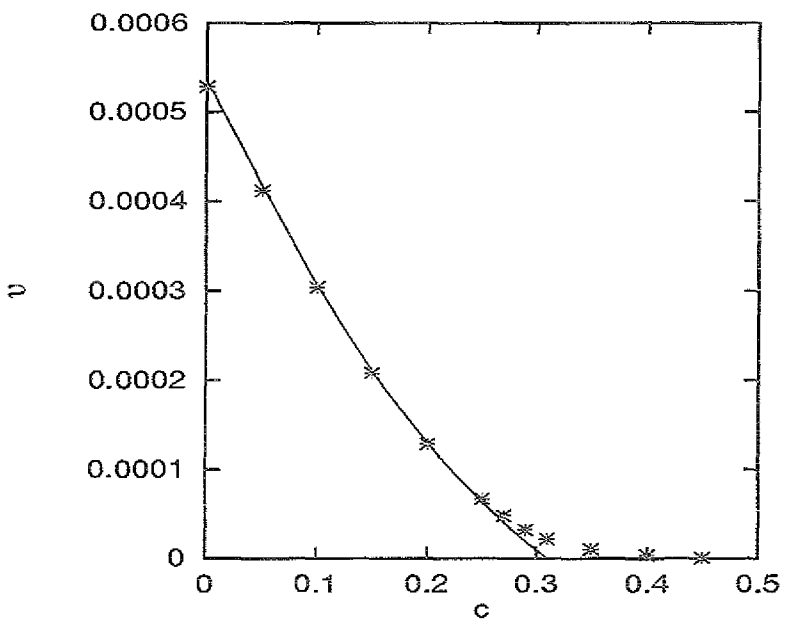


Figure 7.2: Steady-state velocity $v$ versus concentration c for the four-column system: $N = 4$. The solid line represents the theoretical expectation Eq.(5.24), and dots represent MC results.

## 7.2 The Finite Size Effect

Simulation results have shown that the interface of a 2D alloy system has a steady-state solidification velocity in the solid phase region ($c < C_s$) and a steady-state melting velocity in the liquid phase region ($c > C_l$). Naturally, the basic question we want to ask is how the interface in the two-phase coexistence region behaves. There are many parameters which affect the properties of the system but the ones which are new compared to the 1D system are the bond energy $\epsilon$ and the system size $N$. In the following, we shall systematically study the effect of these two parameters on the dynamics of the interface. The values of other parameters are kept fixed to reproduce the same equilibrium phase diagram, Fig.1.1: $T_A = 0.9$, $T_B = 0.1$, $L_A/T_A = L_B/T_B = 1$. We choose the concentration $c = 0.4$ and the temperature $T = 0.5$ so that the corresponding phase point is located in the two-phase coexistence region with a solid phase favored (see Fig.1.1). Then the choice of $\omega_{-A} = \omega_{-B} = 1$ leads to solidification frequencies $\omega_{+A} = 1/\omega_{+B} = 2.226$ at $T = 0.5$. For simplicity, the bond energies $\epsilon_s$ and $\epsilon_l$ take always the same value: $\epsilon_s = \epsilon_l = \epsilon$. We shall keep the values of the above parameters through chapter 7, otherwise they will be specified.

We first study the time dependence of the interface displacement $\langle h(t) \rangle$ for various system sizes $N$ at a given bond energy $\epsilon$. Figure 7.3 depicts the raw data in the log-log plot for six different sizes $N$ ranging from 20 to 80 at the fixed bond energy $\epsilon/T_A = 2.0$. The simulation is performed up to the time $10^6$ and $\langle h(t) \rangle$ have been averaged over $50 \sim 150$ samples. Two different behaviors of interface separated by a cross-over time $t_\times$ are observed:
(i) Initially, the displacement, $< h(t, N) >$, increases linearly with time t,

$$< h(t, N) > \sim t \qquad [t \ll t_\times] \tag{7.2}$$

which is reflected by the unity slope of the initial part of curves and is independent of the system size $N$.

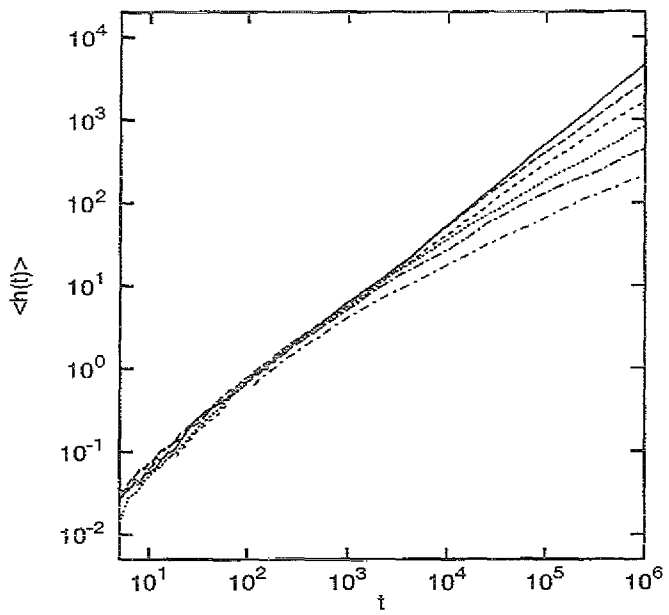


Figure 7.3: Log-log plot of the mean displacement $< h(t) >$ as a function of time t for various system sizes: $N$ =20,30,40,50,60 and 80 from the bottom to the top. The bond energy is $\epsilon = 2.0T_A$.

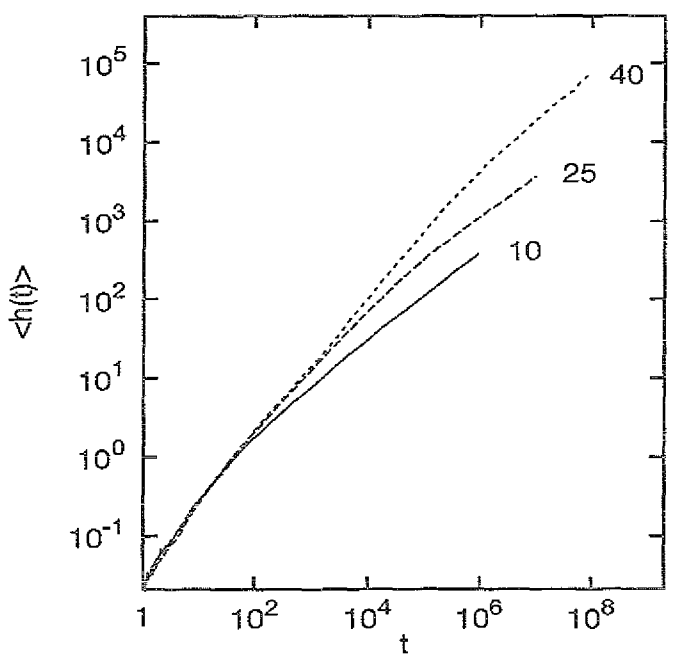


Figure 7.4: Log-log plot of the mean displacement $< h(t) >$ as a function of time t for three system sizes: $N$ =10, 25 and 40. The bond energy is $\epsilon = 1.5T_A$.

(ii) The liner increase in displacement does not continue indefinitely, but followed by a power-law increase

$$< h(t,N) > \sim t^{\nu_1} \qquad [t \gg t_\times]. \tag{7.3}$$

Up to a simulation time $T = 10^6$ we obtain a dynamic exponent $\nu_1$ which varies from around 0.51 to 0.97 as the system size $N$ increases from 25 to 80. The same tendency is also observable for a system with a smaller bond energy, $\epsilon/T_A = 1.5$ as that depicted in Fig.7.4. Here the simulation is performed longer up to the time $t = 10^8$ and $\langle h(t) \rangle$ verse $t$ have been averaged over 900,300 and 80 samples for $N = 10, 25$ and 40, respectively. The asymptotics slopes of the three curves of $\langle h(t) \rangle$ verse $t$ in double-logarithm are around 0.51. This result suggests us strongly that the interface of a finite size system in the long time limit (see tails of the curves in Fig.7.4) behaves similarly and it is independent of size like the initial growth phase. The tails of the curves in Fig.7.3 are just the intermediate behaviors between depinned and pinned states.

In the simulation, the solidification starts from a straight interface. As atoms on the interface change their states between the liquid and the solid states, the interface gradually roughens and bumps appear. At the beginning, bumps are so small and isolated from each other that the interfaces of systems can not tell one system size from the other and therefore display a common linear law behaviors. However at a time near the cross-over time when the typical bump size reaches the system size, the system is affected strongly by its size. Obviously it takes longer time for a larger system when a typical bump develops and finally reaches the system size. This leads to what we can see in Fig.7.3 and 7.4: the larger the system is, the later the cross-over takes place. In the long time limit (see Fig.7.4) all systems lose the memory of the size and present a common behavior: a quasi-1D behavior which is characterized by the power law behavior of the displacement with $\nu_1 = 0.51$.

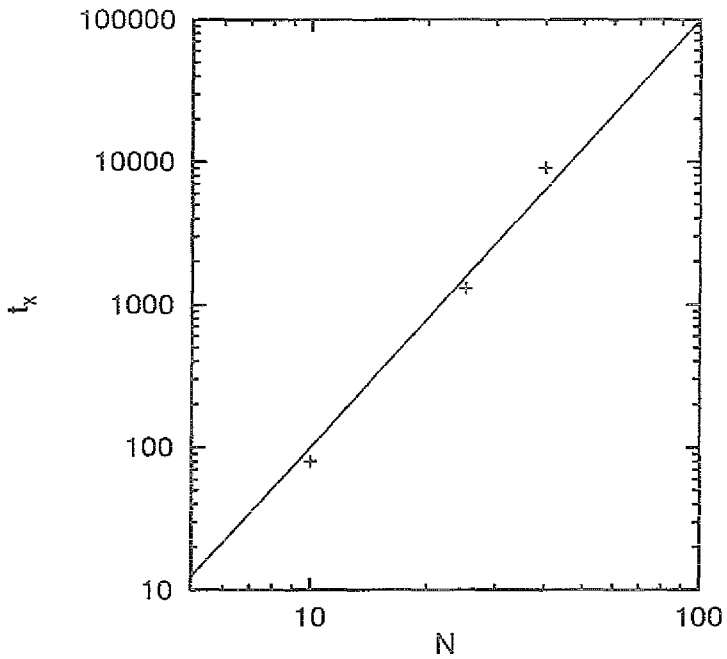


Figure 7.5: Log-log plot of the cross-over time $t_x$ as a function of the system size N. The fitting line is $t_x \sim N^3$.

Fitting the initial behavior and the asymptotic behavior of each curve in Fig.7.4 to two straight lines, we estimate the cross-over time for the three systems. Fig.7.5 shows the size-dependence of the cross-over time on the log-log plot and it can be fitted by a straight line with a slope around 3. So the cross-over time $t_x$ at which the interface cross over from the behavior of (7.2) to that of (7.3) dependents on the system size,

$$t_x \sim N^z, \tag{7.4}$$

where $z$ is the dynamic exponent.

So for a finite-size system with moderate bond energy at the very beginning of growth ($t \ll t_x$) the interface advances steadily in a undepinned state and at the long time limit ($t \gg t_x$) it becomes pinned; In between it is strongly affected by its size. This scenario will be further elucidated later in the section 7.3.2.

## 7.3 The Bond Energy Effect

### 7.3.1 Bond Energy Dependence of the Exponent $\nu_1$

Now we examine the effect of the bond energy $\epsilon$ on the dynamic exponent $\nu_1$ for a given system size $N$. The exponents $\nu_1$ are obtained from the simulations up to the time $t = 10^5 \sim 10^6$ and $\langle h(t) \rangle$ have been averaged over $100 \sim 1000$ realizations of randomness. We studied seven systems with sizes ranging from 25 to 2000 and the results of the bond energy $\epsilon$ dependence of the exponent $\nu_1$ are summarized in Fig.7.6. It clearly shows that there is an evident size- and bond energy-dependence of the interface dynamics. We can divide the bond energy dependence of $\nu_1$ into four characteristic regimes; (a), (b), (c) and (d), as is exemplified in Fig.7.6 for the system with a size $N = 40$.

(a) Jump Regime – For $\epsilon = 0$, $\nu_1$ has theoretically the value 0.51 since the 2D lattice becomes 1D one due to lacking correlations among atomic columns. The exponent $\nu_1$ increases sharply from the 1D value, 0.51, to unity in a very short range of energy from 0 to $0.1T_A$.

(b) Steady-state velocity regime – For moderate bond energies ($> 0.1T_A$), the interface obtains a steady-state velocity and its displacement grows linearly with time; The exponent has the value 1 in this regime: $\nu_1 = 1$. This is quite a surprise since the interface of a 1D chain gets completely pinned at the concentration $c = 0.4$ and temperature $T = 0.5$. The energy range where $\nu_1$ remains unity varies with the system size. The larger the system size N is, the wider the range becomes. For example, this range falls in $0.1T_A \sim 1T_A$ and $0.1T_A \sim 1.5T_A$ for $N = 40$ and 70, respectively. However, the interface of a system with size 2000 moves always steadily in our time-limited simulations.

(c) Transit Regime –If the bond strength $\epsilon$ exceeds the critical value $\epsilon_c(N)$ then $\nu_1$ starts to decrease. For the reason of easy operation we define $\epsilon_c$ as the value of the bond energy when $\nu_1$ drops from 1 to 0.9. The so defined critical value $\epsilon_c$ is found to increase linearly with the system size $N$, as is shown in Fig.7.7. Note that the results in Fig.7.3 belong to this regime.

(d) Pinned Regime– For a strong enough bond energy $\epsilon$, the exponent $\nu_1$ eventually approaches to the 1D value 0.51. This regime has been studied

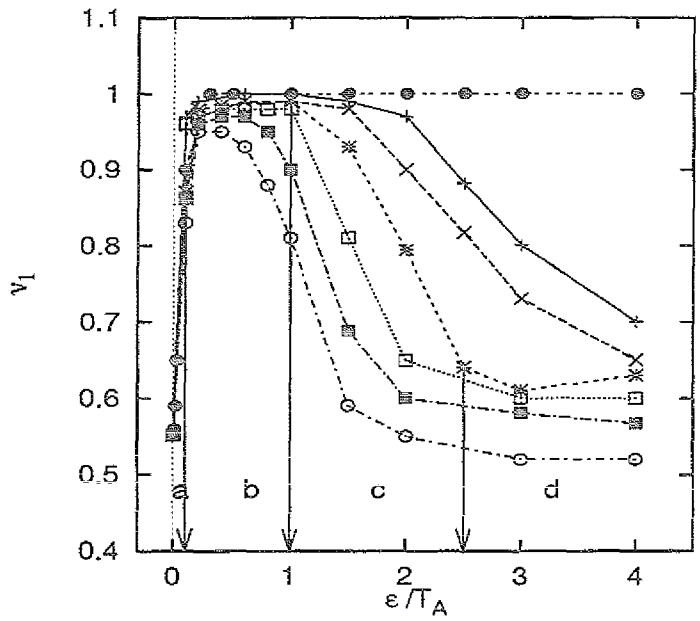


Figure 7.6: Dependence of the dynamical exponent $\nu_1$ on the bond energy $\epsilon$. Curves from bottom to top correspond to system sizes $N$ =25,30,40,50,70,80 and 2000. data are obtained from the simulations performed up to the time $10^6$.

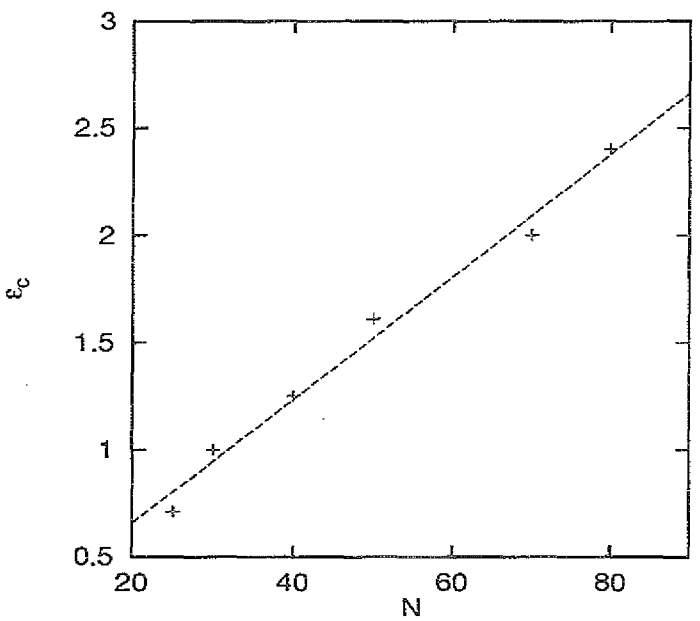


Figure 7.7: Dependence of critical bond energy $\epsilon_c$ on the system size $N$.

in detail in the previous section 5 theoretically and in the section 7.1 by the simulations.

It is worth mentioning that the results presented in Fig.7.6 are obtained from time-limited ($10^5 \sim 10^6$) simulations. If we could perform simulations for infinite time ($t \gg t_\times$ or $t \to \infty$), then the picture in Fig.7.6 should look totally different; all $\nu_1$ have the 1D value 0.51!

### 7.3.2 Very Small Bond Energy Regime

For very small but non-zero bond energy ($\epsilon/T_A \ll 1$ ), namely the jump regime of the two-phase region in Fig.7.6, the interface is pinned and therefore does not have a steady-state velocity. The fact that the exponent $\nu_1$ increases from the value 0.51 of a 1D system, or namely the case $\epsilon = 0$ in a 2D system, to 1.0 when $\epsilon$ is around $0.1T_A$ reveals that the 2D effect on the system gets stronger as $\epsilon$ increases. Pinning for small bond energy $\epsilon$ can be understood by the following picture: treat the very small energy $\epsilon$ as a perturbation for the zero-$\epsilon$ case. In the absence of the bond energy, there exists no correlation between neighboring atomic columns in the 2D system and it becomes simply a pile of 1D chains. Once an atom is pinned, it will stay in the pinned state until be excited into unpinned state by the external driving force $H$ and gets no help from its neighbors. Therefore, the interface is rather corrugated and interspersed with many ditches with a B atom sitting at the bottom. Therefore, the dynamic exponent $\nu_1$ can be approximately expressed as

$$\nu_1 \approx \frac{H}{H_c} = \frac{C_0 - c}{C_0 - C_s}. \tag{7.5}$$

Here $H_c$ is the critical driving force which separates the moving interface (when $H > H_c$) from the pinned interface (when $H < H_c$) for a one-dimensional diffusionless disordered alloy system. The above formula (7.5) shows a linear dependence of $\nu_1$ on c. The suitability of this approximation (7.5) can be verified by Fig.3.5 where the solid line shows a approximately linear decrease of $\nu_1$ from 1 at $c = C_s$ to 0 at $c = C_0$ in the solid side of the two-phase region.

As the small bond energy is introduced, the atoms in different columns start to affect each other. The bond energy plays a role of an extra driving

force which always tries to make the pinned atomic column catch up with its two neighboring advancing columns. In consequence, when the pinned atom solidifies the system gets energy gain not only from the driving force $b(C_0 - c)$ but also from the bond energy $2\epsilon$ with its two neighboring atoms. According to (7.5), $\nu_1$ can be now approximately written as

$$\nu_1 \approx \frac{H}{H_c} = \frac{b(C_0 - c) + 2\epsilon/T_A}{b(C_0 - C_s)}. \tag{7.6}$$

This formula shows a linear dependence of $\nu_1$ on $\epsilon$. Roughly speaking, this is what we have seen in the jump regime of Fig.6. Because of the extra driving force $2\epsilon$, the real external driving force $b(C_0 - c)$ required to keep the interface steadily moving becomes smaller than that $(b(C_0 - C_s))$ in the zero $\epsilon$ case. In other words, even for $b(C_0 - c) < H_c$, or $c > C_s$, it is still possible that the interface moves steadily provided that $\epsilon$ is bigger than a critical value $\epsilon^*$ which satisfies the condition: $\nu_1(\epsilon^*) = 1$. In the case studied here ($c = 0.4, b = 0.8, C_s = 0.31$ and $C_0 = 0.5$), $\epsilon^*$ is about $0.04T_A$ from the formula (7.6) by letting $\nu_1 = 1$. The value of $\epsilon^*$ measures from the simulation as around $0.1T_A$ (see Fig.7.6). This means that the interface gets pinned when $\epsilon < \epsilon^*$, but unpinned when $\epsilon > \epsilon^*$ in the two-phase region of the equilibrium phase diagram for very small $\epsilon$. In addition, $\epsilon^*$ varies with the concentration and the temperature. Note that this argument applies only to the very small $\epsilon^*$ case where such an interface structure of a single pinned atomic column surrounded by two much advanced columns could exist and $\epsilon^*$ can be considered as a perturbation. Thus both for very large and very small bond energy in a finite system the interface is pinned. However that the latter result applies only to models of SOS-type and probably not to systems with overhangs.

## 7.4 Depinning of Large Systems

In the previous sections, we have seen that the properties of a 2D system depends strongly on the two parameters: the size N and the bond energy $\epsilon$. In the limit of large energy ($\epsilon \to \infty$) the system loses its 2D features and behaves

effectively like its 1D counterpart. On the contrary, in the limit of large system size ($N \to \infty$), the crystal grows steadily for the concentrations $c < C_0(T)$ if $\epsilon > 0.1T_A$ (see Fig.7.6 for $N = 2000$). Here the critical concentration $C_0$ is defined in Eq.(3.49), and takes the value 0.5 at $T = 0.5$.

Our concern hereafter in this section is the growth law in the two-phase region; how does the growth depend on the driving force $H \propto C_0 - c$ for a very large system in the two-phase region? Fig.7.8 shows the simulation results of the velocity of a solidification front as a function of the driving force $H \propto 0.5 - c$ for a large system with size $N = 2000$. Three different bond energies are considered: $\epsilon/T_A = 1.0$, 1.5 and 2.0. The simulation has been performed only once for each parameter set, but statistics are sufficiently good due to the large system size.

Figure 7.8 clearly shows that the velocity of the front increases systematically with the driving force $H$. Generally, we can not formulate the $H$-dependence of $v$, but for a very small driving force we shall make it in the spirit of a driven elastic manifold[60, 81, 62, 63]. Our picture of the interface motion is as follows. In the absence of an external driving force $H = 0$ or $c = C_0 = 0.5$, the interface moves until it finds a configuration with a local minimum of the energy, whereupon it is pinned. If we drive a system with a non-zero force

$$H = b(0.5 - c), \tag{7.7}$$

the interface tends to move in the direction of $H$, but the pinning force $f$ tends to block the motion. Here above $b$ is a constant. As soon as the pinning force $f$ is overcome by the external driving force $H$ and the restoring force $F_s$ generated by the local curvature of the interface (or surface), the interface begins to move with a finite velocity. For a very small field $H$ the motion may not be uniform. At a given instant the interface may consist of pinned and unpinned regions. The height difference between the pinned and unpinned region increases in time, and thus the interface should be randomly corrugated with large amplitudes. But once the combined effect of the driving and restoring forces overcome the pinning forces in some pinned region, the interface jumps over the pinning sites and begins to move until it is stopped

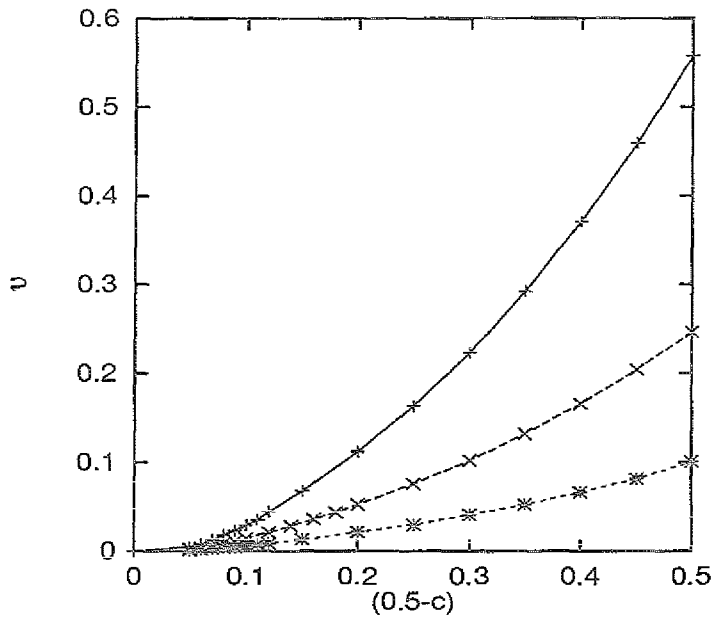


Figure 7.8: Dependence of the velocity $v$ on the concentration difference $(0.5 - c)$. The system size is $N = 2000$ and the bond energies are :$\epsilon$=$1.0T_A(+), 1.5T_A(\times)$ and $2.0T_A(*)$, respectively.

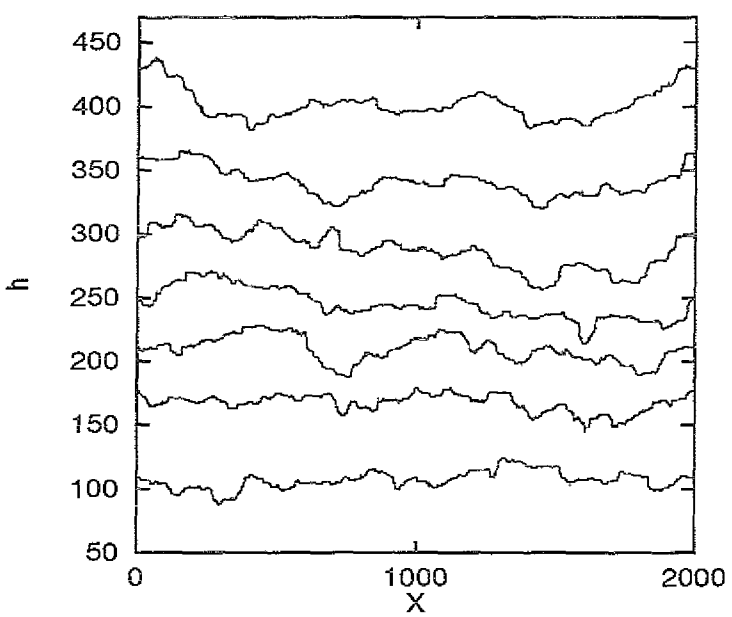


Figure 7.9: Time evolution of an interface profile of a 2D system under a small driving force : $0.5 - c = 0.08$. The system size is $N = 2000$ and the bond energy is $\epsilon = 2.0T_A$. Time increases from the bottom to the top. Note that the vertical and horizontal scales are different.

again by another region of strong pinning sites. Thus the interface exhibits a slow, smooth motion interspersed with jumps. After waiting times which are typically long in comparison with the time to move from one pinned state to the next the interface jumps over the pinning center and then moves on continuously until the next stop at a pinning site. The interface velocity $v$ thus is expected to be inversely proportional to the waiting time $t_w$ for a jump. Typical interface profiles of the system are shown in Fig.7.9. From the bottom to the top one can observe the time evolution of an interface profile and the eye can readily recognize that the roughness increases in time.

We now estimate this waiting time $t_w$. The randomly quenched B atom on the site $i$ corresponds to a pinning center against the solidification front with a pinning force $f_i$. Let us consider the case that the interface has to jump over a pinning region with an extension $l$ and a height $h$. This region pins the solidification front because it has more B atoms than the expected average value and the liquid phase is favored with an energy gain $\sim \Delta(hl)^{1/2}$. Here $\Delta$ is a prefactor characterizing the effective strength of the random pinning force and is proportional to the quantity $< f_i f_j >$. For the interface to pass over this region, it has to pay the energy penalty

$$u_r \sim \Delta(hl)^{\frac{1}{2}}. \tag{7.8}$$

in order to pass over this region. However the interface deformation costs surface energy and therefore the jump makes the interface to gain the surface energy

$$u_s \sim \gamma(\frac{h}{l})^2 l, \tag{7.9}$$

where $\gamma$ is the surface tension. The solidification of the volume $hl$ by the uniformly applied driving force $F$ leads to the energy gain

$$u_d \sim Hlh. \tag{7.10}$$

By assuming that the jump takes place when all the competing energies are of the same order as $u_s \sim u_r \sim u_d$, the pinning region to be jumped over has the following characteristic length scales

$$l \sim \gamma^{\frac{1}{3}}\Delta^{\frac{2}{3}}/H, \qquad h \sim \Delta^{\frac{4}{3}}/H\gamma^{\frac{1}{3}}, \tag{7.11}$$

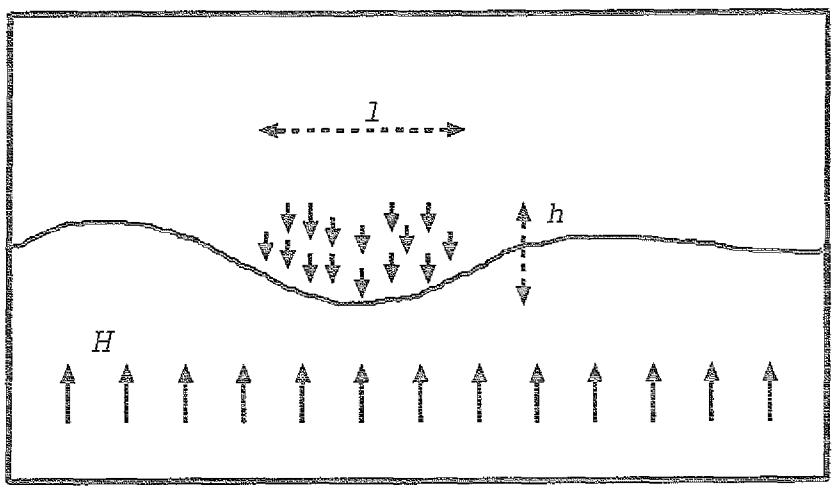


Figure 7.10: Schematic illustration of the pinning of an interface portion of length $l$ and height $h$. The local impurities (small arrows) oppose the motion of the interface, acting against the external driving force $F$ and the elastic force generated by the local curvature of the interface.

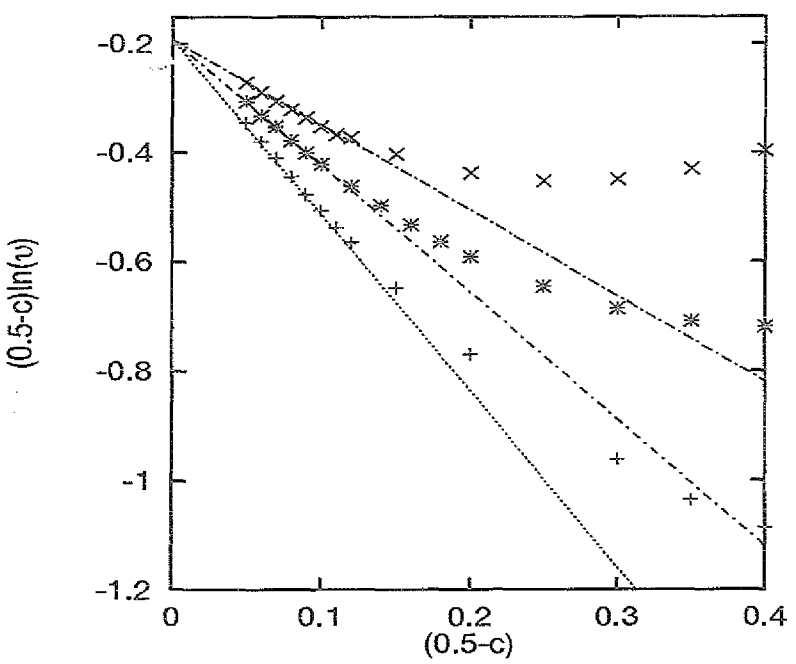


Figure 7.11: Dependence of the normalized velocity $(0.5 - c)\ln(v)$ on the concentration difference $(0.5 - c)$. The parameters are: $N = 2000$ and $\epsilon$=$1.0T_A(\times)$, $1.5T_A(*)$ and $2.0T_A(+)$, respectively.

and the characteristic energy

$$u = d\Delta^2/H, \tag{7.12}$$

where $d$ is some constant of order unity. Assigning $u$ to be the height of the energy barrier over which the interface has to jump, we estimate the waiting time for the interface as

$$t_w \sim e^{u/T}. \tag{7.13}$$

The velocity of the interface is simply the inverse of the waiting time, and can be expressed as

$$v = g \exp\left(\frac{-d\Delta^2}{HT}\right) \tag{7.14}$$

where $g$ is a prefactor. Thus for small driving force $H$ the velocity $v$ is expected to decrease exponentially with $H^{-1}$.

In order to check the above ideal, we obtain the following relation by inserting $H$ in Eq.(7.7) into (7.14) and then taking the logarithm of its both sides

$$(0.5 - c)\ln(v) = -\frac{d\Delta^2}{bT} + (0.5 - c)\ln(g). \tag{7.15}$$

As the driving force $(0.5-c)$ approaches zero the value of $(0.5-c)\ln(v)$ changes linearly and reaches the value $-d\Delta^2/bT$ at $H = 0$. The linear law is verified by the numerical simulations. Fig.7.11 shows the value of $(0.5 - c)\ln(v)$ as a function of $(0.5 - c)$ for three various bond energies: $\epsilon/T_A = 1, 1.54$ and 2. In the vicinity of zero driving force all data points can be fitted by three different straight lines which cut the vertical axis at the same point 0.192 independent of $\epsilon$ at $H = 0$. Since the temperature is $T = 0.5$, so $d\Delta^2/b$ is estimated about 0.096.

Next we shall now estimate the constant $b$ and the strength of the pinning force $\Delta$. One starts from the analysis of the free energy of a binary lattice system without concentration fluctuation. By solidifying $M = hl$ atoms, the system gain free energy which can be written as

$$u_d = -M[\Delta\mu_A(1 - c) + \Delta\mu_B c]. \tag{7.16}$$

The two terms on the RHS of the above equation represent the free energy gained by solidification of an A and a B atoms, respectively. Now introducing the local concentration fluctuations, we can write the total free energy gain as

$$\begin{aligned} u &= -\sum_{i=1}^{M}[\Delta\mu_A(1-c_i)+\Delta\mu_B c_i] \\ &\approx -M[\Delta\mu_A[1-(c\pm\overline{\Delta c})]+\Delta\mu_B(c\pm\overline{\Delta c})] \\ &= -M[\Delta\mu_A(1-c)+\Delta\mu_B c]+\pm M\overline{\Delta c}(\Delta\mu_B-\Delta\mu_A) \\ &= -MH\pm M\overline{\Delta c}(\Delta\mu_B-\Delta\mu_A). \end{aligned} \tag{7.17}$$

Here $\overline{\Delta c}$ is the concentration fluctuation, $\overline{\Delta c}=\sqrt{<(\Delta c)^2>}$, and is estimated as follows. Since the probability $p(M,m)$ of finding $m$ B atoms at $M$ given sites obeys the binomial distribution

$$p(M,m)=\frac{M!}{m!(M-m)!}c^m(1-c)^{M-m}. \tag{7.18}$$

For a sufficiently large number of lattice sites ($M\to\infty$), the above distribution becomes Gaussian distribution

$$p(M,m)\approx\frac{1}{\sqrt{2\pi Mc(1-c)}}exp(-\frac{(m-Mc)^2}{2Mc(1-c)}). \tag{7.19}$$

The mean value and the mean square fluctuation of the number $m$ of B atoms can be read off directly from the above Gaussian distribution as

$$<m>=Mc \tag{7.20}$$

$$<(m-Mc)^2>=Mc(1-c). \tag{7.21}$$

Then

$$\overline{\Delta c}=\sqrt{\langle\left(\frac{m}{M}-c\right)^2\rangle}=\sqrt{\frac{c(1-c)}{M}}. \tag{7.22}$$

Substituting the expressions (7.22) into formula (7.17) and using the parameters $L_A/T_A=L_B/T_B=1, T_A=0.9, T_B=0.1$ and $T=0.5$, the free energy gain is found to be

$$u=-0.8M(0.5-c)\pm 0.8\sqrt{M}\sqrt{c(1-c)}. \tag{7.23}$$

Notifying that $M = hl$, the first term on the RHS corresponds to the bulk driving energy $u_d$, (7.10) and the second term corresponds to the random field contribution $u_r$, (7.8). Then the driving field is identified from (7.10) and (7.23) as

$$H = 0.8(0.5 - c), \tag{7.24}$$

and the strength of the random field (7.8) and (7.23) as

$$\Delta = 0.8\sqrt{c(1-c)}. \tag{7.25}$$

At the mean concentration, $c$ =0.5 the driving force $H$ becomes zero and the strength of the random force $\Delta$ becomes 0.4. From the expression (7.24) and (7.7), we obtain the prefactor $b$ being 0.8. From $\Delta = 0.4$, $b = 0.8$ and the estimate $d\Delta^2/b \approx 0.096$ obtained by the simulation, $d$ is determined to be 0.5, of order unity as expected.

It is worth mentioning that the driving force $H$ used here is two times of $F$ used in the RFI model (4.11): $H = 2F$. The factor 2 results from the fact that the energy gain is $2\,u_d$ when atoms change states from liquid to solid, or in terms of RFI model, spins flip from downwards ($s_i = -1$) to upwards ($s_i = +1$).

## 7.5 The Velocity for Very Large Bond Energy

The interface velocity of a large system should be a function of bond energy and the driving force at fixed temperature : $v(\epsilon, H)$ or $v(\epsilon, c)$ which generally can not decoupled. Although we do not have a theory to write $v(\epsilon, c)$ down explicitly, by computer simulation we do can investigate some properties of $v(\epsilon, c)$ in some extreme conditions. In the previous section we have found that $\epsilon$ and $c$ affect $v$ separately in the vicinity of zero driving force, namely $v(\epsilon, H)$ can be written as

$$v(\epsilon, c) = \varphi_1(\epsilon)\varphi_2(c), \tag{7.26}$$

with $\varphi_1(\epsilon) = g$ in (7.14), where $\varphi_1(\epsilon)$ is a function of $\epsilon$ and $\varphi_2(c)$ is a function of c. Now we ask how $v$ depends on $\epsilon$ when $\epsilon$ is large. Obviously, the larger

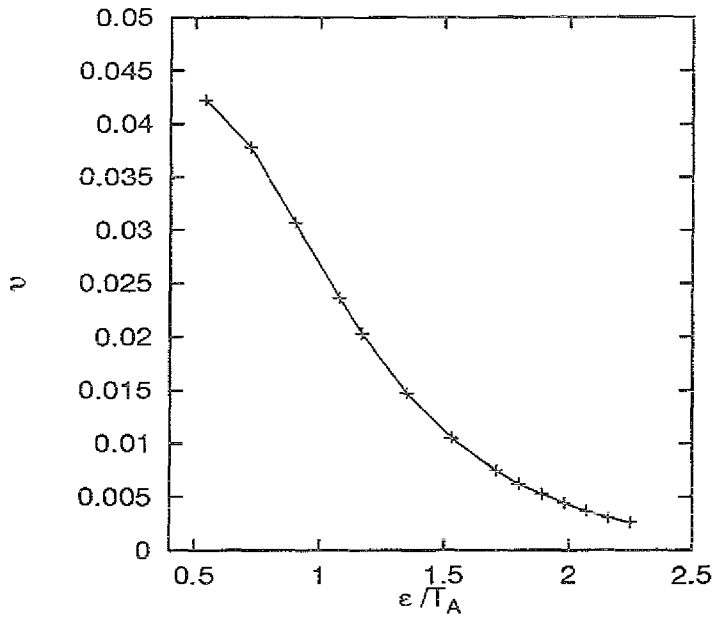


Figure 7.12: Dependence of the interface velocity $v$ on the bond energy $\epsilon$. The parameters are: $N$ =2000, $T$ =0.5, $c$ =0.4. Simulation is performed up to the time $10^5$.

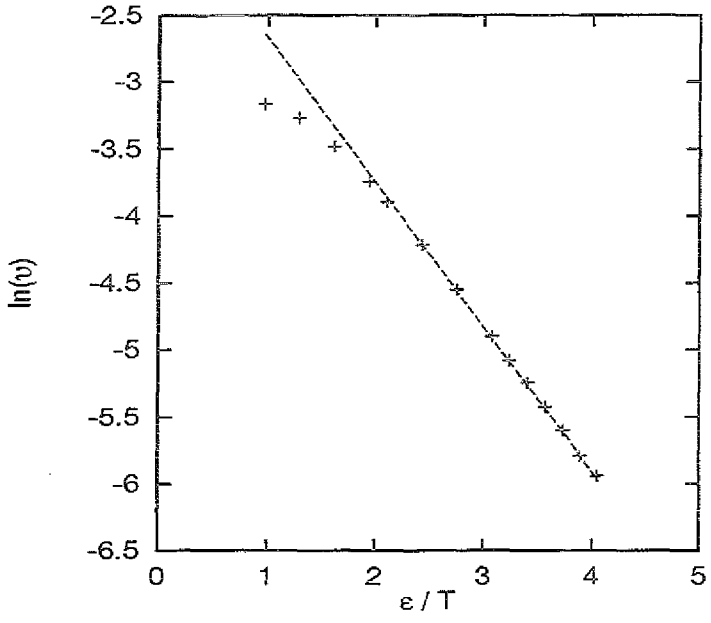


Figure 7.13: Logarithm of the velocity $ln(v)$ versus the bond energy $\epsilon/T$. The parameters are: $N$ =2000, $T$ =0.5, $c$ =0.4. Simulation is performed up to the time $10^5$. The fitting line has the slope around 1.06.

the bond energy is, the more difficult it is for the interface to move. Fig.7.8 clearly shows this tendency where the velocity curve for larger $\epsilon$ is lower than that for smaller $\epsilon$. For a systematic study of the $\epsilon$-dependence of the velocity, we fix the concentration $c = 0.4$ and vary $\epsilon$. Fig.7.12 shows the result for the system size $N = 2000$ and $T = 0.5$. From the figure we can see that the velocity decays with increasing the energy $\epsilon$. Generally we cannot formulate the velocity as a function of $\epsilon$, but for large energy things become simple. For large energy the interface is almost flat, but still a few kinks are always excited thermally since the system size is large enough. The density of those thermally excited kinks is proportional to $\exp(-\epsilon/T)$ and they act as a solidification center. With increasing energy the difficulty of creating a kink increases as well and therefore fewer kinks exist. Because the propagation of a kink along the interface is much faster than creating it, we can safely predict that the velocity decays in the same manner as the number of kinks: $v \sim \exp(-\epsilon/T)$. Fig.7.13 shows the data of Fig.7.12 in a semilogarithmic way. The data in the large $\epsilon/T$ range can be fitted by a straight line with slope around unity, which agrees quite well with the prediction! This argument is not applicable for small $\epsilon$ because multi-kinks exist on the interface.

Combining the above argument with the result (7.14), we get the velocity of the solidification front for an infinite system with large bond energy under very small driving force ($c$ being in the vicinity of 0.5) as

$$v = 1.5\, e^{-\epsilon/T} e^{-0.5\Delta^2/HT} \qquad when \quad \begin{cases} N & \to & \infty \\ H & \to & 0 \\ \epsilon & \to & \infty. \end{cases} \tag{7.27}$$

Here the prefactor 1.5 is estimated from Fig.7.11.

Some comments may be necessary concerning a small system. As is shown in chapter 5 explicitly the velocities of small systems are proportional to $\exp(-2\epsilon/T)$ for $\epsilon_s = \epsilon_l = \epsilon$. This is due to the fact that the creation of an initial nucleus is required in these small systems, because there exists usually no kinks at all at sufficiently large bond energy and low enough temperature.

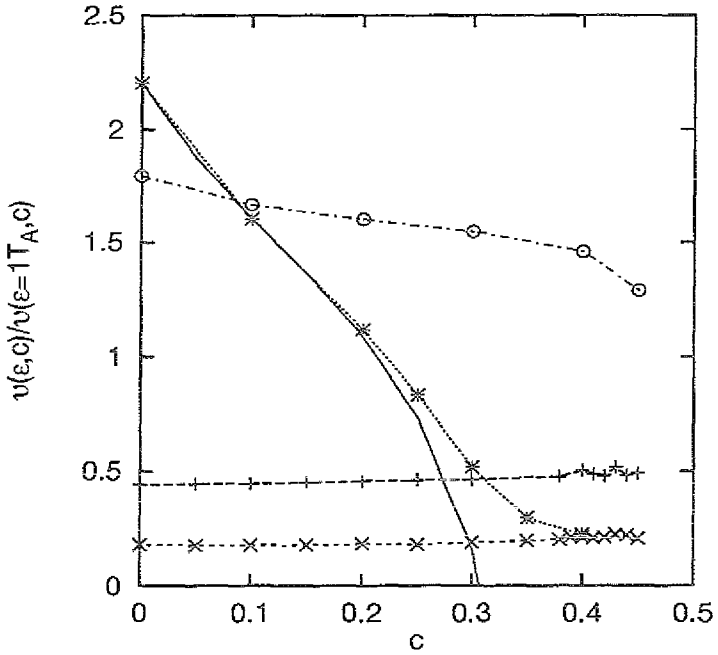


Figure 7.14: The ratio of the velocity $v(\epsilon, c)$ to the velocity $v(\epsilon = 1\,T_A, c)$ versus the concentration c for four various $\epsilon$. The bond energies are : $\epsilon = 0$ (symbol $*$), $0.5\,T_A$ (symbol $\circ$),$1.5\,T_A$ (symbol $+$) and $2.0\,T_A$ (symbol $\times$). The solid line represents the exact 1D results from (3.53). Other parameters are: $N$ =2000, $T$ =0.5 and $c$ =0.4. Simulation is performed up to the time $10^5$.

The Eq.(7.27) tells us that in the two phase region( c=0.4) for very large $\epsilon$, the bond energy-dependence and concentration-dependence of the steady-state velocity of the interface can be decoupled. Actually this is not a unique property for the two phase region, but for one-phase region too. So if formally we can write the velocity as

$$v(\epsilon, c) = \varphi_1(\epsilon)\varphi_2(c), \tag{7.28}$$

then we can get the following ratio of two velocities for same concentration

$$\frac{v(\epsilon_1, c)}{v(\epsilon_2, c)} = \frac{\varphi_1(\epsilon_1)}{\varphi_1(\epsilon_2)} = \varphi(\epsilon_1, \epsilon_2). \tag{7.29}$$

The means that the ratio of velocities of two systems with bond energies $\epsilon_1$ and $\epsilon_2$ is independent of the concentration, if $\epsilon_1$ and $\epsilon_2$ are large enough.

This prediction has an excellent agreement with the compute simulations(see Fig.7.14)! Fig.7.14 shows the ratio $v(\epsilon, c)/v(\epsilon = 1T_A, c)$ versus the concentration c for four various $\epsilon_1$. For the large energies: $\epsilon = 1.5\,T_A$ (symbol +) and $2.0\,T_A$ (symbol $\times$ ), the ratio is almost a constant in the whole range of concentration; For the moderate energy: $\epsilon = 0.5\,T_A$ ( symbol $\circ$ ), the ratio decreases with c increases; For zero energy: $\epsilon = 0$ (symbol $*$), the ratio should follow the solid line which is the exact 1D results from (3.53), but actually it does not vanish in the two-phase region due to the limited simulation time.

So we conclude that for very large bond energy the influences of the bond energy and concentration on the velocity of a large system can be always decoupled as the product of a function of $\epsilon$ : $\varphi_1(\epsilon)$ and another function of $c$ : $\varphi_2(c)$. Although we do not know the expressions of $\varphi_1(\epsilon)$ and $\varphi_2(c)$ generally, we have found : $\varphi_1(\epsilon) = e^{-\epsilon/T}$ in the two phase region and $\varphi_2(c) = e^{-d\Delta^2/HT}$ in the vicinity of $C_0$.

## 7.6 Correlation Length

In the section 7.2 we have observed that the interface displacement crosses over from an initially depinned to a finally pinned state as time proceeds. This question may appear elementary, but it has no simply answer. The fact that the cross-over time, $t_\times$, increases with the system size $N$ suggests that cross-over phenomena constitute a finite size effect. But What is the mechanism that leads to the transition? How does the system know when to undergo a depinning-pinning transition? To answer these questions, we must discuss a very important property of most surfaces, the existence of correlations in the system which imply that different sites of the interface are not completely independent, but upon the heights of the neighboring sites. Through a close examination of the growth process, we can gather some clues about it. Figure 7.15 illustrates our growth model. Shown is the case $N = 11$, where N is the number of columns. There are four most possible sites where atoms can change their states from liquid to solid state. After the transition, the height of the column will be equal to or larger than that of its neighbors. From the

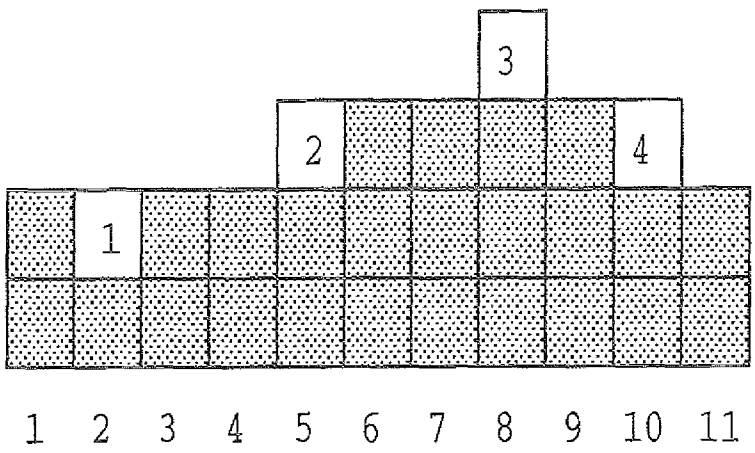


Figure 7.15: The lattice model. Shown is the case $N = 11$, where $N$ is the number of columns.

model, the interface of a column has less chance to move if it is higher than its neighbors in both sides after moving (case 4). However, those columns with interfaces lower than at least one of the two neighbors are easy to move. In this way the neighboring columns are strongly influenced by each other. The height fluctuation will spread laterally, because the newly growing interface of a column must have height equal to or larger than its neighbors, but the height difference can not be very large. Although the growth process is local, through this lateral growth the information about the height of the neighbors spreads globally.

The correlation length $\xi_{//}$ is just the typical distance over which the heights know about each other. At the beginning of the growth, the sites are uncorrelated. During the growth $\xi_{//}$ grows as well. For a finite system $\xi_{//}$ can not grow indefinitely, because it is limited by the size of the system N. When $\xi_{//}$ reaches the system size, the entire system becomes correlated, resulting in the cross-over of the interface behavior from (7.2) to (7.3). Thus after cross-over the correlation length $\xi_{//}$ is about the system size N,

$$\xi_{//} \sim N \qquad [t \gg t_\times]. \tag{7.30}$$

Depinning-pinning transition occurs at a time $t_\times$ given by (7.4). Replacing

N with $\xi_{//}$, we obtain $\xi_{//} \sim t_{\times}^{\frac{1}{z}}$, which in fact holds for $t < t_{\times}$ as well

$$\xi_{//} \sim t^{\frac{1}{z}} \qquad [t \ll t_{\times}]. \tag{7.31}$$

We define the following height-height correlation function

$$G(x,t) = \left\langle h(x',t)^2 \right\rangle - \left\langle h(x',t)\, h(x'+x,t) \right\rangle . \tag{7.32}$$

Here $x'$ and $x+x'$ are two different lattice sites separated by a distance $x$ and $h(x',t)$ denotes the height of the interface at site $x'$ at time $t$. $< ... >$ means the average over all sites $x'$ keeping the separation $x$ fixed. The simulation results of $G(x,t)$ versus the $x$ at various times on the log-log plot are shown in Fig.7.16. It is apparent in Fig.7.16 that there are two regions separated by the correlation length $\xi_{//}$ at a given time:
(i) For small separation distance $x$, the correlation function increases as a power of x,

$$G(x) \sim x^{\beta} \qquad [x \ll \xi_{//}]. \tag{7.33}$$

Here $\beta$ is an exponent.
(ii) The power-law increase in correlation function does not continue indefinitely, but is followed by a saturation regime ( the horizontal region of each curve in Fig.7.16), during which the correlation function reaches a saturation value, $G_{sat}(t)$. In Fig.7.16, twelve different curves correspond to the correlation functions at twelve different times t. As time increases, the saturation value, $G_{sat}(t)$, increases as well.

(iii) The correlation length $\xi_{//}$ at which the correlation function, $G(x,t)$, crosses over from the behavior of (7.33) to saturation has been found by the simulation to increase with the time. Fig.7.17 shows the simulation results (symbols) of the correlation length $\xi_{//}$ as a function of time for a system with size $N$ =2000, concentration $c$ =0.4 and bond energy $\epsilon = 1.5\, T_A$ at temperature $T$ =0.5. The fitting curve $\xi_{//} \sim t^{\frac{1}{3}}$ is drawn just as a guide to the eyes. At a given time the correlation function increases with the separation $x$ but saturates for $x$ larger than the correlation length $\xi_{//}$: The correlation extends up to $\xi_{//}$ but two points on the interface separated by more than $\xi_{//}$

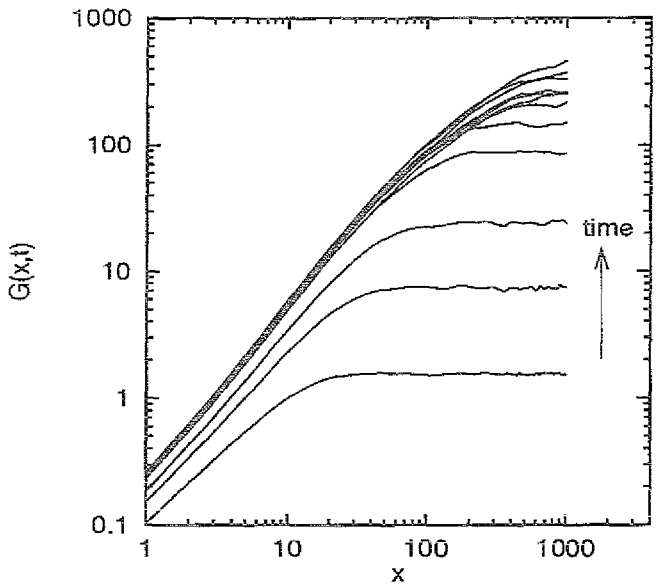


Figure 7.16: The height-height correlation function $G(x,t)$ versus the separation distance $x$ at various times on the log-log plot. From the bottom to the top time increases up to $10^5$. The chosen parameters are : $N$ =2000, $c$ =0.4, $T$ =0.5, $\epsilon = 1.5\,T_A$. Data is obtained for 50 independent runs.

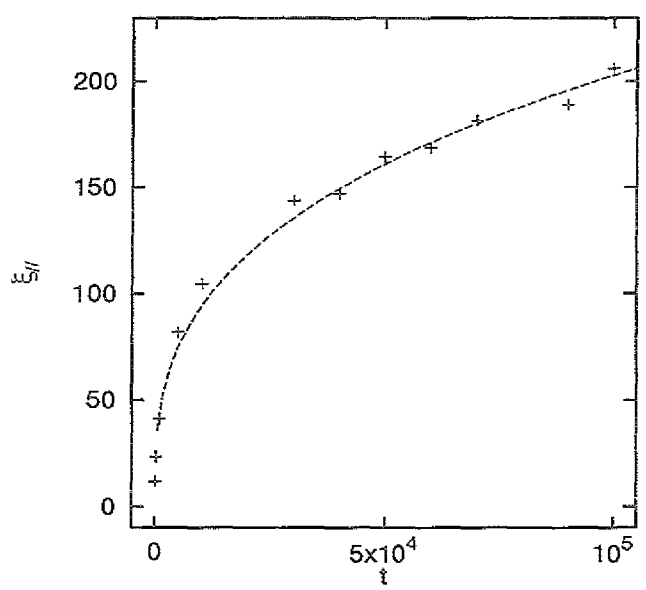


Figure 7.17: Correlation length $\xi_{//}$ versus the time $t$. The simulation is performed with the system size $N$ =2000, $\epsilon = 1.5T_A$, $T$ =0.5 and $c$ =0.4. The curve $\xi_{//} \sim t^{\frac{1}{3}}$ is just for the guide to the eyes.

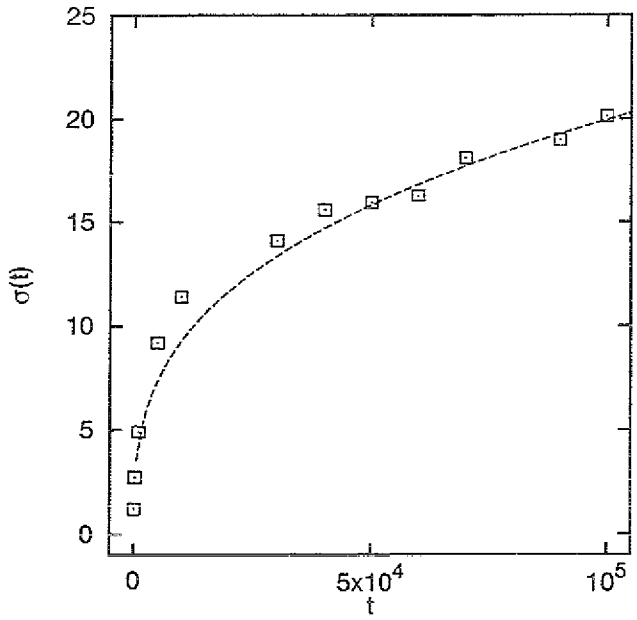


Figure 7.18: Time evolution of the width of the interface $\sigma(t)$. The curve $\sigma(t) \sim t^{\frac{1}{3}}$ is just for the guide to the eyes.

are uncorrelated. As time proceeds the correlation-length $\xi_{//}$ increases with time, as is shown in Fig.7.17.

For $x \gg \xi_{//}$ when $t \ll t_\times$ the correlation of the interface at two sites is lost, and therefore the $< h(x') >$ is independent of $< h(x+x') >$. In this case the correlation function (7.32) has the following property

$$\begin{aligned} & \lim_{x\to\infty} G(x,t) \\ = \; & < h(x',t)^2 > - \lim_{x\to\infty} < h(x',t)h(x'+x,t) > \\ = \; & < h(x',t)^2 > - < h(x',t) >< h(x'+x,t) > \\ = \; & < h(t)^2 > - < h(t) >^2 \\ = \; & \sigma^2(t) \end{aligned} \tag{7.34}$$

This means that the saturation value $G_{sat}(t)$ of the correlation function in the limit of large separation $x$ is equal to the variance $\sigma^2(t)$ of the interface position $h(t)$. Note, however, that the width of the interface at long times scales with the systems size as $\sigma \sim N^{0.69}$ as can be read off the Fig.7.16.

Fig.7.18 shows the interface width $\sigma(t)$ as a function of time t. At time $10^5$, $\sigma(t)$ is about 20, which is at least less than one-fiftieth of the width of the interface in a 1D system with the same concentration (c=0.4)(see Fig.3.3(b)). The thin interface width in the 2D system is due to the surface tension which tends to keep the interface as flat as possible.

The pinning-depinning crossover phenomena can be understood in terms of the correlation length and the finite size of the system. From the simulation of a rather large system $N = 2000$, we know how the correlation develops as time proceeds, as shown in Fig.7.17. For systems with small sizes the correlation should develop similarly. Therefore the time-dependence of the velocity can be related to the $\xi_{//}$-dependence of the velocity, as shown in Fig.7.19. It contains the information of four systems with different sizes. At the very beginning the interface is not affected by the system size and all systems behave in the same way. This corresponds to the common slope ($\sim 0.0263$) of the initial part of curves in Fig.7.4. As time passes and when the correlation length approaches the system size the interface starts to slow down and eventually the velocity becomes zero. This crossover from depinning to pinning takes place later if the system size becomes larger. For very large system ($N = 2000$), $\xi_{//}$ remains much smaller than $N$ and the interface stays in the depinned state with a steady-state velocity.

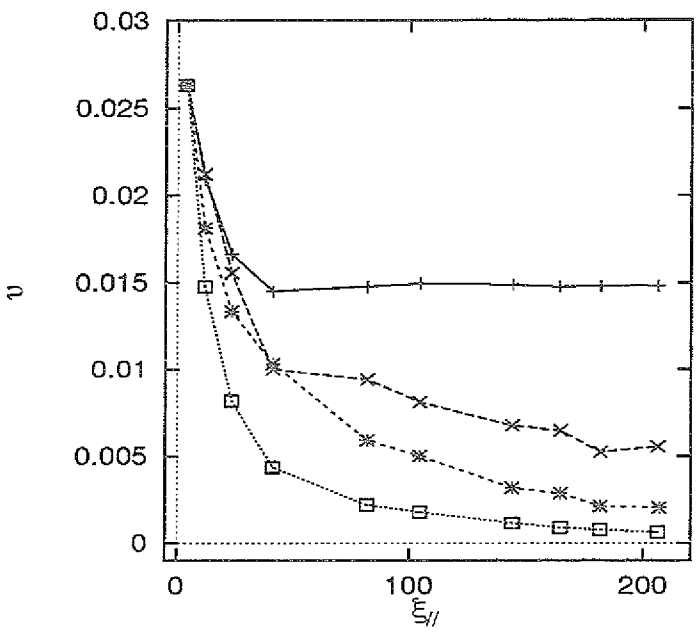


Figure 7.19: The velocity $v$ of the interface versus the correlation length $\xi_{//}$. The system sizes are $N$ =10,25,40 and 2000 from the bottom to the top, respectively.

# Chapter 8

# Solidification of a One-Dimensional System with Diffusion

In the previous chapters we study the propagation of the solidification front of an alloy system with quenched atomic configuration, i.e. no rearrangement of atoms allowed. We found that for a one-dimensional system with a zero-dimensional interface the interface does not advance steadily but shows an anomalous time dependence in the two-phase region. For a two-dimensional finite sized system with a one-dimensional interface, similar asymptotics is found in the limit of the large energy of kink formation.

In reality , however, atoms are not completely quenched but are moving and the concentration follows the diffusion law. The natural question then is how the diffusion affects the motion of the interface. In this chapter, we shall address this question by Monte Carlo simulation of a one-dimensional system and compare the results with an approximate analysis which neglects the correlations in the concentration distribution.

## 8.1 One-Dimensional Lattice Model with Diffusion

We use the same one-dimensional lattice model as the one described in the section 3.2 but with diffusion of atoms in stead of no diffusion. We consider a binary alloy system composed of atomic species of A and B, and denote the concentration of B atoms by $c$. Each atom can be either in solid or liquid state. We introduce the state variable $n_i$ which assumes the value zero or unity according to whether the site $i$ is occupied by an A or B atom, respectively. The average of $n_i$ over the whole lattice sites $L$ should be the given concentration $c$:

$$c = \frac{1}{L}\sum_{i=1}^{L} n_i \,. \tag{8.1}$$

On this chain we assume a single interface which separates the solid and liquid phases, for example, liquid above solid. The interface position $h$ is defined then as the lattice site of the highest solid atom. It can be either a species of A or B. If it melts the interface-height decreases by one lattice unit: $h \to h-1$. If the liquid atom above the interface solidifies, the interface advances by one unit: $h \to h+1$. The interface motion is assumed to take place stochastically following the master equation

$$\begin{aligned} \frac{\partial P(h,t)}{\partial t} &= \sum_{\delta=\pm 1} W(h+\delta \to h)\, P(h+\delta,t) \\ &- \sum_{\delta=\pm 1} W(h \to h+\delta)\, P(h,t) \end{aligned} \tag{8.2}$$

where $P(h,t)$ is the probability that the interface is at the site $h$ at time $t$. The transition probabilities $W$ depend on the atomic configurations around the interface. We consider a model where the transition probability $W$ depends only locally on the type of particle which changes its state during melting or solidification. If the solid site $h$ is occupied by an X (= A or B) atom and the liquid site $h+1$ by a Y (= A or B) atom, then transition probability of the interface advancement is given by

$$W(h \to h+1) = \omega_{+Y} \tag{8.3}$$

and that of the interface retardation as

$$W(h \to h-1) = \omega_{-X} \tag{8.4}$$

The detailed balance condition requires that the kinetic ratio $\omega_{-X}/\omega_{+X}$ should be equal to the one $\exp(-\mu_X/T)$ determined by the thermodynamics:

$$\frac{\omega_{-X}}{\omega_{+X}} = e^{-\mu_X/T} \tag{8.5}$$

where X=A or B.

If the interface motion is so fast that there is no time for the atomic configurations to change while the interface traverses the whole system, the configuration can be regarded as being quenched. In reality the atoms are moving and the configuration changes according to the diffusion law;

$$\begin{aligned}\frac{\partial Q(\{n\},t)}{\partial t} &= \sum_{\delta=\pm 1} W_D(n'_i, n'_{i+\delta} \to n_i, n_{i+\delta}) Q(\{n'\},t) \\ &- \sum_{\delta=\pm 1} W_D(n_i, n_{i+\delta} \to n'_i, n'_{i+\delta}) Q(\{n\},t)\end{aligned} \tag{8.6}$$

where $Q(\{n\},t)$ is the probability of finding the atomic configuration $\{n\}$ at the time $t$. The configurations $\{n'\}$ are different from the configurations $\{n\}$ by the exchange of states at the site $i$ and its neighbor $i+\delta$. Here we assume a simple diffusion such that the transition probabilities $W_D$ are constant and equal to the diffusion coefficient. In principle the diffusion coefficient in the solid, $D_S$, is different from that of liquid $D_L$. In this paper two typical cases are considered: the symmetric diffusion where $D_S = D_L$, and the one-sided diffusion where $D_S = 0$.

## 8.2 Monte Carlo Simulation

The motion of the interface is simulated by the Monte Carlo method. In the simulation, in principle, all the atoms in the chain have the possibility to move stochastically but the influence upon the interface motion is localized within the diffusion length $D_{S(L)}/v$ near the interface, when the interface is moving with the instantaneous velocity $v$. In the two-phase region the asymptotic

velocity is expected to vanish but within our simulation time less than $10^5$ one obtains a finite velocity. In order to save computing time we allow the diffusion of atoms within ranges of $l_S$ and $l_L$ from the interface in the solid and liquid phases, respectively, which are chosen sufficiently larger than the diffusion lengths.

The simulation proceeds as follows. Let the interface be located at a site $h$ between a solid X and a liquid Y atom, where both X and Y can be either of type A or B. After the time increment of

$$\Delta t = \frac{1}{(\omega_{-X} + \omega_{+Y} + D_S l_S + D_L l_L)}, \tag{8.7}$$

the interface advances forward with a probability

$$P_+ = \omega_{+Y}\, \Delta t, \tag{8.8}$$

recedes backward with a probability

$$P_- = \omega_{-X}\, \Delta t, \tag{8.9}$$

or one of the solid or liquid atoms in the range $l_S$ or $l_L$ from the interface exchanges its position with its neighboring solid atom above or liquid atom below with a probability

$$P_0 = D_S\, \Delta t \qquad \text{or} \qquad P_0 = D_L\, \Delta t. \tag{8.10}$$

Parameters are chosen to be the same as those in the work [34] for comparison; $T_A = 0.9$, $T_B = 0.1$, $L_A/T_A = L_B/T_B = 1$, $T = 0.5$ and $\omega_{+A} = \omega_{+B} = 1$. Thus the equilibrium concentrations are $C_S = 0.310$ and $C_L = 0.690$, and the melting probabilities are $\omega_{-A} = e^{-0.8} = 0.4493$, and $\omega_{-B} = e^{0.8} = 2.226$. The new parameters in the present study are the diffusion constants $D_S$ and $D_L$. They are chosen as $D_S = D_L = 1$ for the symmetric diffusion and $D_S = 0, D_L = 1$ for the one-sided diffusion. The length of the chain is chosen such as to be sufficiently larger than the displacement of the interface during the simulation. The range of diffusion is chosen in the largest case as $l_S = l_L = 1500$.

From the simulation we calculate the interface mean displacement $\langle h(t)\rangle$ and its variation $\sigma(t) \equiv \sqrt{\langle (h(t) - \langle h(t)\rangle)^2\rangle}$. Here $\langle A\rangle$ means the sample average of the quantity $A$ over at least 100 samples simulated. Their time variations are shown in Fig.8.1 for the case with the symmetric diffusion and in Fig.8.2 for the case with the one-sided diffusion. They depend on time asymptotically in power laws ; $\langle h(t)\rangle \sim t^{\nu_1}$ and $\sigma(t) \sim t^{\nu_2}$. The estimated exponents $\nu_1$ and $\nu_2$ are shown in Fig.8.3. In the diffusionless case ($D_S = D_L = 0$) our model can be mapped to the directed random walk with a waiting time distribution for forward interface jumps $F(\tau) \sim \tau^{-(1+\gamma)}$ with $\gamma = 1.25\ln(c^{-1} - 1)$, where the exact behavior of $\nu_1$ and $\nu_2$ are known

$$\begin{aligned} \nu_1 = 2\nu_2 = 1 \quad &\text{for} \quad 0 < c < c_2 = 0.168, \\ \nu_1 = 1, 2\nu_2 = 3 - \gamma \quad &\text{for} \quad c_2 < c < C_S, \\ \nu_1 = \nu_2 = \gamma \quad &\text{for} \quad C_S < c < 0.5. \end{aligned} \tag{8.11}$$

These exact results for the diffusionless growth are also shown in Fig.8.3 as solid and dashed lines. In the diffusionless growth the exponent $\nu_2$ increases anomalously above $1/2$ in the concentration range $c_2 < c < c_3 = 1/(1 + e^{0.4}) \approx 0.401$ due to the strong pinning effect of B atoms. With diffusion the anomalous increment of the interface width seems to be healed such that $\nu_2$ becomes closer to $1/2$. The reason might be that the large cluster of B atoms which pins the solidification front will be resolved by the diffusion of B atoms. Close to $c = 0.5$ the exponent $\nu_2$ seems to remain smaller than $1/2$ even with diffusion as in the case without diffusion. Concerning the exponent $\nu_1$ for the mean displacement one can observe that it takes the value close to $1/2$ in the region $c_3 < c < 0.5$ and remains larger than $1/2$ in the region $C_S < c < c_3$ at least in our time limited simulations. This result can be understood by the approximate analysis in the next section if the growth is controlled by the diffusion.

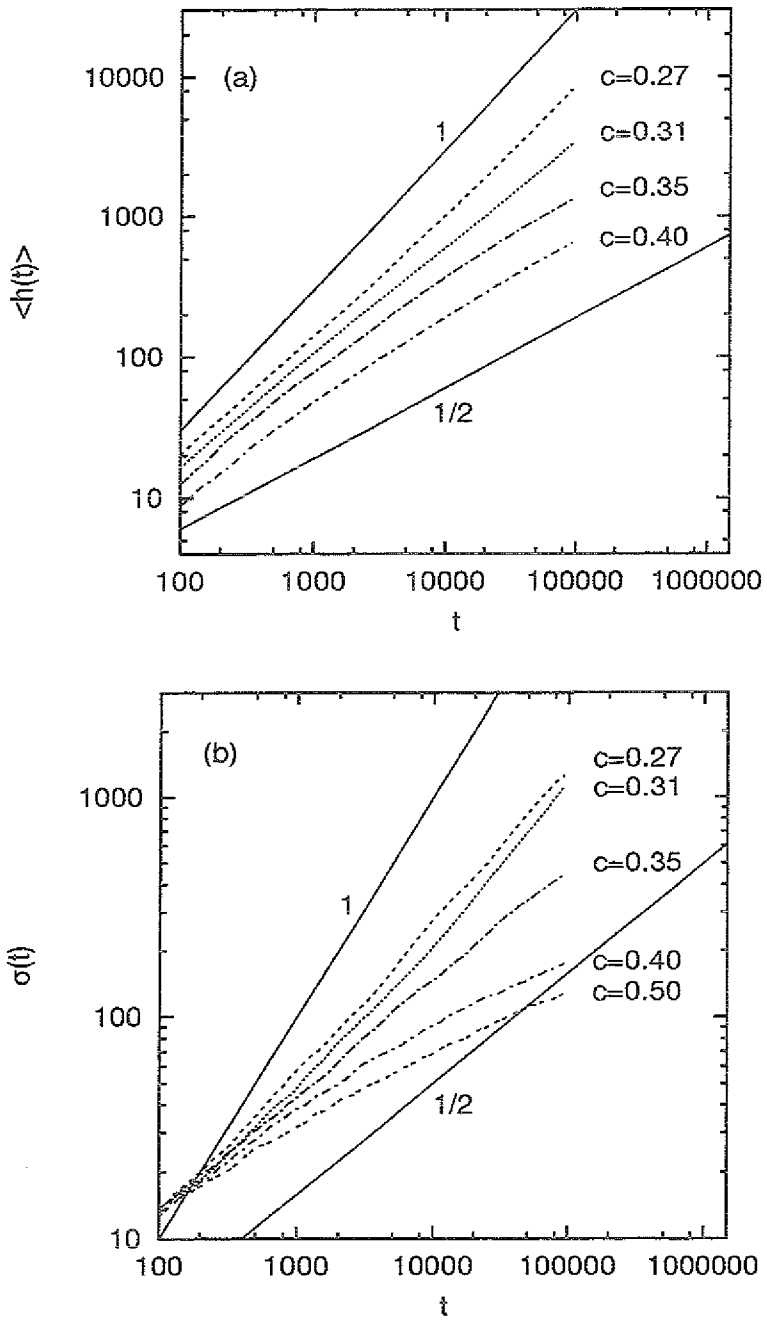


Figure 8.1: Time evolution of (a) the interface position $\langle h(t) \rangle$ and (b) its width $\sigma(t)$ for the symmetric diffusion model. Two straight solid lines represent the asymptotic behavior with exponent 1 and 1/2.

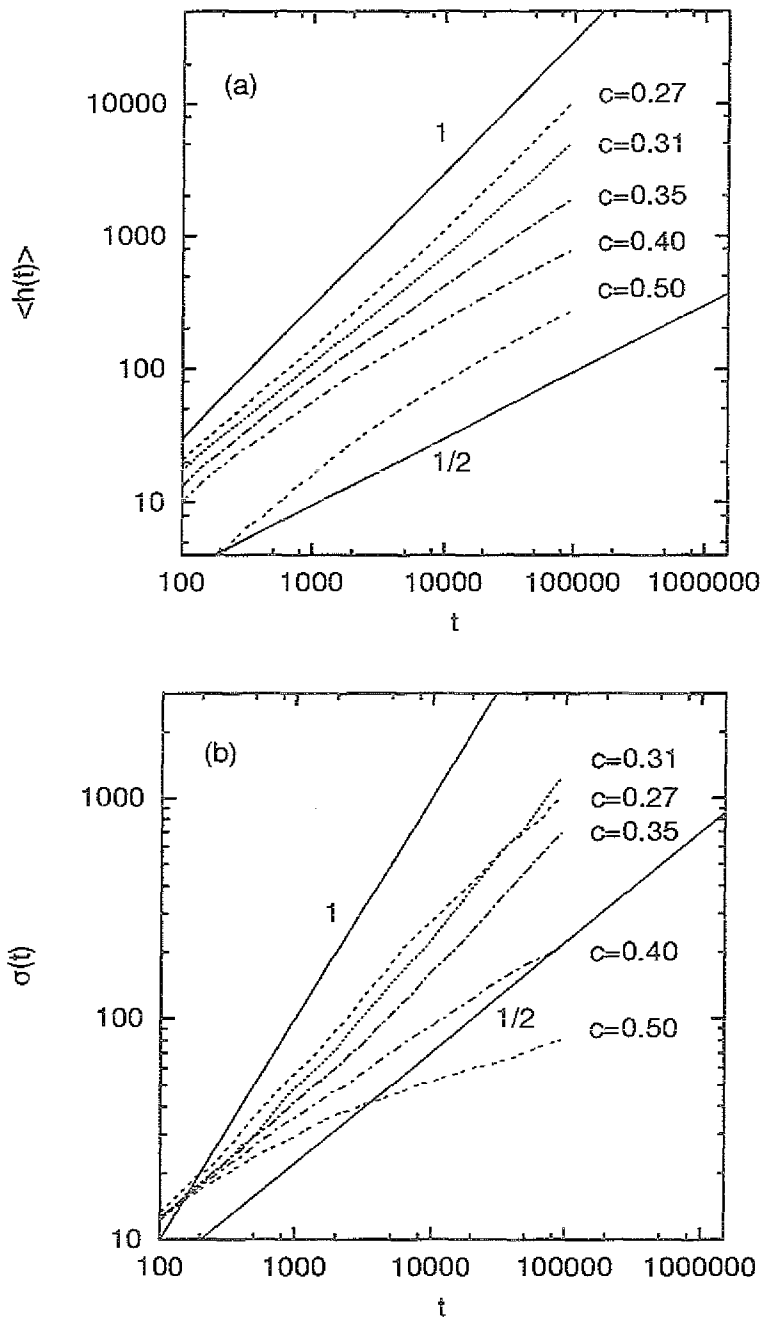


Figure 8.2: Time evolution of (a) the interface position $\langle h(t) \rangle$ and (b) its width $\sigma(t)$ for the one-sided diffusion model.Two straight solid lines represent the asymptotic behavior with exponent 1 and 1/2.

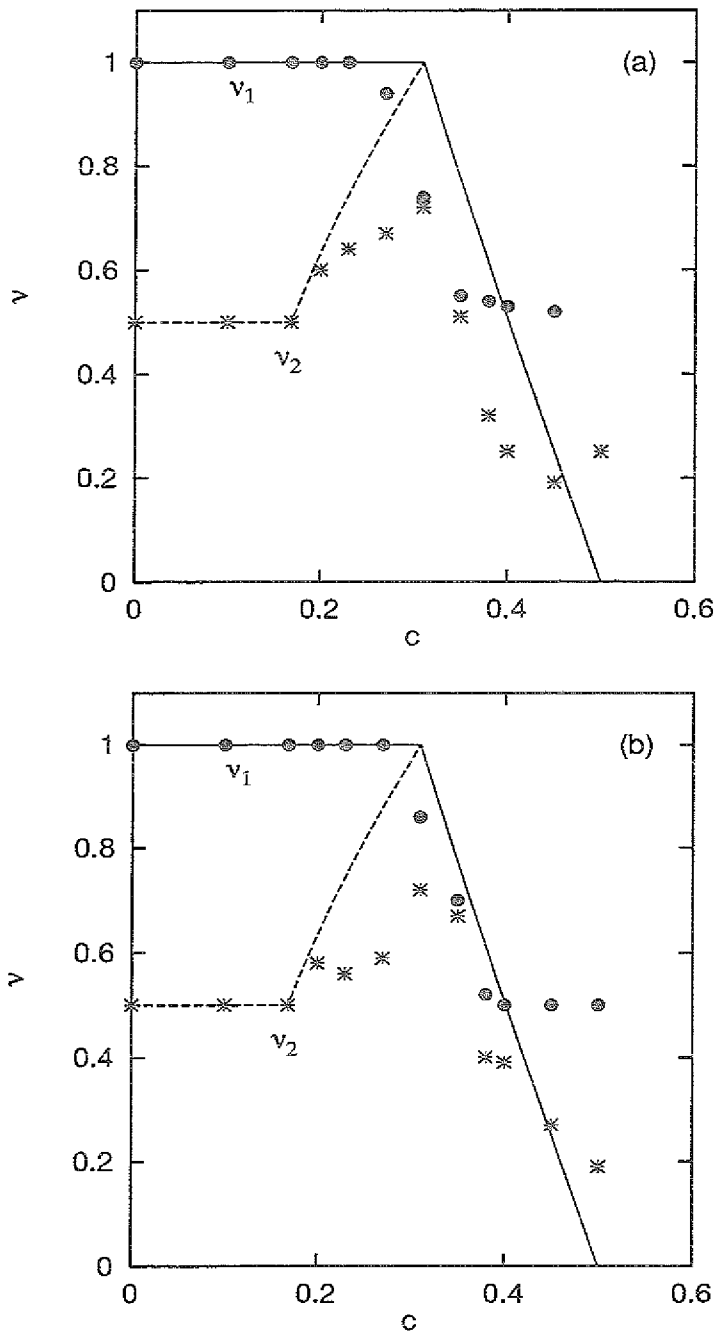


Figure 8.3: Exponent $\nu_1$ for the interface position and $\nu_2$ for its width versus the B-atom concentration $c$ for (a) symmetric diffusion model and (b) one-sided diffusion model. Solid and dashed lines are the exact diffusionless behaviors of $\nu_1$ and $\nu_2$, respectively. The symbol dots and stars represent the estimated $\nu_1$ and $\nu_2$ from the Monte Carlo simulation with diffusion, respectively.

## 8.3 Diffusion Equations

### 8.3.1 Distribution Function

The results described in the preceding section have shown that in an infinite disordered chain there is no steady-state motion of the interface with a nonvanishing velocity under conditions corresponding to the two-phase region of the equilibrium diagram. Accordingly, if we are interested in the interface motion in the two-phase region or in the transient period in a single phase regions, we should take into account the dependence of the state of the system on the time t. This analysis can be based on the kinetic equations for the distribution of components with respect to the moving interface. Therefore we introduce the probability $W(n;t)$ of finding B atom on the site n respective to the interface at the time t, $W(n,k;t)$ of finding B atoms on the sites n and k respective to the interface simultaneously at the time t, etc. Here $n \geq 0$ represents the liquid state and $n \leq -1$ represents the solid state. The drift velocity is equal to the average difference between the frequencies of rightwards and leftwards jumps of the interface and is given in terms of $W(0;t)$ and $W(-1;t)$ by

$$\begin{aligned} v(t) &= \omega_{+A}[1 - W(0;t)] + \omega_{+B}W(0;t) \\ &- \omega_{-A}[1 - W(-1;t)] - \omega_{-B}W(-1;t). \end{aligned} \tag{8.12}$$

### 8.3.2 Infinite System of Equations

The kinetic equations for $W(n;t)$ and $W(n,k;t)$ have been given in [32] and following are the equations only for $W(n;t)$:

$$\begin{aligned} \frac{dW(n;t)}{dt} &= \omega_{+A}\left[W(n+1;t) - W(n;t)\right] \\ &+ \omega_{-A}\left[W(n-1;t) - W(n;t)\right] \\ &+ (\omega_{+B} - \omega_{+A})\left[W(0,n+1;t) - W(0,n;t)\right] \\ &+ (\omega_{-B} - \omega_{-A})\left[W(-1,n-1;t) - W(-1,n;t)\right] \\ &\quad \text{for} \quad n \geq 1 \quad \text{and} \quad n \leq -2 \end{aligned} \tag{8.13}$$

$$\begin{aligned}\frac{dW(0;t)}{dt} &= \omega_{+A}\,W(1;t) - \omega_{+B}\,W(0;t) \\ &+ \omega_{-B}\,W(-1;t) - \omega_{-A}\,W(0;t) \\ &+ (\omega_{+B} - \omega_{+A})W(0,1;t) \\ &- (\omega_{-B} - \omega_{-A})W(-1,0;t), \end{aligned} \tag{8.14}$$

$$\begin{aligned}\frac{dW(-1;t)}{dt} &= \omega_{+B}\,W(0;t) - \omega_{+A}\,W(-1;t) \\ &+ \omega_{-A}\,W(-2;t) - \omega_{-B}\,W(-1;t) \\ &- (\omega_{+B} - \omega_{+A})W(-1,0;t) \\ &+ (\omega_{-B} - \omega_{-A})W(-2,-1;t). \end{aligned} \tag{8.15}$$

These are a set of "coupled" equations, in which the equations for the single-component function $W(n;t)$ contain the binary functions $W(n,k;t)$; the binary functions $W(n,k;t)$ contain the ternary functions $W(n,k,l;t)$, etc. So they are nonlinear equations. However, if we have $c \ll 1$, these equations uncouple in the first approximation in c. For example, in the equations for $W(n;t)$ we can discard the terms containing $W(n,k;t)$, since they are proportional to $c^2$. This approximation results in linear equations for $W(n;t)$.

### 8.3.3 Closed Equations for the Distribution Functions

A situation in which the type of solution changes qualitatively as a function of the parameters of the problem, is characteristic of nonlinear problems and should be described by nonlinear equations. We will therefore use a "coupling" of the equations which is related, not to the small magnitude of c, but to the auxiliary assumption that there is no correlation of components in different spatial positions :

$$W(n,k;t) = W(n;t)W(k;t). \tag{8.16}$$

In the following, we will write equations for $W(n;t)$ in this approximation (8.16). Despite the absence of correlation far from the interface, we note

that there is such a correlation in the liquid phase near the interface, i.e., we have $W(n,k;t) \neq W(n;t)W(k;t)$ for $n$ and $k \geq 0$. However, the correlation of concentrations in different spatial points needs time to develop. At the beginning of crystal growth, the correlation is so small that we can neglect it and in this case the approximation (8.16) is applicable. We consider a situation in which A and B atoms in the solid and liquid phase can exchange positions with their nearest neighbors by means of diffusion with frequencies $D_S$ and $D_L$, respectively, but we do not permit exchange across the interface. Then the kinetic equations for $W(n;t)$ are [35]

$$\begin{aligned}\frac{dW(n;t)}{dt} &= [\omega_{+A} + (\omega_{+B} - \omega_{+A})W(0;t)]\,[W(n+1;t) - W(n;t)] \\ &\quad + [\omega_{-A} + (\omega_{-B} - \omega_{-A})W(-1;t)]\,[W(n-1;t) - W(n;t)] \\ &\quad + \begin{cases} D_L\,[W(n+1;t) - 2\,W(n;t) + W(n-1;t)] & for \quad n \geq 1, \\ D_S\,[W(n+1;t) - 2\,W(n;t) + W(n-1;t)] & for \quad n \leq -2, \end{cases}\end{aligned} \tag{8.17}$$

$$\begin{aligned}\frac{dW(0;t)}{dt} &= \omega_{+A}\,W(1;t)\,[1 - W(0;t)] - \omega_{+B}\,W(0;t)\,[1 - W(1;t)] \\ &\quad + \omega_{-B}\,W(-1;t)\,[1 - W(0;t)] - \omega_{-A}\,W(0;t)[1 - W(-1;t)] \\ &\quad + D_L\,[W(1;t) - W(0;t)],\end{aligned} \tag{8.18}$$

$$\begin{aligned}\frac{dW(-1;t)}{dt} &= \omega_{+B}\,W(0;t)\,[1 - W(-1;t)] - \omega_{+A}\,W(-1;t)\,[1 - W(0;t)] \\ &\quad + \omega_{-A}\,W(-2;t)\,[1 - W(-1;t)] - \omega_{-B}\,W(-1;t)[1 - W(-2;t)] \\ &\quad + D_S\,[W(-2;t) - W(-1;t)].\end{aligned} \tag{8.19}$$

The meaning of these equations is easily understood from (8.17). We assume that there are M chains and M is a large number. By definition of the quantity $W(n,t)$, there there is a B atom in $M\,W(n,t)$ chains on the site n respective to the interface at the time t. This number changes as a result of two types of processes: motion of the interface to the right (the terms with $\omega_{+A}$ and $\omega_{+B}$ in (8.17)) or to the left (the terms with $\omega_{-A}$ and $\omega_{-B}$ in (8.17))

and diffusive interchange of atoms in the $n$-th position with nearest neighbors (the terms with $D_S$ and $D_L$). As an example, we consider the contribution to $d[MW(n;t)]/dt$ due to motion of the interface to the right for the case in which there a B atom on the right side of the interface. This contribution is positive and equal to

$$\omega_{+B}M[W(0,n+1;t) - W(0,n,n+1;t)] \tag{8.20}$$

if there is an A atom on the $n$-th position of the chain and a B atom on the $(n+1)$-th position of the chain. Here (8.20) is the number of chains in which there are a B atom on the 0-th position, an A atom on the $n$-th position, and a B atom on the $(n+1)$-th position at the time t. If there is a B atom on the $n$-th position and an A atom on the $(n+1)$-th position, the contribution due to the interface motion to the right is negative and equal to

$$-\omega_{+B}M[W(0,n;t) - W(0,n,n+1;t)]. \tag{8.21}$$

The sum of this contributions is

$$(8.20) + (8.21) = \omega_{+B}M[W(0,n+1;t) - W(0,n;t)] \tag{8.22}$$

and it does not contain a ternary distribution function. According to the assumption of no correlation (8.16), the binary functions can be replaced by a product of corresponding single-component functions and therefore we have

$$(8.22) = \omega_{+B}W(0)M[W(n+1;t) - W(n;t)] \tag{8.23}$$

Equations (8.17)-(8.19) should be supplemented with initial conditions. Let us consider the case in which the initial distribution of components with respective to the interface is uniform :

$$W(n;0) = c, \quad W(n,k;0) = c^2 \quad for\ -\infty < n < \infty, \tag{8.24}$$

which correspondents to the connection at time $t = 0$ of semiinfinite solid and liquid phase chains, in each of which the distribution is random and the concentration is equal to c. Far from the interface the concentration is kept to c of the mother-phase :

$$W(-\infty;t) \;=\; W(\infty;t) = c. \tag{8.25}$$

It is not difficult to show that the solution of steady-state equations (8.17)-(8.19) $[dW(n;t)/dt = 0]$ in the case of a L→S transition is

$$W(n) = \begin{cases} c & for \quad n \leq -1, \\ c + [W(0) - c]s^n & for \quad n \geq 0, \end{cases} \tag{8.26}$$

where

$$s = \frac{\omega_{-A} + c(\omega_{-B} - \omega_{+A}) + D_L}{\omega_{+A} + W(0)(\omega_{+B} - \omega_{+A}) + D_L} \tag{8.27}$$

and

$$W(0) = \frac{c + c(1-c)[\omega_{+A} - \omega_{-A} - \omega_{+B} + \omega_{-B}]}{\omega_{+B} + c(\omega_{+A} - \omega_{+B})}. \tag{8.28}$$

The concentration distribution does not depend on the frequency $D_S$. The $W(-1)$ and $W(0)$ values given by this equations are the same as those given by diffusionless growth equations [32], so regardless of the $D_L$ and $D_S$ values, the velocity of the interface should be given by the same formula [32]

$$v_{L\to S} = \frac{\omega_{+A}\omega_{+B} - c\omega_{+A}\omega_{-B} - (1-c)\omega_{-A}\omega_{+B}}{c\omega_{+A} + (1-c)\omega_{+B}}. \tag{8.29}$$

The values of the front velocity is determined only by the kinetics ($\omega_{\pm A,B}$). A correlation, neglected in Eqs.(8.17)- (8.19), arises because of the fluctuation of the boundary during its directed motion. There are no such fluctuations and thus no correlation in the case of $\omega_{-A} = \omega_{-B}$. In the case of rapid solidification, the fluctuation of the boundary is so small that man can neglect it. Fig.(8.4) shows the concentration distribution $W(n)$ versus the lattice layer respective to the interface for a chain with $c = 0.2$ at time $10^5$. $W(n)$ has been averaged over 200 different realizations of randomness. The results of the Monte Carlo simulations (zigzag lines) are in a very good agreement with results from equation (8.26) (symbols × on the right side of the figure). The concentration in the whole solid region ($n \leq 0$) as well as in the liquid region ($n \geq 0$) but far from the interface remains the average value c (= 0.2), however near the interface in the liquid side the concentration varies from $c = 0.2$ to $c = W(0)$ (= 0.484) when the lattice layer gets closer to the interface. In addition, the steady-state velocity of the chain is measured by MC simulation as 0.203,

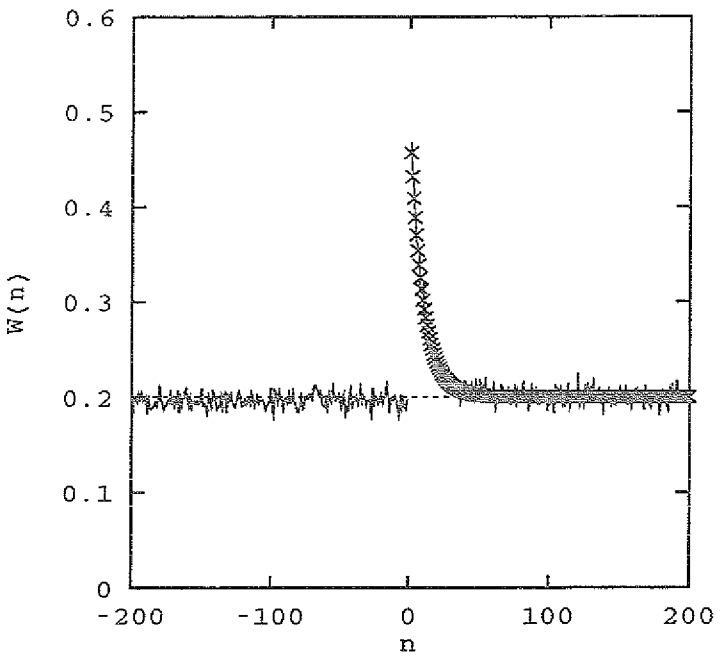


Figure 8.4: The concentration distribution $W(n)$ versus the lattice layer n respective to the interface for a chain with $c = 0.2$ at time $10^5$.

which has only 2.4% deviation from the expected value 0.1953 from (8.29). The front velocity (8.29) remains finite only in the one-phase solid region, but it vanishes at the solidus line $C_S$. In the two-phase region the steady growth with a finite velocity is impossible and it follows from the sets of equations (8.17)-(8.19).

### 8.3.4 From Difference Equations to Differential Equations

In order to study the transient behavior of equations (8.17)-(8.19) numerically, we write the difference equations into differential equation; this is permissible change provided that the characteristic distances for the changes in the functions $W(n;t)$ are much larger than unity. Instead of the discrete variable $n$

we introduce a continuous variable $x$, and then we have:

$$\begin{aligned} W(x,t) &= W(n;t) \quad \text{when } x = n \geq 0, \\ W(x,t) &= W(n-1;t) \quad \text{when } x = n \leq 0. \end{aligned} \tag{8.30}$$

So that the concentrations $W(0;t)$ and $W(-1;t)$ at the interface are $W(+0;t)$ and $W(-0;t)$, respectively. Replacing the differences in (8.17) by derivatives, we have

$$\begin{aligned} \frac{\partial W(x,t)}{\partial t} &= D_S^e(t)\frac{\partial^2 W(x,t)}{\partial x^2} + v(t)\frac{\partial W(x,t)}{\partial x} \\ &\quad \text{for} \quad x < 0 \quad \text{in the solid phase,} \\ \frac{\partial W(x,t)}{\partial t} &= D_L^e(t)\frac{\partial^2 W(x,t)}{\partial x^2} + v(t)\frac{\partial W(x,t)}{\partial x} \\ &\quad \text{for} \quad x > 0 \quad \text{in the liquid phase,} \end{aligned} \tag{8.31}$$

where

$$\begin{aligned} D_S^e(t) &= D_S + \frac{1}{2}[j_+(t) + j_-(t)], \\ D_L^e(t) &= D_L + \frac{1}{2}[j_+(t) + j_-(t)], \\ v(t) &= j_+(t) - j_-(t), \\ j_+(t) &= \omega_{+A} + (\omega_{+B} - \omega_{+A})W(+0,t), \\ j_-(t) &= \omega_{-A} + (\omega_{-B} - \omega_{-A})W(-0,t)]. \end{aligned} \tag{8.32}$$

Here $D_S^e$ and $D_L^e$ are the effective diffusion coefficients in the solid and liquid phase, which differ from the actual or bare diffusion coefficients $D_S$ and $D_L$ due to taking into account both diffusion of atoms and fluctuations of the interface; $j_+(t)$ is the flux of atoms from the liquid side to the solid side at the interface; $j_-(t)$ is that from the solid side to the liquid side ; $v(t)$ is the interface velocity : $v(t) = d\langle h(t)\rangle/dt$. The ratio $D_S/v$ and $D_L/v$ are characteristic distances for changes in function $W(x,t)$. We can thus transform the discrete equations (8.17)-(8.19) to continuous eauqtions (8.31)-(8.32) under the conditions $D_S/v \gg 1$ and $D_L/v \gg 1$. These conditions hold either with

$D_S$ and $D_L \gg \frac{1}{2}(j_+ + j_-)$, i.e., when the atomic diffusion coefficients are much grater than the interface diffusion coefficient $D_i \equiv \frac{1}{2}(j_+ + j_-$ (this is an approximate expression for the interface expression coefficient, with correlation effect neglected.) or with $\frac{j_+ - j_-)}{j_+} \ll 1$ when $D_S$ and $D_L$ are of the same order of magnitude as $D_i$ or smaller (the index $i$ refers to the interfaces).

Equations (8.18) and (8.19) are local equations of motion for the interface, which can serve as a boundary condition for the differential equation (8.31). Transforming (8.18) and (8.19) to the continuous relations, we find the two boundary conditions:

$$v(t)W(+0) + D_L^e(t)\frac{\partial W(+0)}{\partial x} = \omega_{+B}\,W(+0) - \omega_{-B}\,W(-0), \quad (8.33)$$

$$v(t)[W(+0) - W(-0)] = D_S^e(t)\frac{\partial W(-0)}{\partial x} - D_L^e(t)\frac{\partial W(+0)}{\partial x}. \quad (8.34)$$

Equation (8.33) corresponds to Eq.(8.18), and Eq.(8.34) corresponds to both Eqs.(8.18) and (8.19). The quantities $(D_S + j_+)$ and $(D_L + j_+)$, rather than $D_S$ and $D_L$ which they replace, should appear in Eqs.(8.33) and (8.34). However, this replacement is justified when we can transform from the discrete description to the continuous description. In the transformation from Eqs.(8.18) and (8.19), the time derivatives are discards since they are quantities of a higher order of smallness.

Relations (8.35) are replaced by

$$\begin{aligned} &W(x,0) = c, \qquad -\infty < x < \infty, \\ &W(-\infty,t) = W(\infty,t) = c. \end{aligned} \quad (8.35)$$

Problem (8.31)-(8.35) differs from the ordinary problem of the growth of a new phase due to a redistribution of alloy components because the boundary or interface fluctuations are taken into account. As a result, effective diffusion coefficients $D_S^e$ and $D_L^e$ replace the actual diffusion coefficients.

For the growth of a new phase, the behavior of the solution of Eqs.(8.31)-(8.35) at large t depends strongly on the parameters of the problem. For parameters corresponding to the single-phase regions of the equilibrium diagram, the system tends toward a steady-state as $t \to \infty$ which is characterized

by a constant interface velocity and by time-independent distributions of the components with respective to this interface. Under conditions corresponding to the two-phase region, the system tends to separate into two phases of equilibrium concentrations $C_s$ and $C_l$, and the interface velocity tends toward zero.

## 8.4 Numerical Results and Discussions

In the two-phase region of the equilibrium phase diagram it was found from equations (8.31)-(8.34)[32] that the velocity of the interface asymptotically falls off as $t^{-1/2}$. For an arbitrary time we can numerically integrate the set of equations (8.31) -(8.34) under the initial condition (8.35) in order to get an instantaneous velocity of the interface and thus obtain the position of the interface $\langle h(t) \rangle$. Time dependence of the interface position obtained by numerical integration is compared with that obtained by Monte Carlo simulation in Fig.8.5. For example for the symmetric diffusion model ($D_S = D_L = 1$) at the concentration $c = 0.35$ in Fig.8.5(a) the numerical integration gives a position $\langle h(t) \rangle$ in excellent quantitative agreement with the Monte Carlo result. A similar quantitative agreement is found for both the one-sided diffusion model and the symmetrical model at the concentration $c = 0.40$ as shown in Fig.8.5(b) and (d). At the concentration $c = 0.50$ for the symmetrical model the interface does not move in average $\langle h(t) \rangle = 0$. For the one-sided model the Monte Carlo data for the initial interface motion still agree with numerical integration with the effective diffusion coefficients. However, for larger time the data agree with the numerical integration with bare diffusion constants, $D_S = 0$ and $D_L = 1$, rather than that with the effective ones, $D_S^e$ and $D_L^e$, as shown in Fig.8.5(e).

For the one-sided diffusion model at $c = 0.35$ in Fig.8.5(c), the Monte Carlo data still agree with numerical integration during some initial time but we observe a deviation increasing with time, and even bigger deviations from the results obtained with bare diffusion constants. So far from these data for $c = 0.35$ and our long but limited simulation times we cannot make a clear

statement if the exponent $\nu_1$ approaches to the diffusionless value $\nu_1 \approx 0.77$ or the diffusional value $\nu_1 = 1/2$, or even other nontrivial value ! We will come back to this point in the conclusion.

The given effective description does not take into account the correlation of concentration between different spatial points. Indeed those correlations are absent in the initial distribution of atoms in our chains and their formation requires some time.

We think that this explains the fact that all our Monte Carlo data agree well with the results based on the effective equations for the small time where nontrivial correlations have not yet built up.

It is clear that correlations become smaller with an increase of the diffusion coefficients and thus the time when the deviation from the correlationless description starts should increase. Qualitatively we can see this effect from the different data for $c = 0.35$. Agreement for the symmetrical model ( $D_S = D_L = 1$, Fig.8.5(a)) holds for all our simulation time while for the one-sided model ($D_S = 0, D_L = 1$, Fig.8.5(c)) the increasing deviation can be observed already at $t \cong 10^3$.

The other parameters which affect the correlations are $(\omega_{+B} - \omega_{+A})$ and $(\omega_{-B} - \omega_{-A})$. The correlations (together with two-phase region) disappear when both parameters are zero. We have performed the Monte Carlo simulations without diffusion for two sets of the parameters $\omega_{+B} = \omega_{+A} = 1$ , $\omega_{-B} = 1/\omega_{-A} = 2.226$ , $c = 0.35$ (Fig.8.6(a)) and $\omega_{+B} = \omega_{+A} = 1$ , $\omega_{-B} = 1/\omega_{-A} = 1.4$, $c = 0.435$ (Fig.8.6(b)). The parameters are so chosen that the exponents $\nu_1$ of the interface position in the above two diffusionless cases are the same and are around 0.77 from the formula $\nu_1 = ln(\frac{1-c}{c})/ln(\omega_{-B})$[8]. In the second case the parameter $(\omega_{-B} - \omega_{-A})$ is smaller and one can see that the deviation of the Monte Carlo data from the effective description starts later. It is interesting to note that even without diffusion the initial behavior can be described by the system of effective diffusion equations with diffusion coefficients which come only from the interface fluctuations.

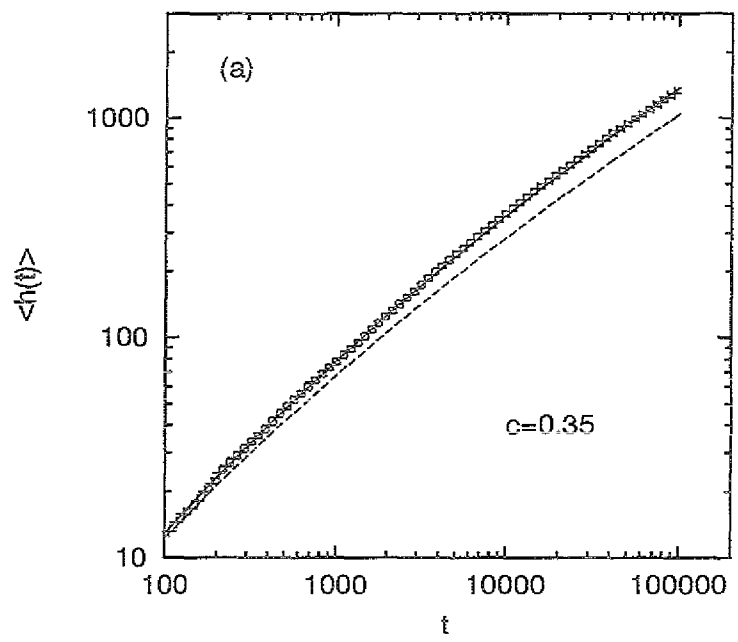
(a)
1000
100
10
<h(t)>
c=0.35
100
1000
10000
100000
t

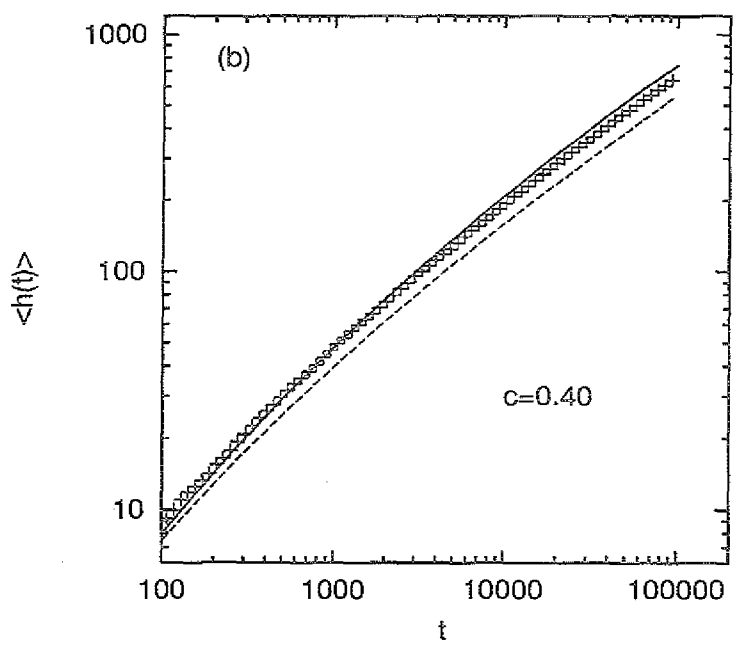
(b)
1000
100
10
<h(t)>
c=0.40
100
1000
10000
100000
t

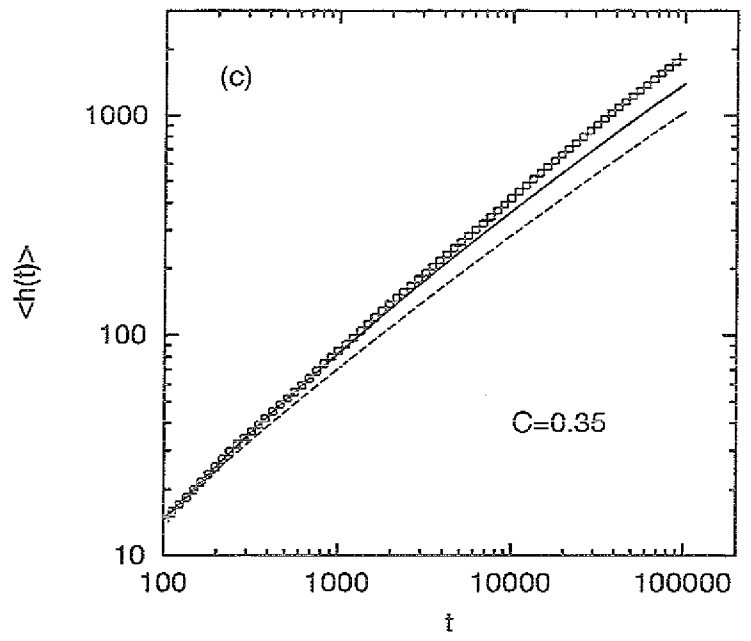
(c)
1000
100
10
<h(t)>
C=0.35
100
1000
10000
100000
t

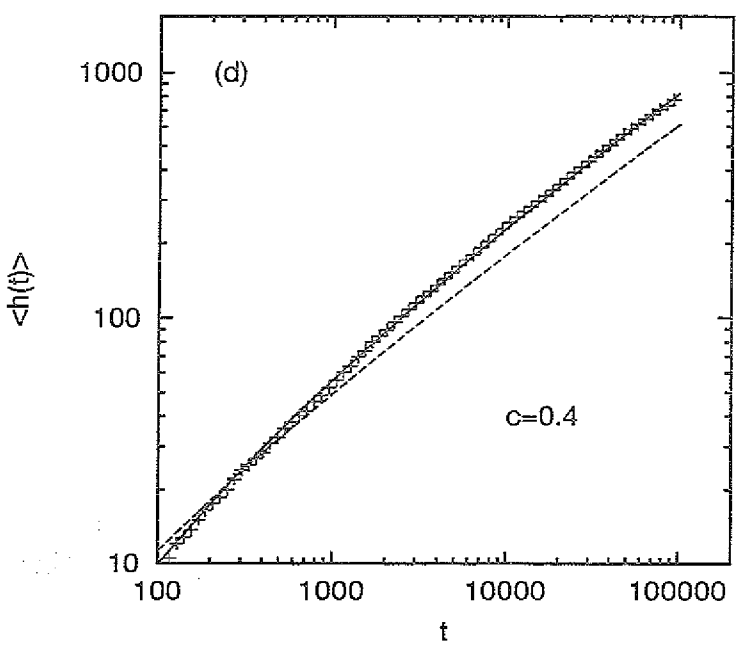
(d)
1000
100
10
<h(t)>
c=0.4
100
1000
10000
100000
t

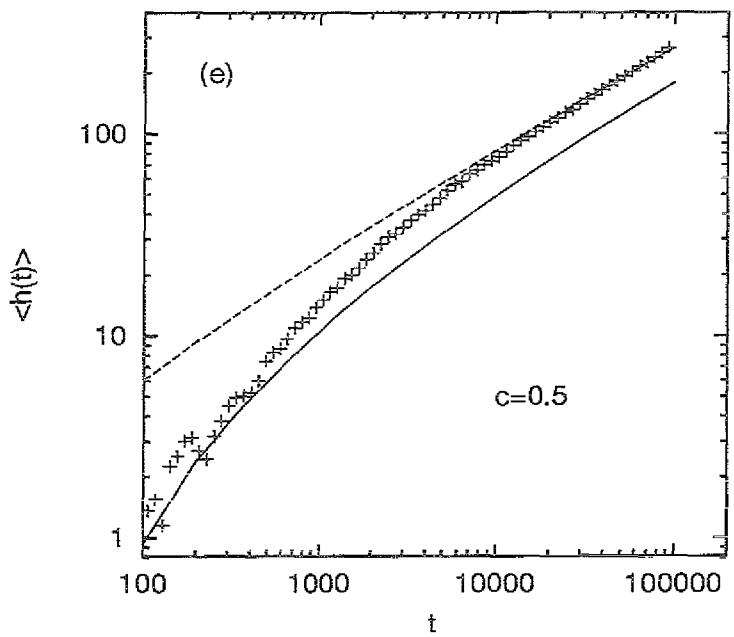


Figure 8.5: The interface position $h(t)$ calculated by the analytical approximation with effective diffusion coefficients $D_S^e$ and $D_L^e$ (solid lines) and bare diffusion coefficients $D_S$ and $D_L$ (dashed lines) compared with the Monte Carlo results (symbols) for (a-b) symmetric diffusion and (c-e) one-sided models. Concentrations are (a) $c = 0.35$, ($b$)c=0.40, ($c$)c=0.35, ($d$)c=0.40, and (e) $c = 0.50$.

For the two-phase region in the long-time asymptotics the system goes to equilibrium (even without diffusion) and correlations decay. However, the asymptotic behavior of the interface velocity which also goes to zero still depends on these small correlations. For example for $c = 0.5$ the dependence $\langle h(t) \rangle$ on $t$ deviates substantially from the dependence calculated without correlations. It seems that the asymptotic behavior can be described by bare diffusion constants rather than by effectives ones (fig.8.5(e)). We think that the correlations renormalize the effective diffusion coefficients back to the bare ones. The description with bare diffusion constants should exactly correspond to the system without interface fluctuations. As can be seen from the Fig.8.1 and fig.8.2 the variation $\sigma(t)$ for $c = 0.5$ grows slower than $t^{1/2}$ which means that the interface fluctuations are indeed small.

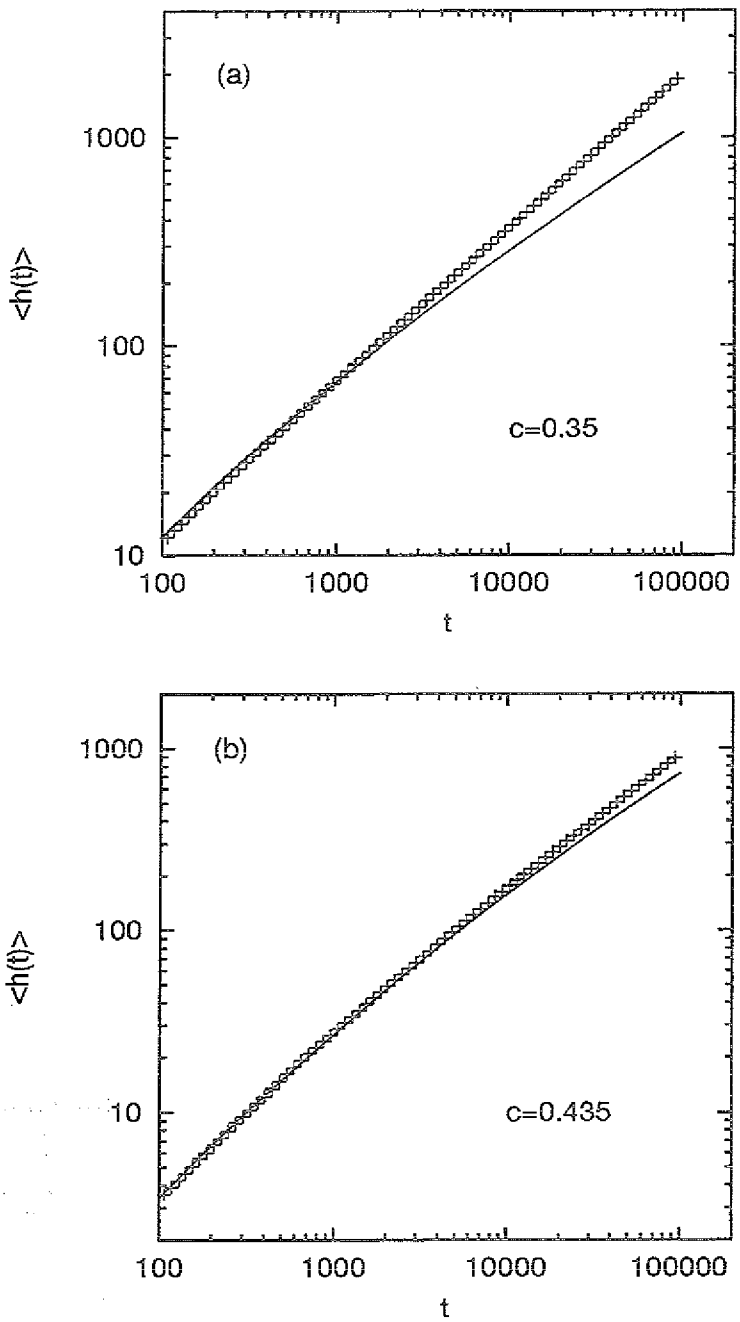


Figure 8.6: The interface position $< h(t) >$ calculated by the diffusionless Monte Carlo simulations (symbols) and by the numerical integration with effective diffusion coefficients $D_S^e = D_L^e = 1$ (solid lines). Concentrations are (a) c=0.35 and (b) c=0.435.

# Chapter 9

# Conclusion

We have studied the diffusionless solid-liquid phase transformation in a disordered binary alloy by observing the motion of the solid-liquid interface. For a 1D system the equilibrium phase diagram is found to determine regions, where pinning-depinning transitions of the interface occur. The solidus line $C_s$ and the liquidus line $C_l$ separate the static and moving state of the interface. In the one-phase region the interface moves steadily but the velocity vanishes in the two-phase region and the displacement of the interface follows a power law of time t as $h \sim t^{\nu_1}$ with

$$\begin{aligned} \nu_1 &= 1 \qquad \text{when} \qquad c < C_S \quad \text{or} \quad c > C_L, \\ \nu_1(c,T) &< 1 \qquad \text{when} \qquad C_S < c < C_L. \end{aligned} \tag{9.1}$$

Here $\nu_1(c,T)$ is not a universal exponent but depends strongly on the concentration c and the temperature T.

For a 2D system Monte Carlo simulations show that in the one-phase region the interface moves with a steady-state velocity, and its bond energy-dependence and concentration-dependence can be decoupled as $v(\epsilon,c) = f_1(\epsilon)f_2(c)$ when the bond energy $\epsilon$ is not very small (see Fig.7.14). There is no explicit theory on this $\epsilon$- and c-dependence of $v$ so far.

In the two-phase region, the interface shows a complicated behavior depending upon the system size N, the bond energy $\epsilon$ and the simulation time $t$.

For a finite sized system under finite simulation time ( up to $t = 10^5 \sim 10^6$), the effective growth exponent $\nu_1$ depends strongly on $\epsilon$ (see Fig.7.6) :

$$\begin{aligned} \nu_1 &< 1 \qquad \text{for} \qquad \epsilon < 0.1T_A \\ \nu_1 &= 1 \qquad \text{for} \qquad 0.1T_A < \epsilon < \epsilon_c(N) \\ \nu_1 &< 1 \qquad \text{for} \qquad \epsilon > \epsilon_c(N) \\ \nu_1 &= \nu_1(1D) \qquad \text{for} \qquad \epsilon \to \infty \end{aligned}$$

The critical bond energy $\epsilon_c(N)$ increases with system size $N$. Unlike the one-dimensional system, the two-dimensional system can realize a steady growth in the two-phase region provided that the bond energy satisfies the condition: $0.1T_A < \epsilon < \epsilon_c(N)$. However when $\epsilon > \epsilon_c(N)$, the interface becomes pinned such that the spatial disorder of the alloy leads to a decay of the interface velocity. In the large energy limit ($\epsilon \to \infty$) theoretical analysis and computer simulations show that the exponent $\nu_1$ has the same value as its one-dimensional counterpart $\nu_1(1D)$.

A peculiar result occurs for small but nonzero bond energies, less than about $0.1T_A$ as discussed in section 7.3.2. Here pinning occurs as would be the case for vanishing bond energy but the exponent $\nu_1$ is increased above the value of the one-dimensional case. In this region $\epsilon$ acts as an extra driving force and $\nu_1$ increases with increasing $\epsilon$. Therefore both for very large and very small bond energy in a finite system the interface will be pinned. Note, however that the latter result applies only to models of SOS-type and probably not to systems with overhangs.

For a very large system ($N \to \infty$) with a finite bond energy, the simulation reveals that the interface always moves steadily within a finite simulation time, that means the critical bond energy $\epsilon_c \to \infty$ when $N \to \infty$. This corresponds to the thermal creep motion. A finite temperature washes out the sharp pinning-depinning transition and the mean velocity is then finite for all driving forces when the bond energy is neither very small nor infinite. We found that the influences of the bond energy $\epsilon$ and the driving force H on the velocity $v$ of the interface growth are decoupled as indicated in Eq.(7.27). The velocity $v$ decays exponentially with $\epsilon$ and $H^{-1}$ in the vicinity of zero $H$

and for sufficiently large $\epsilon$.

In addition, we have also studied the development of correlations along the interface and their relevance to finite size effects on the interface dynamics. The correlation length $\xi_{//}$ along the interface increases very slowly with the time. Once it reaches the system size $N$ the whole interface becomes correlated and the interface-motion asymptotically behaves like the one in a one-dimensional system. So principally the system will lose its 2D character in the infinite time limit. However, as long as the system size is much larger than $\xi_{//}$ and the thermal creep wins over the pinning force, the interface can obtain a steady velocity. Thus for the system studied here the limits $N \to \infty$ and $t \to \infty$ do not commute.

Besides the diffusionless solidification we have also studied the propagation of the solidification front of a binary alloy growing from its melt including diffusion of material in a one-dimensional model, which should remain relevant also in more realistic two- and three-dimensional systems within certain parameter-ranges. The Monte Carlo simulation shows that in the one-phase region the alloy grows steadily with a velocity controlled solely by kinetics. In the two-phase region the observed anomaly for the diffusionless growth is cured by the diffusion of atoms and the $t^{1/2}$ growth law is confirmed at least in the range of concentration $0.401 = c_3 < c < 0.5$ (at $T$=0.5 in Fig.1.1). We can quantitatively explain this behavior by an approximate analytical treatment leading to two types of bare and effective diffusion coefficients.

Because of the limited simulation time we can only suggest two possible scenarios for the general long time asymptotic behavior $\langle h(t) \rangle$ of the interface movement with diffusion included. The first scenario is that in the two-phase region the behavior is governed by a set of effective diffusion equations (8.31)-(8.35). For arbitrary but non-zero bare diffusion constants $D_S$ and $D_L$, the interface position $\langle h(t) \rangle$ obeys the following time-dependence. For a point exactly on the solidus or liquidus line (see [90]) one obtains:

$$\langle h(t) \rangle \sim t^{2/3} \quad \text{for} \quad c = C_{S(L)}.$$

Inside the two-phase region we have the usual diffusion law:

$$\langle h(t) \rangle \sim t^{1/2} \quad \text{for} \quad C_S < c < C_L,$$

within this scenario. The concentration point $c^*$ where solidification is replaced by melting is [35]

$$c^* = (C_S \sqrt{D_S^e} + C_L \sqrt{D_L^e})/(\sqrt{D_S^e} + \sqrt{D_L^e}).$$

We note that this point $c^*$ in general differs from the corresponding point $C_0$ for the diffusionless process,

$$c_0 = \ln \frac{\omega_{+A}}{\omega_{-A}} \Big/ \ln \frac{\omega_{+A}\omega_{-B}}{\omega_{-A}\omega_{+B}}.$$

For our choice of parameters $\omega$, $c_0 = 1/2$ and this coincides with $c^*$ for the symmetrical diffusional model. This scenario is based on the solution of the effective equations (8.31)-(8.35) but with the effective diffusion coefficients renormalized by the correlation effects. This is in agreement with Figs. 8.5(a), (b), (d) and (e), but in some disagreement with long time behavior seen in Fig. 8.5(c) We should remark that this scenario does not reproduce the limiting case of the diffusionless process where $\langle h(t) \rangle \sim t^{\nu_1}$.

The second scenario is that the asymptotics with diffusion would not be slower than that without diffusion, meaning

$$\langle h(t) \rangle \sim t^{\nu_1} \quad \text{for} \quad \nu_1 > 1/2,$$

and

$$\langle h(t) \rangle \sim t^{1/2} \quad \text{for} \quad \nu_1 < 1/2,$$

with $\nu_1$ being the anomalous exponent of diffusionless growth. Unfortunately, however, we have no explicit analytical explanation at hand for this second scenario other than the argument, that the faster of two processes running in parallel wins (in contrast to two processes in series, where the slower one is rate-controlling). This second scenario has some support from the long time

behavior of Fig. 8.5(c) and the corresponding Fig. 8.3(b) for the concentration $c = 0.35$, indicating that the otherwise nice agreement of the simulation results with scenario one may be lost for very long simulation time in this parameter ranges. In order to understand which of these scenarios is correct for the diffusional process or if still some other nontrivial exponents can appear in the range where the diffusionless exponent is $\nu_1 > 1/2$, further numerical and analytical efforts will be necessary.

# Bibliography


[1] A. -L. Barabási, S. V. Buldyrev, S. Havlin, G. Huber, H. E. Stanley and T. Vicsek, "Imbibition in Porous media: experiment and theory," in Surface disordering: Growth, roughening and phase transitions, edited by R. Jullien, J. Kertész, P. Meakin and D. E. Wolf (Nova Science, New York, 1992), pp.193-204.

[2] R. Bidaux and R. B. Pandey, Phys. Rev. **E 48**, 2382 (1993).

[3] S. V. Buldyrev, A. -L. Barabási, F. Caserta, S. Havlin, H. E. Stanley and T. Vicsek, Phys. Rev. **A 45**, 8313 (1992).

[4] M. Dong, M. C. Marchetti, A. A. Middleton and V. Vinokur, Phys. Rev. Lett. **70**, 662 (1993).

[5] S. Havlin, A. -L. Barabási, S. V. Buldyrev, C. K. Peng, M. Scwartz, H. E. Stanley and T. Vicsek, "Anomalous interface roughening: experiment and models," in Growth Patterns in physical Sciences and Biology, edited by E. Louis, L. Sander and P. Meakin, Proc. 1991 NATO Advanced Research Workshop, Granada, Spain. (Plenum, New York, 1992), pp.85-98.

[6] M. H. Jensen and I. Procaccia, J. de Physique II **1**, 1139 (1991).

[7] Z. Jiang and H. G. E. Hentschel, Phys. Rev. **A 45**, 4169 (1992).

[8] M. J. Leaseburg and R. B. Pandey, Phys. Rev. **E 50**, 3730 (1994).

[9] H. Leschhorn, Physica **A 195**, 324 (1993).

[10] S. Pal and D. P. Landau, Phys. Rev. B 49, 10597 (1994).

[11] G. Parisi, Europhys. Lett. 17, 673 (1992).

[12] K. Sneppen, Phys. Rev. Lett. 69, 3539 (1992).

[13] K. Sneppen and M. H. Jensen, Phys. Rev. Lett. 71, 101 (1993).

[14] D. Spasojevic and P. Alstrom, Physica A 201, 482 (1993).

[15] L. -H. Tang and H. Leschhorn, Phys. Rev. A 45, R8309 (1992).

[16] T. Vicsek, "Kinetic roughening with multiplicative noise," in Surface Disordering: Growth, Roughening and Phase Transitions, edited by R. Jullien, J. Kertész, P. Meakin and D. E. Wolf, Nova Science, New York, 1992), pp.155–162.

[17] T. Vicsek, E. Somfai and M. Vicsek, J. phys. A 25, L763 (1992).

[18] R. Bruinsma and G. Aeppli, Phys. Rev. Lett. 52, 1547 (1984).

[19] J. Koplik and H. Levine, Phys. Rev. B 32, 280 (1985).

[20] A. E. Scheidegger, *The Physics of Flow in Porous Media*, University of Toronto Press, Toronto (1984).

[21] D. S. Fisher, M. P. A. Fisher and D. A. Huse, Phys. Rev. B 43, 130 (1991).

[22] T. Nattermann, Phys. Rev. Lett 64, 2454 (1990).

[23] D. S. Fisher, "Collective Transport: From Superconductors to Earthquakes", Lectures at Summer School "Fundamental Problems in Statistical Mechanics IX" , August 20-23, 1997, Alternberg in Germany

[24] H. Fukuyama and P. A. Lee, Phys. Rev. B 17, 535 (1978).

[25] P. A. Lee and T. M. Rice, Phys. Rev. B 19, 3979 (1979).

[26] K. B. Efetov and A.I. Larkin, Sov. Phys. JETP 45, 1236 (1977).

[27] D. S. Fisher, Phys. Rev. Lett **50**, 1486 (1983); Phys. Rev. B **31**,1396 (1985).

[28] O. Narayan and D. S. Fisher, Phys. Rev. Lett **68**, 3615 (1992); Phys. Rev. B **46**, 11520 (1992).

[29] P. G. Gennes, Rev. Mod. Phys. **57**, 827 (1985)

[30] J. F. Joanny and P. G. de Gennes, J. Chem. Phys. **81**, 552 (1984).

[31] M. Kardar, "Nonequilibrium Dynamics of the Interfaces and Lines", Lectures at Summer School "Fundamental Problems in Statistical Mechanics IX" , August 20-23, 1997, Alternberg in Germany

[32] D. E. Temkin. J. Cryst. Growth **5**, 193 (1969).

[33] D. E. Temkin, Dokl. Akad. Nauk SSSR **206**, 27 (1972) [Sov. Math. Dokl. **13**, 1172 (1972)].

[34] Y. Saito, N. Tanabe and D. Temkin, Phys. Rev. E**48**, 2028 (1993).

[35] D. E. Temkin, Kristallografiya **17**, 77 (1972) [Sov. Phys. Crystallogr. **17**, 60 (1972)].

[36] S. Alexander, J. Bernasconi, W. R. Schneider, R. Orbach, Rev. Mod. Phys. **53**, 175(1981).

[37] J. Bernasconi, S. Alexander and R. Obach, Phys. Rev. Lett. **41**, 185 (1978).

[38] J. Bernasconi, W. R. Schneider and W. Wyss, Z. Phys. **B 37**, 175 (1980).

[39] J. Bernasconi and W. R. Schneider, Phys. Rev. Lett. **47**, 1643 (1981).

[40] J. Bernasconi and W. R. Schneider, J. Phys. A **15**, L729 (1982).

[41] B. Derrida and H. Hilhorst, J. Phys. **C 14**, L539 (1981).

[42] B. Derrida and Y. Pomeau, Phys. Rev. Lett. **48**, 627 (1982).

[43] B. Derrida, J. Stat. Phys. **31**, No.3, 433 (1983).

[44] B. Derrida and R. Orbach, Phys. Rev. **B 27**, (1983).

[45] H. Kesten, M. V. Koslov and F. Spitzer, Compositio MAth. **30**, 145 (1975).

[46] T. Odagaki and M. Lax, Phys. Rev. Lett. **B 45**, 847 (1980).

[47] T. Odagaki and M. Lax, Phys. Rev. **B 24**, 5284 (1981).

[48] Ya. G. Sinai, in *Mathematical Problems in Theoretical Physics* edited by R. Schneider, R. Seiler and P. Uhlenbrock, Lecture Notes in Physics Vol. 153 (Springer, Berlin, 1982), p.12.

[49] F. Solomon, Ann. Prob. **3**:1 (1975)

[50] M. J. Stephen, J. Phys. **C 14**, L1077 (1981).

[51] I. Webman, Phys. Rev. Lett. **47**, 1496 (1981).

[52] I. Webman and J. Klafter, Phys. Rev. **B 26**, 5950 (1982).

[53] J. Machta, Phys. Rev. **B 24**, 5260 (1982).

[54] R. Zwanzig, J. Stat. Phys. **28**, 127 (1982).

[55] C. Asulangul, M. Barthelemy, N. Pottier and D. Saint-James, J. Stat. Phys. **59**, 11 (1990).

[56] J. P. Bouchaud and A.Georges, Phys. Rep. **195**, 127 (1990).

[57] J. P. Bouchaud, A. Comtet, A. Georges and P. Le Doussal, Ann. Phys. **201**, 285 (1990).

[58] D. E. Temkin, Sov. Phys. Crystallogr., **19**, 291 (1974).

[59] K. A. Jackson, G. H. Gilmer, D. E. Temkin, J. D. Weinberg and K. Beatty, J. Cryst. Growth **128**, 127 (1993).

[60] V. V. Voronkov, Sov. Phys. Crystallogr., **19**, 975(1979)

[61] L. B. Ioffe and V. M. Vinokur, J. Phys. **C20**, 6149(1987)

[62] V. M. Vinokur, J. Phys. France **47**, 1425(1986)

[63] V. M. Vinokur, Physica D **107**, 411(1997)

[64] L. V. Mikheev, B. Drossel and M. Kardar, Phys. Rev. Lett. **C75**, 1170 (1975).

[65] B. Drossel, J. Stat. Phys. **82**, 431 (1996).

[66] T. Nattermann, S. Stepanow, L.-H. Tang, and H. Leschhorn, J. Phys. II (France), **2**, 1483 (1992).

[67] O. Narayan and D. Fisher, Phys. Rev. **B 48**, 7030 (1993).

[68] M. Dong et al., Phys. Rev. Lett. **70**, 662(1993).

[69] H. Kaper et al., Phys. Rev. Lett. **71**, 2973(1993).

[70] H. Leschorn and L. -H. Tang, Phys. Rev. Lett.'**70**, 2973(1993).

[71] H. Leschorn, Physica **A 195**, (1993324).

[72] C. Tang, S. Feng and L. Golubovic, Phys. Rev. Lett. **72**, 1264 (1994).

[73] H. A. Makse and L. A. N. Amaral, Europhys. Lett. **31**, 375 (1995).

[74] P. A. Kazantsev and V. L. Pokrovsky, JETP, **58**, 677 (1968).

[75] Müttiker and B. Landauer, Phys. Rev. **A23**, 1397 (1980).

[76] B. V. Petukhov, Fiz. Tv. Tela **13**, 1445 (1971).

[77] B. V. Petukhov and V. Ya. Sukharev, Fiz. Tv.'Tela **22**, 1981 (1980).

[78] B. V. Petukhov and V.'Ya. Sukharev, Fiz. Tv. Tela **23**, 1093 (1980).

[79] B. V. Petukhov, Fiz. Tv. Tela **25**, 1822 (1983).

[80] B. V. Petukhov, Fiz. Met. **25**, 1179 (1983).

[81] T. Nattermann, Condensed Matter preprint, No. 9705295, 1997.

[82] J. R. Patel and A. R. Chandhuri, Phys. Rev., **143**, 601 (1966).

[83] V. N. Erofeev, V. I. Nikitenko and V. B. Osvenskii, Phys. Stat. Sol., **35**, 79 (1969).

[84] V. N. Erofeev and V. I. Nikitenko, Phys. Stat. Sol., **35**, 79(1971).

[85] S. Alexander, J. Bernasconi, W. R. Schneider, R. Biller, W. G. Clark, G.Grüner, R. Orbach, and Zettl, Phys. Rev. B **24**:7474(1981).

[86] A. -L. Barabási and H. E. Stanley, "Fractal Concepts in Surface Growth", Cambridge University Press, Cambridge (1995).

[87] J. M. Burgers, The Nonlinear Diffusion Equation (Riedel, Boston 1974).

[88] M. Kardar, G. Parisi and Y. -C. Zhang, "Dynamic scaling of growing interfaces", Phy. Rev. Lett. **56**, 889-892 (1986).

[89] G. P. Ivantsov, Dokl. Akad. Nauk SSSR, **81**,2, 172 (1951).

[90] A. R. Umantsev, Kristallografiya **30**, 153 (1984) [Sov. Phys. Crystallogr. **30**, 153 (1984)].

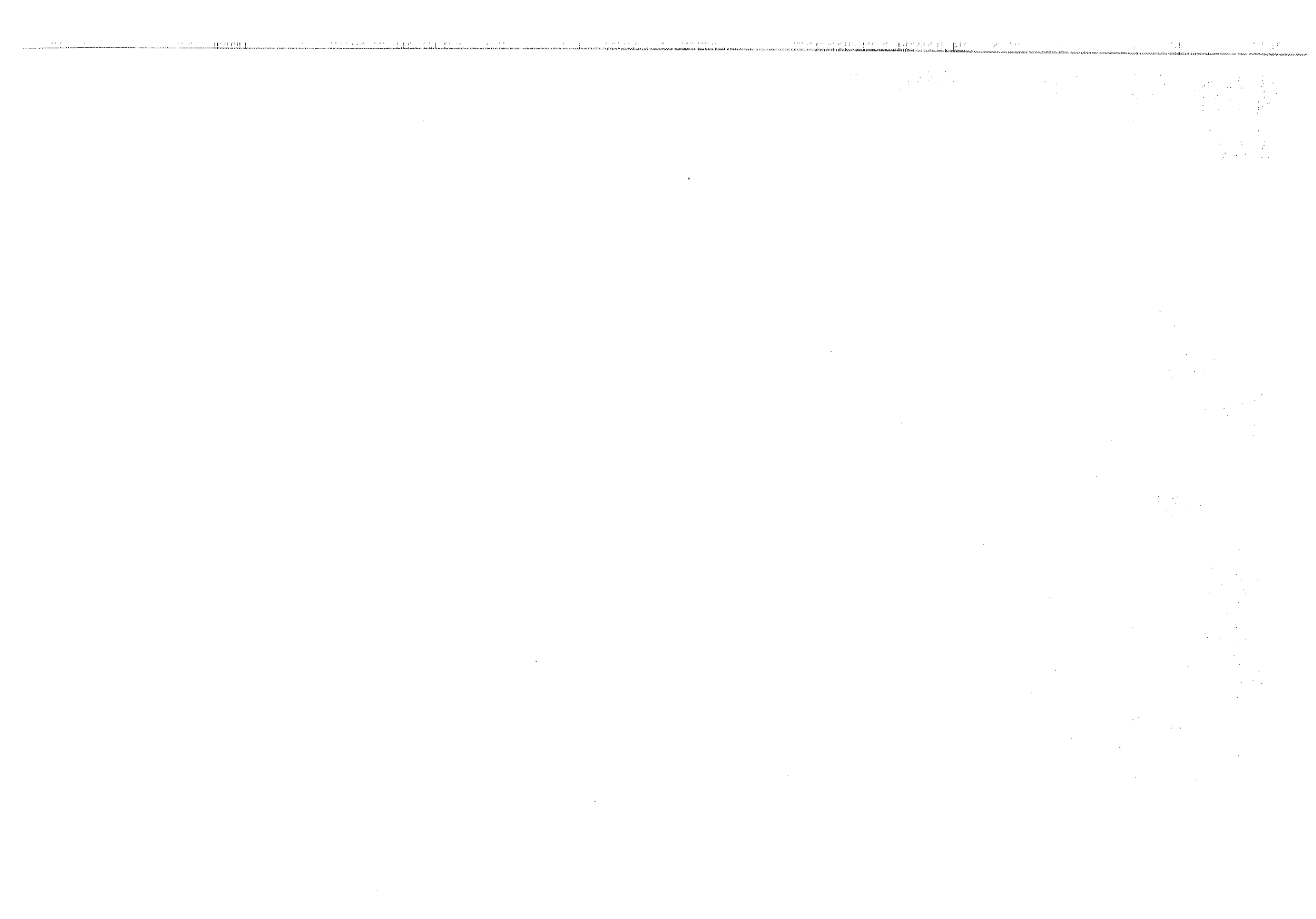

# Veröffentlichungen

Teile der vorliegenden Arbeit werden an folgenden Stellen veröffentlicht:

1) X. Feng, E. Brener, D. Temkin, Y. Saito and H. Müller-Krumbhaar,
*Solidification in the one-dimensional model for*
*a disordered binary alloy under diffusion,*
wird in Kürze in EPJ B veröffentlicht.

2) X. Feng, E. Brener, D. Temkin, Y. Saito and H. Müller-Krumbhaar,
*Creep motion of a solidification front in a two-dimensional binary alloy,*
wird im Januar 1999 in Phys. Rev. **E 59** veröffentlicht.

# Danksagung

Besonders herzlich danke ich Herrn Prof. Dr. H. Müller-Krumbhaar für die Möglichkeit, in Deutschland zu promovieren, für die Betreuung meiner Arbeit, für die interessante Themenstellung und hervorragende Zusammenarbeit, für das freundschaftliche Arbeitsklima und viele wertvolle Anregungen, Hilfestellungen und Ratschläge.

Sehr dankbar bin ich Herrn Dr. E. A. Brener für eine großartige Zeit der Zusammenarbeit, für viele fachliche Gespräche, für seine große Hilfsbereitschaft und stete Ansprechbarkeit.

Herrn Prof. Dr. D. E. Temkin gilt mein Dank für die erfolgreiche Zusammenarbeit, sowie für seine Freundlichkeit.

Herrn Prof. Dr. Y. Saito danke ich für die Hilfe bei der Arbeit mit dem Computer, sowie für die zahlreichen Emails und Faxe über fachliche Fragen.

Herrn Prof. Dr. H. Wenzl gilt mein Dank für die freundliche Übernahme des Korreferats.

Ich danke Frau Dipl. -Phys. B. Montanari, Frau Dipl. -Phys. S. Biermann, Frau Dr. A. Borrmann, Herrn Dipl. -Phys. J. -H. Lin, Herrn Dr. T. Sintes und Herrn Dipl. -Phys. M. Krenzlin für ihre Freundschaft, zahlreiche interessante Diskussionen über das Leben und die Hilfe bei der Arbeit mit dem Computer.

Frau L. Snyders danke ich für die große Hilfsbereitschaft in allen organisatorischen Fragen.

Schließlich bedanke ich mich bei allen Mitgliedern des Institutes Theorie III für die angenehme Arbeitsatmosphäre sowie die stetige Hilfsbereitschaft. Sie haben einen großen Anteil daran, daß die drei Jahre im Forschungszentrum Jülich für mich eine schöne, interessante Zeit waren.

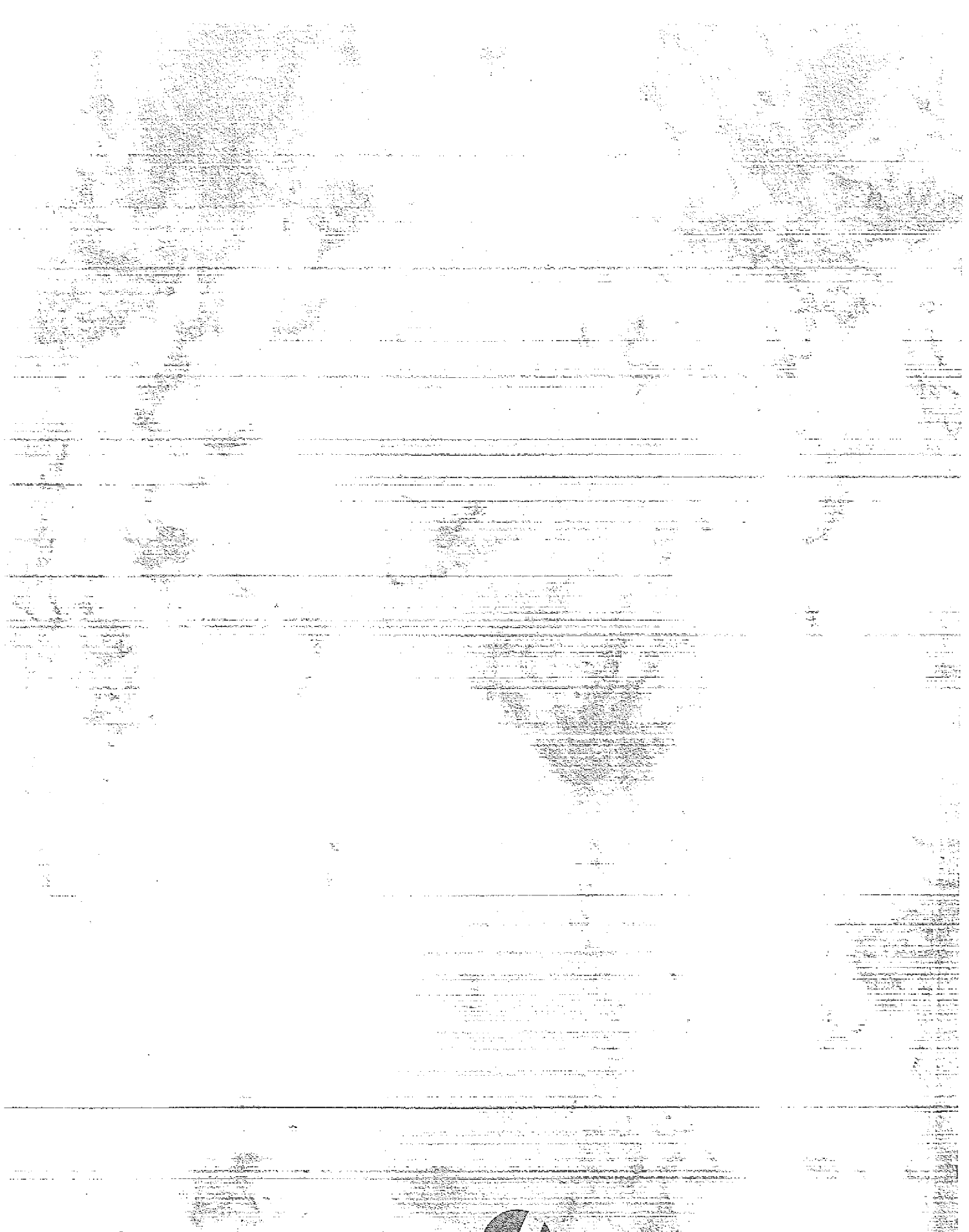

Forschungszentrum Jülich

Jül-3613
December 1998
ISSN 0944-2952